UNIVERSITEIT VAN PRETORIA
UNIVERSITY OF PRETORIA
YUNIBESITHI YA PRETORIA

Assessment of seasonal variations of teal carbon in palustrine wetlands of the Grassland Biome: A case study of Chrissiesmeer, Mpumalanga Lakes District, Mpumalanga Province, South Africa

By

Sisipho Ngebe

21757608

Supervisor: Dr Heidi van Deventer

Co-supervisor: Dr Laven Naidoo

Co-supervisor: Dr Philemon Tsele

A dissertation submitted in fulfilment of the requirements for the degree of

Master of Science in Geoinformatics by research

In the Department of Geography, Geoinformatics and Meteorology

Faculty of Natural and Agricultural Sciences

University of Pretoria

March 2023

SUPERVISORS:

Dr Heidi van Deventer

Council for Scientific and Industrial Research (CSIR),

Smart Places Cluster,

Pretoria, 0001

Department Geography, Geoinformatics and Meteorology,

Faculty of Natural and Agricultural Sciences,

University of Pretoria,

Hatfield, 0028.

Dr Laven Naidoo

Gauteng City-Region Observatory (GCRO),

Braamfontein,

Johannesburg 2050, Gauteng

Dr Philemon Tsele

Department Geography, Geoinformatics and Meteorology,

Faculty of Natural and Agricultural Sciences,

University of Pretoria,

Hatfield, 0028.

DEDICATION

This work is wholeheartedly dedicated to my family especially my beloved parents, Luzuko Ngebe and Ntombikhona Yaliwe-Ngebe under whose constant emotional and mental support, love, and words of encouragement I have completed this dissertation. My special thanks also go to my caring sisters Andisiwe Ngebe, Sibulele Ngebe and my only nephew Liyabona Ngebe who have never left my side.

DECLARATION

I, Sisipho Ngebe, declare that the entirety of the work contained in this dissertation, which I hereby submit for the degree of Master of Science in Geoinformatics at the University of Pretoria, is my own work except where stated otherwise by citation or acknowledgement. I declare that this dissertation has not been previously submitted for a degree at this or any other tertiary institution of higher learning.

Student number: 21757608

SIGNATURE: 

DATE: March 2023

ACKNOWLEDGEMENTS

I am deeply grateful to God who has given me strength, courage, and guidance throughout the course of my research. Words cannot express my gratitude to my supervisor Dr Laven Naidoo for his invaluable patience, guidance, and feedback. I also could not have undertaken this journey without Dr Heidi van Deventer and Dr Philemon Tsele, who generously provided knowledge, expertise, and words of encouragement. The tremendous knowledge, key comments and plentiful experience from my supervisors have motivated me throughout my academic research and daily life. Additionally, this milestone would not have been possible without the extensive support from Mr Mcebisi Qabaqaba whose kind heart, support and insightful inputs have contributed towards the successful completion of this dissertation.

I would like to acknowledge the Water Research Commission (WRC) and the Council for Scientific and Industrial Research (CSIR) who initially funded the project. My gratitude extends to the South African National Space Agency (SANSA) for the financial sponsorship and academic support provided to undertake my MSc studies. I would like to thank the Department of Geography, Geoinformatics and Meteorology, University of Pretoria for providing a safe environment, academic support and ensuring that I have all the necessary skills and material to complete my thesis. Sincere words of gratitude and acknowledgement go to Prof. Moses Cho, Dr Basanda Nondlazi, Ms Ridhwanna Gangat and Ms Seadi Mofutsanyana who assisted during the collection of field data.

Lastly, I would be remiss in not acknowledging my friends, my aunts Lwandiswa Ngebe, Lona Yaliwe, Fikiswa Yaliwe and my uncle Gcinikhaya Yaliwe. Their belief and confidence in me have kept my spirits, hopes, and motivation high during this journey.

TABLE OF CONTENTS

LIST OF EQUATIONS

LIST OF FIGURES

LIST OF TABLES

ABSTRACT

Wetlands are recognised as the important natural ecosystems in the world. The above-ground biomass (AGB) of wetland vegetation is essential for providing ecosystem services related to global climate change due to its crucial role in sequestrating anthropogenic carbon emissions. Seasonal AGB estimation could help to understand carbon changes in wetlands and how vegetation in these ecosystems differs across seasons at regional scales. Remote sensing technology offers time-effective and cost-efficient ways to improve the monitoring of wetlands and understanding of the spatial carbon changes in wetland vegetation. This study aimed to use seasonal derived AGB of palustrine herbaceous vegetation to determine the differences in teal carbon, using active and passive remote sensing data across the summer and winter seasons. The study was carried out in the Chrissiesmeer catchment in the temperate Grassland Biome of the Mpumalanga Province of South Africa. The objectives were to (1) derive different season-specific modelling scenarios from Sentinel-1 and Sentinel-2 imagery to assess the optimal model for estimating AGB of palustrine wetland vegetation AGB, (2) assess the performance of Random Forest (RF) and Support Vector Regression (SVR) in predicting seasonal AGB of wetland vegetation, (3) map the seasonal spatial patterns of teal carbon from the estimated AGB of wetland vegetation, and (4) assess the seasonal variation in the predicted teal carbon. RF and SVR algorithms were used as regression-based algorithms with important variable selection to develop an optimal model from the modelling scenarios, which also incorporated field-measured Leaf Area Index (LAI). The results showed that the combination of Sentinel-1 GLCMs and backscatter channels yielded higher accuracy for the estimation of the AGB of palustrine herbaceous vegetation attaining coefficient of determination (R^2) = 0.735, root mean squared error (RMSE) = 39.848 $g \cdot m^{-2}$, and relative RMSE (relRMSE) = 17.286% compared to a combination of reflectance bands, vegetation indices and red-edge bands (R^2 = 0.753, RMSE = 49.268 $g \cdot m^{-2}$, and relRMSE = 20.009%) in the summer season. For the estimation of AGB in the winter season, Sentinel-1-derived GLCMS textures obtained higher accuracy (R^2 = 0.785, RMSE = 67.582 $g \cdot m^{-2}$, and relRMSE = 20.885%) compared to the combination of reflectance bands, vegetation indices and red-edge bands of optical data (R^2 = 0.749, RMSE= 69.634 $g \cdot m^{-2}$ and relRMSE = 21.248%).

These findings suggested that Sentinel-1 sensor-derived models performed better than the optical models in both seasons. Furthermore, the addition of SAR textural measurements improved the accuracy of modelling AGB and RF model performed better than SVR in estimating the AGB of wetland vegetation. The study observed that there was a significant difference between the summer (77.527 g C/m^{-2} DM) and winter (57.918 g C/m^{-2} DM) seasonal mean carbon ranges ($p < 0.05$), and Tevredenpan wetland vegetation communities stored higher levels of carbon in the AGB vegetation in summer than in winter. The study showed that vegetation of palustrine wetlands is significant for carbon storage and fluctuates significantly between summer and winter. Estimating carbon stock in the AGB vegetation can aid in conserving grasslands and wetlands and notably optimise research on biomass estimation with remote sensing and machine learning systems.

Key words: carbon sequestration; carbon stock; climate change; herbaceous AGB; machine learning; remote sensing; temporal.

ACRONYMS AND ABBREVIATIONS

AFOLU	Agriculture, Forestry and Other Land Use
AGB	Above Ground Biomass
AIC	Akaike Information Criterion
ANN	Artificial Neural Networks
BGB	Below Ground Biomass
BOA	Bottom of the atmosphere
CBD	Convention on Biological Diversity
CO_2	Carbon dioxide
COV	Co-efficient of variation
CS	Carbon Sequestration
DEM	Digital Elevation Model
EBV	Essential Biodiversity Variable
EMS	Electromagnetic Spectrum
ESA	European Space Agency
GBF	Global Biodiversity Framework
GHGs	Greenhouse gases
GLCM	Grey Level Co-occurrence Matrix

GNDVI	Green Normalized Difference Vegetation Index
GPS	Global Positioning System
GRD	Ground Range Detected
GRVI	Green- Red Vegetation Index
HGM	Hydrogeomorphic
IPCC	International Panel on Climate Change
LAI	Leaf Area Index
LiDAR	Light Detection and Ranging
MLD	Mpumalanga Lakes District
MLR	Multiple Linear Regression
MODIS	Moderate Resolution Imaging Spectroradiometer
MSI	Multispectral Instrument
NDVI	Normalized Difference Vegetation Index
NDWI	Normalized Difference Water Index
NIR	Near-infrared
NWA	National Water Act
NWM5	National Wetland Map 5
OLI	Operational Land Imager

QGIS	Quantum Geographic Information System
RBF	Radial Basis Function
RE	Red-Edge
relRMSE	Relative Root Mean Square Error
RF	Random Forest
RFE	Recursive Feature Elimination
RMSE	Root Mean Square Error
RSD	Relative Standard Deviation
RTM	Radiative Transfer Model
SAR	Synthetic Aperture Radar
SD	Standard Deviation
SDG	Sustainable Development Goals
SMLR	Stepwise Multiple Linear Regression
SNAP	Sentinel Application Platform
SPOT	Satellite Pour l'Observation de la Terre
SR	Simple Ratio
SVM	Support Vector Machine
SVR	Support Vector Regression

SWIR	Short-wave infrared
TM	Thematic Mapper
TOA	Top of the atmosphere
UN	United Nations
UNWWD	United Nations World Water Development Programme
VH	Vertical-horizontal
VI	Vegetation Indices
VV	Vertical-vertical
WCM	Water Cloud Model
WRC	Water Research Commission

CHAPTER 1: INTRODUCTION

1.1 General introduction

Wetlands are among the most significant natural ecosystems for the long-term sequestration of atmospheric carbon through carbon sequestration (CS) (Nahlik and Fennessy, 2016; Were et al., 2019). The carbon stored and sequestrated by freshwater wetlands is referred to as teal carbon (Nahlik and Fennessy, 2016). According to the South African National Water Act (Act no. 36 of 1998), a wetland is a "land which is transitional between terrestrial and aquatic systems where the water table is usually at or near the surface, or the land is periodically covered with shallow water, and which land in normal circumstances supports or would support vegetation typically adapted to life in saturated soil" (Republic of South Africa (RSA), 1998). Palustrine wetlands, in particular, their contribution relating to ecosystem services such as supporting biodiversity, livelihoods, and CS is globally recognised. Keith et al. (2020) define palustrine wetlands as spatial heterogeneous systems consisting of seasonally or permanently saturated vegetated wetland types such as seeps, floodplains, and mires. However, intensified impacts of anthropogenic and climatic change pressures are expected to result in a global decline in freshwater ecosystems, thus affecting the distribution and functioning of these ecosystems (Collen et al., 2014).

The ideal anoxic wet environment of wetland ecosystems results in inefficient respiration and decomposition of organic matter, leading to a high accumulation of carbon, making these ecosystems sinks for greenhouse gases (GHGs) (Ribeiro et al., 2021; Salimi et al., 2021). Although the wetland biome is globally vital for providing ecosystem services, including storing carbon, it is highly degraded and endangered. The water abstraction near wetlands can result in the desiccation of these wetlands, and surface fires can ignite the peat, causing possible burning of the substrate to change these sinks to sources of GHGs emissions (Grundling et al., 2015). Despite variability when evaluating the importance of wetlands in the balance of atmospheric GHGs, it is vital to mention that they have continuously been absorbing and releasing GHGs. Therefore, their contribution to carbon sink needs to be modelled over different times (Dayathilake et al., 2021).

The Intergovernmental Panel on Climate Change (IPCC) identified above-ground biomass (AGB) as one of the crucial components with the ability to store, accumulate, and release carbon (Eggleston et al., 2006). AGB is the dry mass of plant organic matter per unit area and is an indicator of plant health in most ecosystems (Pang et al., 2020). Moreover, the AGB contributes significantly to atmospheric carbon changes caused by fire, logging, and land use practices (Dahy et al., 2020). Therefore, it should be monitored and measured throughout the year, not only for single instance mapping. In addition, at different seasonal times, vegetation in wetlands shows differences in the carbon and nutrient cycles, water content and energy during the growing season, which in turn impacts the quantity of AGB in these ecosystems (Mitch et al., 2013; Jin et al., 2014). As a result of these fluctuations in climate variability as well as disturbances (e.g., fire and cattle ranching which can affect seasonal AGB) , the assessment of carbon changes in various natural ecosystems has become crucial for developing sustainable climate change strategies (Dayathilake et al., 2020). However, understanding wetland ecosystem services, including carbon changes, can be very difficult as wetlands are very dynamic and complex ecosystems and thus poses a challenge in knowing their future state (Moomaw et al., 2018; Villa and Bernal, 2018). Thus, timely monitoring systems of carbon changes in freshwater wetlands are still lacking, and the variations in carbon, especially in different seasons, are poorly understood.

Estimation and assessment of seasonal AGB in grass-covered areas would provide valuable information for the evaluation and modelling of seasonal carbon changes, wetland productivity and the health of these ecosystems (Adam and Mutanga, 2012; Nahlik and Fennessy, 2016). Also, grass, sedge and large macrophyte vegetation would offer a significant opportunity to understand and measure how AGB or carbon growth varies in inundated and non-submerged areas since the grasslands are affected by seasonality (Xu and Baldocchi, 2004). There still needs to be more information globally on quantifying teal carbon changes in wetlands (Nahlik and Fennessy, 2016). In the case of South Africa, most work on the quantification of AGB has been done on quantifying biomass of woody structures (Mathieu et al., 2013; Naidoo et al., 2015; Urbazaev et al., 2015) and estimating AGB in grasslands (Cho et al., 2007; Ramoelo et al., 2015; Sibanda et al., 2015; Sibanda et al., 2017). There are no studies that have quantified and assessed the total carbon sink of the herbaceous AGB in palustrine wetland vegetation across the seasons within the Grassland Biome.

Skowno et al. (2019) have highlighted that the wetlands and grasslands of South Africa are severely destroyed because of extensive agriculture and alien invasive species. Consequently, quantifying teal carbon in wetlands in the Grassland Biome is crucial for protecting and monitoring wetland biodiversity.

Previously, AGB was estimated using non-destructive methods, such as allometric equations based on critical variables like diameter, height, and wood density, particularly in forest ecosystems (Chave et al., 2014; Luo et al., 2017). The currently used field-based method for estimating herbaceous AGB is based on destructive- measurements, which involve cutting down vegetation at point locations (Knapp et al., 2020). However, these conventional techniques are laborious, time-consuming, and unable to accurately map wetland carbon or biomass in terms of its spatial and temporal distribution (Barrachina et al., 2015; Otukei and Emanuel, 2015). Despite these constraints, field methods are still valuable and are crucial as calibration and validation datasets for upscaling model approaches (Englhart et al., 2011). The development of remote sensing technology over the years has been among the essential tools for biomass or carbon assessment. In contrast to the limitations of traditional methods, remote sensing allows for frequent wetlands monitoring over broad geographical areas. Several satellite datasets such as Synthetic Aperture Radar (SAR) images, multispectral and hyperspectral optical data, and Light Detection and Ranging (LiDAR) data have previously been used to develop analytical models for extracting biophysical vegetation parameters (Luo et al., 2017; LaRocque et al., 2020; Tavasoli and Arefi, 2020). For example, LiDAR data has unique benefits in obtaining information about an object horizontally and vertically and shows a 3-dimensional (3D) representation of vegetation structure (Fatoyinbo et al., 2018). However, utilisation of LiDAR datasets is constrained in wetlands because of high costs and limited coverage information at both spatial and temporal scales (Guo et al., 2017).

In contrast to the cost limitation of LiDAR data, freely available optical remote sensing imagery of high spatial, temporal, and spectral resolution has been made available over the years, improving hyper-temporal wetland AGB estimation (Li et al., 2021). Estimating herbaceous AGB in wetlands using optical data is based on correlating vegetation indices (VIs) with field-measured vegetation parameters (Kumar and Mutanga, 2017). VIs are spectral indices that are based on quantifying the physical difference in spectral reflectance of vegetation across the visible to shortwave regions of

the electromagnetic spectrum (EMS) (350 nm – 2500 nm) and are derived from optical remotely sensed data (Taddeo et al., 2019). Leaf Area Index (LAI) is also a crucial metric for characterising the growth of grassland and wetland vegetation, and it is a strong proxy for AGB (Van Wijk and Williams, 2005; Masemola et al., 2016). Remote sensing VIs are quite simple and practical algorithms for quantitative and qualitative assessments of vegetation properties and offer the advantage of suppressing soil background while significantly improving the sensitivity of the detection of green vegetation when estimating AGB (Xue and Su 2017). However, VIs such as the Normalized Difference Vegetation Index (NDVI) (Tucker, 1979) is limited in estimating vegetation biomass because it reaches saturation in areas with high-density biomass (Mutanga and Skidmore, 2004). On the other hand, VIs derived from the red-edge (RE) proved to increase the accuracy of AGB estimates (Mutanga et al., 2012). The absence of the RE region in multispectral satellite data, such as Landsat, hampered the estimation of vegetation AGB at regional scales (Ramoelo et al., 2015). Commercial sensors containing the RE bands (RapidEye and Worldview imagery) showed improved accuracy in grass biomass estimates (Ramoelo et al., 2015). However, they are costly, hindering the capability of exploring the RE region in wetland vegetation-related studies at local and regional scales.

The accessibility of free optical sensor imagery developed by the European Space Agency (ESA) has improved the retrieval of vegetation parameters, especially wetland AGB in temperate and semi-arid grasslands (Li et al., 2021). The Sentinel-2 Multispectral Instrument (MSI) sensor has better image acquisition characteristics which significantly enhances the monitoring of aspects of the aquatic, coastal, estuarine, marine, and terrestrial ecosystems (Stratoulias et al., 2015; Shoko et al., 2016). Sentinel-2 has several spectral bands, including the four RE bands (705 nm - 865 nm), which enable wetland assessments at broader scales due to better spectral and spatial resolutions (Shoko and Mutanga, 2017; Li et al., 2021). The RE region has been demonstrated to increase the accuracy and sensitivity of vegetation AGB estimation, overcoming the effect of saturation in areas with dense canopies and moderate to higher AGB (Mutanga et al., 2012; Ramoelo et al., 2015; Sibanda et al., 2017; Shoko and Mutanga, 2017). However, the shortcomings associated with optical data in estimating vegetation AGB include the reduced ability to sense the 3D structure of vegetation given the viewing angle, wavelength, signal saturation and cloud obstruction (Guo et al.,

2017). Additionally, spectral contamination of background water in heterogeneous palustrine wetlands can also be problematic in optical sensors.

SAR has become an attractive technology with several bands such as the C-band, X-band, and L-band that can be used together with optical data to improve wetland AGB estimates regardless of cloudy conditions (Englhart et al., 2011; Sinha et al., 2015). The C-band and X-band have wavelengths of 5.6 cm and 3.1 cm, respectively, and have proved to be suitable for monitoring wetlands herbaceous AGB (Brisco et al., 2011; Naidoo et al., 2019). In areas of dense vegetation cover, longer wavelengths (L-band ~24cm) are more effective in estimating the AGB, particularly in forest ecosystems (Lang et al., 2008). Sentinel-1A SAR sensor by ESA operating at C-band frequently provides free imagery that improves retrieval of vegetation parameters (Sinha et al., 2015; Montgomery et al., 2019) and enables seasonal monitoring of AGB. The assessment of AGB with SAR data involves finding the relationship between vegetation biomass and radar backscatter coefficients (Sinha et al., 2015). Polarised and co-polarised backscatter channels (VH and VV) have shown to effectively estimate wetland AGB (Ye et al., 2010; Naidoo et al., 2019). Even so, radar backscatter signals are limited in estimating AGB in submerged and non-submerged vegetation in wetlands ecosystems (Silva et al., 2008; Gallant, 2015).

The analysis of texture measurements is an image processing method that can improve the estimation of AGB by addressing certain existing saturation problems associated with VIs and C-band (Cutler et al., 2012; Kelsey and Neff, 2014). Image texture, such as the grey level co-occurrence matrices (GLCMs) methods, enables for provision of structural and geometrical information on vegetation properties (Kelsey and Neff, 2014) and can be extracted in both optical and radar satellite imagery. The benefit of texture is that, irrespective of tone (i.e., backscatter or reflectance), it can enhance spatial information retrieval by raising the saturation level and improving the range of biomass that can be estimated using SAR data (Sarker et al., 2011). Thus, the efficiency of potential proxies that may improve discrimination of spatial information in vegetation properties, including RE bands and texture variables, must be well evaluated (Dube and Mutanga, 2015; Sibanda et al., 2017).

Remote sensing methods for assessing AGB in wetlands are based on investigating relationships between vegetation biophysical parameters and predictor variables derived from remote sensing

images using parametric, non-parametric and physical modelling approaches (Darvishzadeh et al., 2008; Verrelst et al., 2015; Wan et al., 2019). Parametric approaches are based on finding the statistical relationship between spectral observations or reflectance and a specific field-measured target variable through a fitting function (Verrelst et al., 2015). The primary benefits of parametric regression techniques are that they are easy, fast to compute, and straightforward to understand (Ramoelo et al., 2015). Due to their empirical nature, they lack generalisation when it comes to up-scaling methods and exhibit a high level of overfitting (Kokaly et al., 2009; Ramoelo et al., 2012). On the other hand, physical-based methods for estimating biophysical parameters from remote sensing data are based on understanding the physical processes involved in energy transfers within plant canopies using physical laws (Darvishzadeh et al., 2008). The most known physical method involves the inversion of Radiative Transfer Models (RTMs) such as PROSPECT (Feret et al., 2008) and PROSAIL (Darvishzadeh et al., 2008). Compared to empirical approaches, the physically-based methods overcome the site- and sensor-specific problems of statistical or empirical approaches (Berger et al., 2018). However, the inversion of RTMs requires site-specific information (e.g., specific in-field backscatter/reflectance measurements during satellite overpass), which makes the calibration of RTM models complex.

Machine learning (ML) algorithms are non-parametric and build a non-linear regression relationship between predictor variables retrieved from remote sensing images and field-collected AGB (Mutanga et al., 2012). Several ML approaches, such as Random Forest (RF), Artificial Neural Networks (ANN) and Support Vector regression (SVR), can be integrated with remote sensing data and field-measured data for the estimation of AGB in wetlands and grasslands (Wan et al., 2018; Naidoo et al., 2019; Li et al., 2021). The most significant advantages of these ensemble algorithms include their ability to improve the robustness and generalisation capacity of regression models through modelling which incorporate many training predictor variables, big data and missing data and can deal with highly collinear variables (Knox et al., 2011; Mutanga et al., 2012). Also, algorithms such as RF offer the advantage of selecting important variables for regression models, enhancing the performance of modelling herbaceous AGB and contributing towards reducing overfitting in predictor models (Naidoo et al., 2019; Li et al., 2021).

The remote sensing technology of biomass estimation is continuously advancing as new and improved techniques, and applications are frequently developed. Thus, incorporating remote sensing variables derived from freely available Sentinel Series imagery (Sentinel-1 and Sentinel-2) for estimating herbaceous AGB in wetlands has been proven to be more accurate than using individual sensors (Huang et al., 2016; Naidoo et al., 2019). This provides a foundation to explore the seasonal variation in teal AGB using remote sensing and machine learning methods to achieve optimum modelling of herbaceous AGB in wetlands for this study. The importance of comprehending and assessing changes in grassland AGB at spatial and temporal scales is, therefore, significant for regional and dynamic carbon accounting.

1.2 Research Problem

Over the years, anthropogenic pressures and changes in the global climate have transformed most wetlands and grassland ecosystems. This results in the inability to observe the relationship between these ecosystems and carbon over time, which significantly impacts carbon estimation accuracy (Salimi et al., 2021). Global freshwater wetland ecosystems hold a remarkable ability to control climate change through their capability to sequester carbon from the atmosphere (Dayathilake et al., 2021). However, in the case of South Africa, the wetlands and grassland ecosystems are amongst the most critically endangered and degraded natural resources (Van Deventer et al., 2020). Due to elevated levels of Grassland Biome degradation in South Africa (covering 26.2% of the country's area) (Fourie et al., 2015; Skowno et al., 2019); palustrine wetlands were not fully presented in the South African National Wetland Maps (NWMs; Van Deventer et al., 2020).

An increase in the geographic footprint and impacts of agriculture, mining, commercial forest plantations, and invasive alien species have contributed to the increasing degradation of South Africa's wetlands and related wetland ecosystems in the Grassland Biome (Fourie et al., 2015). With wetlands increasingly drying because of water abstraction and climate change, transformation may increase, while the integrity of other wetlands may decline. Frequent monitoring of grassy wetlands is required to assess their changes at temporal scales and their potential for CS, especially at local and regional scales. However, most studies based on AGB in South Africa concentrated more on assessing the AGB in woody structures (Mathieu et al., 2013; Naidoo et al., 2015; Urbazaev et al.,

2015). There are no studies focusing on quantifying wetland teal carbon stock from the AGB, particularly across seasons within the Grassland Biome of South Africa. According to Schwieder et al. (2018), this is often influenced by inconsistent data acquisition due to dense vegetation and strong seasonality. This results in significant uncertainties as to whether wetlands and grasslands will respond positively or negatively to the changing climate and whether the variation in seasons affects the amount of carbon stored by wetlands (Chamaillé-Jammes and Bond, 2010; Salimi *et al.,*2021). Therefore, studies on carbon stock quantification in vegetated wetlands are needed.

1.3 Research Aim

This study aimed to use field-measured herbaceous AGB to quantify the seasonal differences in teal carbon across the summer and winter of 2017 in the Tevredenpan study area, which is part of the Mpumalanga Lakes District (MLD) in the Grassland Biome of the Mpumalanga Province of South Africa.

1.4 Research Questions

(i) Which combination of remote sensing predictor variables derived from Sentinel-1 and Sentinel-2 datasets best predict herbaceous AGB or carbon for the different seasons?

(ii) Which machine learning algorithm under investigation best estimate the AGB of wetland vegetation?

(iii) What spatial patterns in the carbon of wetland vegetation are noted between the summer and winter seasons in palustrine wetlands?

(iv) Are there any significant seasonal fluctuations in the estimated carbon of palustrine wetland vegetation?

1.5 Research objectives

The objectives of this study were to:

(i) Derive and test different season-specific modelling scenarios from Sentinel-1 and Sentinel-2 imagery to assess the optimal model for estimating AGB of palustrine wetland vegetation for the summer and winter seasons.

(ii) Assess the performance of RF and SVR algorithms in predicting seasonal AGB of palustrine wetland vegetation.

(iii) Map the spatial distribution of wetland vegetation carbon stock for the summer and winter seasons.

(iv) Assess the seasonal variations and if there is a statistical difference in teal carbon derived from wetland herbaceous AGB in the summer and winter seasons for the year 2017.

1.6 Significance of the study

Wetland ecosystems are essential for providing ecosystem services related to global climate change (Were et al., 2019). Monitoring the state and health of natural ecosystems, particularly freshwater ecosystems, over time is critical, and it is one of the target sub-indicators (sub-indicator 6.6.1.d) for 2030 Sustainable Development Goals (SDGs) set by the United Nations (UN) (UN, 2017). Several studies have highlighted that the AGB of wetland vegetation is a significant indicator of the state and health of wetlands (Mutanga et al., 2012; Li et al., 2019; Naidoo et al., 2019) and a good component for the storage of carbon (IPCC, 2006). Herbaceous AGB is the most dynamic and changing component and is estimated to globally contribute up to 30% of the sequestrated carbon (Houghton et al., 2009; Kumar and Mutanga, 2017). Thus, continuous monitoring and quantification of AGB at different seasons are vital owing to the increasing heterogeneity and complexity of ecosystems (Fernandez-Alaez et al., 2002). Additionally, monitoring results at different seasons may differ as natural ecosystems undergo seasonal changes due to their natural cycles (UN, 2017).

The inundation of wetlands during the summer (wet) season may affect the monitoring assessments and during the winter (dry) season, for example, monitoring may yield different results in ephemeral wetlands influencing the dynamics of nutrient cycles, vegetation growth, and gas emissions from wetlands (UN,2017; Salimi et al., 2021). Therefore, thorough attention must also be given to the winter season, especially in climate change-related studies on wetland ecosystems (Salimi et al., 2021). Estimating the seasonal dynamics of AGB is of key significance for developing our knowledge in monitoring ecosystem natural processes, ecological functions, management, and wetlands protection. Remote sensing models from the integration of remote sensing datasets and

field measurement of vegetation biophysical parameters have improved AGB estimation in various studies at regional scales in wetlands and grasslands (Mutanga et al., 2012; Ramoelo et al., 2015; Naidoo et., 2019; Li et al., 2021). However, fewer studies have considered assessing the seasonality of the AGB of palustrine wetland vegetation, particularly in the Grassland Biome. The study's novelty lies in integrating remote sensing data and field data into season-specific models to assess seasonal variations in teal carbon between the summer and winter. Assessment of season variations of carbon stored in the AGB of wetland vegetation will help to comprehend how vegetation in wetlands differs and functions between seasons, and how it contributes to CS at regional scales in dry and semi-arid places. This, in turn, will further help in ensuring that the SDGs sub-indicator 6.6.1.d goals of sustainable monitoring of the health and changes in natural ecosystems over time are achieved.

1.7 Research Outline

Chapter One: The aim of this chapter is to provide an introduction of the research topic, namely the estimation of South Africa's teal carbon in the Grassland Biome over the summer and winter seasons. Chapter one further presents a detailed description of the research problem in order to highlight why it is important to estimate herbaceous AGB of wetlands across these two seasons, indicate the main aim and objectives that are investigated in the study. In addition, this chapter provides insight on significance of this research.

Chapter Two: This chapter introduces an overview on wetlands and the process of CS in wetlands. It also provided a detailed evaluation of the existing literature studies on the application of satellite imagery data in assessing AGB of palustrine wetlands in the Grassland Biome of a part of the MLD of South Africa. Chapter two gives an important background on the traditional methods of estimating AGB that have been used in other studies and also their disadvantages. The chapter also reviews the utilisation of machine learning methods in non-parametric modelling for the estimation of AGB in palustrine wetlands. The purpose of literature review is to give background on what has been done and what are the research gaps.

Chapter Three: This chapter gives description and setting of the selected region of interest including the climatic conditions of the area. This chapter gives a detailed description on the methodology used in this study. The chapter clearly defines the chronological approach in which

these methods are used to conduct the research and for each objective. Chapter three also presents a detailed information on remote sensing data used, how it was processed , field sampling protocols, and field data collection for the calibration and validation of predictive models.

Chapter Four: This chapter will provide the results of the methods used to achieve and investigate the main objectives and research questions of the research project. The results section describes the observed variations between summer and winter, the significant differences in the vegetation of wetlands and further illustrate the prominent or significant remote sensing variables that have contributed towards the observed trends in the two investigated seasons.

Chapter Five: The aim of chapter five is to present the discussions which involves explaining the results within the context of existing literature. The chapter explains the trend observed in the results of the current study in relation to previous studies, how do the findings differ or correspond to existing in order to find plausible scientific reasons and arguments to validate the observed trend. Additionally the discussions in this chapter further help in knowing whether the objectives of the current research were achieved, and also pave a way for other studies to improve on the seasonal monitoring of AGB of wetland vegetation

Chapter Six: This chapter presents a summary of the current study and shows the importance of remote sensing techniques in temporal monitoring of palustrine wetland ecosystems at regional scales in arid and semi-arid areas. Chapter six also provides the key scientific findings of the study which provide insights for future studies to assess AGB using variables and models of different seasons. The study limitations, recommendations for future research are proposed in this chapter.

CHAPTER 2: LITERATURE REVIEW

This chapter provides an overview of the wetlands and introduces the process of carbon stock quantification in wetlands. It also provides a detailed evaluation of the existing literature studies on the application of satellite imagery data in assessing AGB of palustrine wetlands in the Grassland Biome. It also gives an important background on the traditional methods of estimating AGB that have been used in other studies and also their disadvantages. The chapter also reviews the utilisation of parametric and machine learning methods in non-parametric modelling for the estimation of AGB in palustrine wetlands. The purpose of literature review is to give background on what has been done and what are the research gaps.

2.1 Overview on wetlands

Wetlands are one of the most important ecosystems in the world. They are distinguished by hydric soils that are permanently or seasonally saturated by water, resulting in anoxic environments that support vegetation growth (Mitsch et al., 2013; Nahlik and Fennessy, 2016). It is estimated that wetlands sequester about 20–25% of the world's organic carbon, and wetland macrophytes not only contribute to the sequestration of atmospheric carbon when they are alive, but they are significantly important even during decomposition (Berry et al., 2010; Lolu et al., 2019). The Ramsar Convention on Wetlands defines wetlands as "areas of marsh, fen, peat, and or water, whether natural or artificial, permanent or temporary, with water that is static or flowing, fresh, brackish or salt, including areas of marine water the depth of which at low tide does not exceed six meters." (Matthews, 1993). Wetlands play an essential role in both hydrological and ecological processes (Kaplan and Avdan, 2018). Wetland services include flood mitigation, water supply and quality regulation, erosion control, biodiversity conservation, and food security. The United Nations World Water Development (UNWWD) has indicated that since the start of the 20th century, two-thirds of the world's wetlands have been degraded (UNWWD, 2015).

Intensive water extraction for agriculture, deforestation, industrial expansion, reservoir construction, increasing sea levels (Schmitt and Brisco, 2013) and altered climate patterns (Salimi et al., 2021) are threats to wetlands. Previous studies on wetlands have indicated that warming climate

and land use practices result in changes in the composition of wetland vegetation and vegetation degradation in some areas, which subsequently affects net primary productivity and significantly affects the functioning of wetlands as carbon sequesters (Hemes et al., 2019; Salimi et al., 2021). Furthermore, due to wetlands occupying a small extent (i.e., approximately 3-8%) of the world's land surface, little attention has been given to CS of teal carbon in these ecosystems and their associated macrophytes, particularly freshwater wetlands (Mitsch et al., 2013; Villa and Bernal, 2018; Lolu et al., 2019). Due to the dynamic nature of wetlands, they are subject to change on a seasonal or temporal and spatial basis in terms of the amount of water present, the water table, and the development of the quantity of vegetation. As a result, the provision of wetland services could continue to deteriorate (Mitchell, 2013). Currently, studies that quantified CS have primarily been conducted in forested terrestrial ecosystems (Berry et al., 2010; Powell et al., 2010;). However, the land surface is also occupied by other systems, such as grasslands and wetlands, which significantly contribute to carbon accounting at global and regional scales. Hence it is vital to quantify carbon in these ecosystems. Freshwater systems were listed by Emerton (2005) as one of Africa's most vulnerable resources. Furthermore, it was projected that mining methods, commercial agriculture, and urban expansion had destroyed more than half of the wetlands in semi-arid Africa (Cowan, 1995). Due to the decline in the extent of wetlands, assessing their condition is an essential concern. Moreover, the evaluation of wetlands demands reliable tools to monitor the vast majority of wetlands. Hence it is vital to assess and monitor wetlands continuously.

2.2 AGB as an important Essential Biodiversity Variable

Environmental problems on a global scale, such as the impacts of climate change and the loss of freshwater biodiversity, are critical problems that must be addressed (Turak et al., 2017). These issues are presented in various initiatives such as Post-2020 Global Biodiversity Frameworks (GBFs) and the Aichi Targets set by Convention on Biological Diversity (CBD) (Osborn et al., 2015; Turak et al., 2017). Improving the monitoring of these challenges and determining biodiversity changes in freshwater ecosystems, for example, at multiple spatial and temporal scales, could address the 2030 SDG targets (Target 15) set by the UN (Osborn et al., 2015). To date, there is still a need for more data on changes within the palustrine wetlands and only changes in the extent of open water bodies were reported to the SDG sub-indicator 6.6.1a (Turak et al., 2017).

The Essential Biodiversity Variables (EBVs), defined as derived biological state variables sensitive to changes over time, could form the basis of monitoring plans for freshwater ecosystems, including palustrine wetlands, which are currently underrepresented under SDG 15 (Turak et al., 2017). Regarding EBVs, "The vertical distribution of biomass in ecosystems, above and below the land surface", linked to the Ecosystem Structure EBV class (Pereira et al., 2013; Turak et al., 2017). Thus, AGB is a significant continuous and direct EBVs that can be measured with remote sensing to quantify changes in the structure of freshwater ecosystems. In turn, this could indicate the extent of freshwater ecosystems and extent of natural habitats that significantly store carbon (Pereira et al., 2013) and also help to meet the Aichi CBD target (Target: five, 11, 14 and 15) and SDG targets on freshwater biodiversity conservation.

2.3 The various categories of carbon in natural ecosystems

Quantifying the different categories of carbon could help to understand and monitor changes in the carbon cycle (Zinke, 2020). Thus, according to Zinke (2020), the different categories of carbon can be described using a full spectrum of colour-based descriptions. For instance, some of the colour-based descriptions of carbon include green, blue, and teal and these colours are mostly carbon sinks, and they illustrate the influence of CS on natural ecosystems in light of the changing climate. Green carbon is the form of carbon that is retained in the biosphere and is absorbed by terrestrial plants from the atmosphere (Berry et al., 2010). Terrestrial ecosystems must be a part of a complete response to the climate change issue because they are crucial in controlling greenhouse gas concentrations in the atmosphere (Berry et al., 2010). The term "blue carbon" describes the organic carbon is sequestrated by vegetated oceans and coastal ecosystems such as tidal marshes, mangrove forests and seagrass meadows (Macreadie et al., 2019).

Blue carbon ecosystems capture carbon at 30 – 50 times the rate of terrestrial forest ecosystems (Macreadie et al., 2019; Blue carbon lab, 2021). Teal carbon refers to the carbon stored in freshwater wetlands found inland (Nahlik and Fennessy, 2016). According to Nahlik and Fennessy (2016), numerous studies have primarily investigated and quantified green and blue carbon, while inland wetland teal carbon is given less attention. The preliminary study indicates that inland freshwater wetlands have the potential to store about 20% to 30% of the world's soil carbon (Mitch and

Gosselink, 2007; Lal, 2008). Precise and reliable carbon accounting is essential for mitigating the risk of climate change effects through identification and conservation of wetlands or wetland-dominated landscapes that store large carbon stocks and allowing wetlands to be included in carbon-offset programs.

2.4 Carbon sequestration in freshwater wetlands

The increase in the atmospheric concentration of CO_2 has resulted in changes in the functioning of natural ecosystems worldwide. The IPCC's fifth assessment report showed a global increase in the atmospheric concentration of CO_2 from approximately 280 to 400 parts per million (ppm) over the years (Pachauri et al., 2014). According to Sundquist et al. (2008), in order to stabilise atmospheric CO_2 during the next century, the world's annual CO_2 emissions must be reduced by more than 75% of their current level. When the effects of climate change are not consistently addressed, both natural and human processes may be severely impacted. Hence, climate change has become humanity's most serious and complex environmental matter over time (Solomon et al., 2007; Erwin, 2009; Pachauri et al., 2014). The projected increase of CO_2 emissions in the changing global climate requires important initiatives to monitor AGB vegetation ecology within wetlands that assist with regulating excessive carbon sources. Such interventions help to ameliorate possible severe effects on biodiversity.

CS is the process whereby the atmospheric CO_2 is absorbed and stored in carbon pools such as above ground live biomass, soils, below biomass for a long-time (Villa and Bernal, 2018). CS in wetlands results from high rates of deposition in organic matter and low decomposition rates (Pant et al., 2003). To maintain and understand the atmospheric carbon dynamics, the sequestration of C and its storage in large quantities, whether below or above ground in wetlands, is significant (Villa and Bernal, 2018). The total quantity of carbon that wetland ecosystems can sequestrate at given spatial and temporal scales is referred to as CS potential (Were et al., 2019). CS potential indicates the maximum rate at which carbon is stored over a certain period. For example, the plant growth rate and the maximum amount of carbon that can be accumulated in plants AGB and below-ground biomass (BGB) (Were et al., 2019).

Wetlands' CS potential is controlled by various factors such as vegetation, climate, anthropogenic activities, as well as significant variations in the rate of transformation and decomposition of plant material, which have caused significant complexities in the spatial distribution and composition of carbon in wetlands (Villa and Bernal, 2018; Were et al., 2019; Salimi et al., 2021). Some of these factors have severely put most wetlands under threat, for example, direct and indirect anthropogenic factors such as deforestation, animal grazing, fires, and invasive alien species, to mention a few (Mitchell, 2013). Due to the changing climate variables, such as increased temperatures, erratic rainfall, and anthropogenic pressures, wetland vegetation communities have been destroyed (Carrington et al., 2001: Kang et al., 2007; Moncrieff et al., 2015). Consequently, these wetland alterations increase the chances of large amounts of carbon stocks being released into the atmosphere. Therefore, CS is crucial for understanding the regional carbon cycle, especially since it is a significant aspect of semi-arid environments.

2.5 Quantification of carbon stocks from biomass estimates

Vegetation biomass is linked to a variety of crucial elements such carbon stock quantification, and peat formation (Sawadogo et al., 2010; Mutanga et al., 2012; Munyati et al., 2022). Quantifying wetland AGB would allow for the identification and prediction of potential variations in AGB, which is critical for developing climate change early warning systems (Wan et al., 2018; Li et al., 2021). Furthermore, it has been highlighted that due to the dynamic nature of the AGB, continual and frequent AGB observations are needed to quantify variations in carbon efficiently (Eastman et al., 2013; Diouf et al., 2015; Shoko et al., 2016). Kumar and Mutanga (2018) stated that estimations in the AGB vegetation still need to be fully documented, especially in African regions. As a result, there are still questions concerning about their estimated temporal variations. Biomass is critical to comprehending and calculating carbon stocks in plant communities, particularly grassland vegetation.

Although comprehensive biomass estimates are essential for precise and reliable carbon accounting, there are few reliable estimates of the carbon stock from dry biomass (Houghton et al., 2009). The IPCC has then established guidelines to convert AGB to carbon stocks, assuming that carbon concentrations are 50% of the AGB (Penman et al., 2003). Conversion of carbon stock is

formulated as ΔC= AGB x CF, where ΔC = Total carbon content in the AGB; AGB = estimated AGB; and CF = Carbon Fraction (Otukei and Emanuel, 2015; Behera et al., 2016). Research on the quantification of carbon stocks has been chiefly done in converting biomass of forest ecosystems (Barrett, 2014; Salas Macias et al., 2017; Tavasoli et al., 2019). For instance, Barret (2014) used a carbon fraction of 0.50 to calculate carbon stock from AGB in the Tongass National Forest. The results indicated that the forest stores large amounts of forest carbon, with an estimated 650 million tons of carbon compared to other national forests in the United States of America. On the other hand, both Tavasoli et al. (2019) and Oliveria et al. (2019) used the carbon fraction of 0.47 to calculate the carbon stocks from dry biomass of forests in urban forests and Brazil's open savannahs, respectively.

There has also been a growing interest in quantifying carbon stocks from biomass in wetlands ecosystems however most studies focused of yearly carbon estimation(Villa and Bernal, 2018; Dai et al., 2020; Dayathilake et al., 2020). Dai et al. (2020) estimated yearly CS of herbaceous vegetation in Poyang wetland, China. Their study indicated that herbaceous wetland vegetation sequestrated a total carbon amount of about 193–1221 g C m^{-2} $year^{-1}$. Fewer studies have estimated the carbon stock in the AGB of wetland vegetation across the seasons (Costa and Henry 2010; Lolu et al., 2019). Lolu et al. (2019) investigated the seasonal carbon stock from the dry AGB of 12 wetland macrophytes (i.e *Epilobium hirsutum, Hippuris vulgaris, Lycopus europaeus, Menyanthes trifoliata, Nymphoides peltatum, Phragmites australis, Ranunculus lingua, Myriophyllum spicatum, Saggitraria safittifolia, Sparganium erectum, Trapa natans and Typha angustata)* in the Hokersar wetland. The results of this study indicated the macrophytes to have an average of 244.86 g C/m^{-2} in the summer season and an average of 188.790 g C/m^{-2} in the winter season. Costa and Henry (2010) evaluated CS of aquatic macrophytes and documented lower carbon range of 114.3 g C/m^{-2} in summer compared to the range of 203 g C/m^{-2} in winter in the lakes of Brazil.

Research on estimating carbon stocks between seasons from wetland vegetation biomass is still lacking, particularly in African regions. Large-scale changes in vegetation cover, degradation of biomass, and increasing climate change effects are occurring throughout Southern African regions, with substantial implications on the functioning of the natural ecosystem (IPCC, 2014; King, 2014). According to David et al. (2022), in Southern African regions this has resulted in many uncertainties

regarding the rate of loss, regrowth in AGB and the carbon stocks estimations in the AGB are largely undocumented. Consequently, temporally, and spatially investigated variations in distributions of vegetative biomass can aid in conserving grasslands and wetlands and notably optimise research on biomass estimation with remote sensing systems. This, in turn, helps improve and understand the accuracy of carbon models, leading to more accurate future predictions of global climate change.

2.6 Methods for estimating AGB in wetlands

Section 2.6 provides a review on methods that are utilised for estimating AGB in wetlands based on existing literature. The section first reviews the field based or traditional methods which are categorised into destructive and non-destructive techniques. Secondly this section provides a review on the role of different remote sensing datasets and indices derived from satellite images in estimating the AGB of wetland vegetation.

2.6.1 Field-based methods

Traditional methods for field-based quantification of herbaceous AGB generally consist of collecting and estimating vegetation biomass using conventional methods such as field surveys and harvesting procedures for biomass assessments (García et al., 2010; Melton et al., 2013). Field surveys allow for the provision of high-quality point data (David et al., 2022). Harvesting is a destructive technique that involves physically cutting and collecting vegetation in non-forested wetlands (Lauck and Benscoter, 2015). Destructive methods have also been applied in wetland vegetation AGB estimation. Cutting wet vegetative biomass is often done at individual sample plots using the average of a number of sub-plots or a quadrant of a particular size. Destructive techniques typically require intensive fieldwork, which is laborious and time-consuming (Lauck and Benscoter, 2015; Han et al., 2019). Also, the destructive sampling is spatially constrained and does not fully describe the AGB variability across the landscape as some parts of the wetlands are inaccessible by foot. However, these approaches still have value, and the collected data are used for field validation.

Estimating plant biomass in wetlands can also be done using non-destructive methods. For example, non-destructive methods for estimating AGB involves developing models using allometric equations based on the correlation between biomass and vegetation metrics such as diameter-at-breast height (DBH) (Houghton et al., 2001; Chave et al., 2005). However, it is essential to note that

allometric equations are suitable for some wetlands species, such as *Carex* and *Phragmites*, which are large but not applicable for small species. The synergy between in-situ measurements and non-destructive methods based on satellite data provides a solid foundation for a practical understanding and analysis of results obtained from secondary data such as remote sensing images (Stephenson et al., 2020). Despite the efficiency and importance of traditional methods, the dynamic nature of wetlands in terms of water level, presence and growth of vegetation, and water-inundated areas cause these habitats to change annually or inter-annually (Mitsch et al., 2013). Wetlands are also hard to access in the field due to the presence of water, peat caps and other hazards which make physical sampling difficult. Therefore, estimating plant AGB in wetlands requires additional means to monitor the vast majority of wetlands distributed over large geographical areas.

The role of remote sensing technology in estimating wetland AGB

Remote sensing is an act of acquiring information from a target object without being physically in contact with it and the first multispectral remote sensing data was made available to the public in the 1970s (Fussell et al., 1986). Over the years, there has been considerable improvement on the use of satellite technology for estimating/predicting AGB in natural ecosystems because of the accessibility of these images to the public at relatively low costs. Satellite imagery data for monitoring and mapping wetlands can be acquired using different satellite platforms that are categorised as either active or passive (Wu, 2017). Active sensors provide their own energy source and acquire images at any time while passive sensors use the natural available energy from the sun to measure the reflected electromagnetic radiations (Campbell and Wynne, 2011). For example, images obtained from passive sensors are multispectral imagery, aerial photographs and hyperspectral imagery and remote sensing images from active sensors include LiDAR and SAR data. Several satellite remote sensors, with varying image acquisition features have been invented offering improved ways for monitoring of herbaceous AGB in wetland ecosystems over seasonal and long-term scales. These inevitable developments in remote sensing sensors offer better and finer spectral, temporal, and spatial resolutions that make it feasible for mapping large-scale wetlands dynamics (Lang et al., 2015). The following subsections will give more detailed information on the

application of different remote sensing datasets in estimation of AGB more specifically for palustrine wetlands in the Grassland Biome.

2.6.1.1 Estimation of wetland herbaceous AGB using optical remote sensing

Optical remote sensing technology has expanded in terms of applications due to exceptional technological improvements in the specifications of these sensors (Sibanda et al., 2015). Optical sensors make it feasible to obtain spectral data for AGB vegetation monitoring in different spectral regions of the EMS, which enables the detection of vegetation biomass, two-dimensional (2D) representation of vegetation, and its estimation within wetlands ecosystem (Gallant, 2015; Guo et al., 2017). Optical remote sensing data is available from several sensors, such as IKONOS, Quickbird, Worldview, *Satellite Pour l'Observation de la Terre* (SPOT), Sentinel series, Landsat, and the Moderate Resolution Imaging Spectroradiometer (MODIS). These sensors vary according to their spatial, radiometric, temporal, and spatial resolutions. This provides an opportunity to investigate the capabilities of these sensors for earth observation applications, including estimating biomass in wetlands and grasslands.

Multispectral data with coarse to moderate resolution, such as MODIS (250 m, 500 m, and 1000 m) and Landsat (30 m, 60 m) datasets, are currently freely available online. The space-based sensors provide images with a repeated global coverage, which is necessary for continuous AGB assessment at regional to global scale. These satellite data characteristics have resulted in numerous remote sensing images gaining more popularity for regional AGB mapping (Mutanga et al., 2012; Barrachina et al., 2015). Barrachina et al. (2015) used Landsat-5 Thematic Mapper (TM) to model the AGB of pastures and obtained satisfactory results of AGB estimation with a coefficient of determination (R^2) of 0.76 and root mean square error (RMSE) of 95 $g.m^2$. Landsat 8 Operational Land Imager (OLI) has nine bands that can be used to calculate vegetation AGB (Dube and Mutanga, 2015). Dube and Mutanga (2015) quantified the AGB of a forest plantation using Landsat 8 and Landsat 7 datasets in the uMngeni catchment in the KwaZulu-Natal Province of South Africa. Their results suggested that Landsat 8 performed better than Landsat 7 in estimating the AGB of *E. dunii* species, obtaining accuracies of an R^2 of 0.71, RMSE of 10.66 t ha^{-1} and mean of 6.26% for Landsat 8 and R^2 of 0.68, RMSE of 11.81 t ha^{-1}; and mean of 6.93% for Landsat 7.

Previous studies, however, on vegetation biomass estimation with moderate-resolution images reveal some gaps and shortcomings, such as the inability to measure the 3D structure of vegetation. For instance, it has been argued that using optical satellite images such as Landsat TM and MODIS may limit the quantification of AGB due to low to moderate spatial and spectral resolution in these sensors (Dube and Mutanga, 2015; Shoko et al., 2016; Li et al., 2021). Furthermore, moderate-resolution sensors are limited in the AGB estimation due to the unavailability of RE bands within these sensors. According to the literature, the wavelengths of the RE region are sensitive to leaf structure reflection (i.e., LAI and leaf angle distribution), reducing the saturation effect due to lower absorption in this region (Cho and Skidmore, 2006; Mutanga et al., 2012). Thus, the RE region provides more information on the characterisation of vegetation parameters and has proven to be beneficial for AGB and vegetation structure estimation (Ramoelo et al., 2015; Naidoo et al., 2019; Li et al., 2021). Therefore, one of the main aspects to consider when using remote sensing images in evaluating vegetation AGB is their capability to extract biophysical vegetation characteristics such as structure over space and time (Forkel et al., 2013).

The development of improved sensors (RapidEye, Sentinel-2 MSI, and Worldview) with designated strategically-positioned spectral bands and frequent revisit times over the years have improved the mapping and estimation of the vegetation biomass in grasslands and wetlands (Sibanda et al., 2017; Li et al., 2021). The presence of RE bands in optical sensors such as Worldview and RapidEye offers improved capabilities for precise and timely prediction of AGB in grasslands and wetlands ecosystems at both local and regional scales. These sensors have shown outstanding capabilities in mapping vegetation biomass in numerous studies (Ramoelo et al., 2012; Ramoelo et al., 2015; Sibanda et al., 2017; Naidoo et al., 2019; Li et al., 2021). While RapidEye and Worldview images are suitable for fine-scale monitoring and estimating teal AGB, they are very costly. Moreover, this causes limitations in multi-temporal or seasonal assessments of biomass and hinders exploring RE bands' ability for AGB estimation at regional scales.

ESA developed the Sentinel-2 MSI sensor system, which consists of two orbiting twin satellites, Sentinel-2A (launched in 2015) and Sentinel-2B (launched in 2017). Sentinel-2 is an optical satellite with 13 spectral bands operating at spatial resolutions of 10 m, 20 m, and 60 m, with frequent revisit times of 5-7 days compared to the nine spectral bands of Landsat 8, which has a revisit time of 16

days. Furthermore, the imagery is available free of charge providing the opportunity to utilise the RE bands, which are not available within the Landsat and MODIS imagery; hence, this study sought the use of Sentinel-2 imagery. Several contributions using Sentinel-2 images in estimating vegetation AGB of wetlands and grasslands have been made in numerous studies (Ramoelo et al., 2015; Sibanda et al., 2015; Naidoo et al., 2019; Li et al., 2021). For example, a study by Ramoelo et al. (2015) investigated the use of the RE band of Sentinel-2 in assessing grass biophysical properties. Li et al. (2021) used Sentinel-2A MSI images for modelling wetland vegetation AGB with ensemble algorithms at accuracies of R^2 = 0.84 and R^2 = 0.87. Despite the capabilities and significant accuracies demonstrated by optical data, they have shorter wavelengths that result in loss of information during cloudy and rainy weather and provide limited structural information (Gallant, 2015). Additionally, water in wetlands mixes the spectral responses of semi- and full-submerged vegetation. Therefore, the estimation of AGB in wetlands with dense vegetation using solely optical datasets may be limited (Gallant, 2015).

Although optical remote sensing data have shown great capabilities in providing vegetation canopy information, including AGB estimates in different environments, the canopy structure tends to have significant differences between months and even across seasons. Powell et al. (2010) and Zhu and Liu (2019) contend that seasonal optical images can potentially result in significant variations in AGB estimates. However, the literature reveals that to date, previous quantification of AGB across seasons has been done during the peak growing season in forested environments using medium-resolution images like Landsat (Gasparri et al., 2010; Powell et al., 2010). On the other hand, studies on quantifying the AGB of wetland vegetation between seasons are still lacking and underrepresented. Some studies, for example, Gasparri et al. (2010) developed predictive models by utilising an optical image obtained at one season to correlate to AGB from various seasons, while Powell et al. (2010) estimated AGB of multiple years; however, using a single Landsat for each year. Thus, these studies did not entirely explore the use of complete seasonal variation information from multi-temporal optical remote sensing images obtained at different seasons.

Satellites with a longer revisit time (i.e., Landsat) often result in limitations in collecting enough cloud-free images during the vegetation growing season. The temporal challenges cause significant uncertainties during model parameterisation and could potentially increase biomass estimation

errors. According to Zhu and Liu (2019), the benefits and shortcomings of seasonal AGB estimation from optical images obtained at different seasons require further investigation. Given this need, a knowledge gap exists regarding whether seasonally obtained optical datasets affect the accuracy of AGB estimations and whether the AGB estimations vary between vegetation types. Consequently, integration of VIs or biophysical variables (e.g., LAI) derived from sensors with better temporal coverage (Sentinel-2) can reduce these data gaps and creates an opportunity to expand the monitoring of wetland conditions and estimation of AGB in wetlands and grasslands at regional scales.

2.6.1.1.1 Optical vegetation indices and estimation of AGB

The optical remote sensing technology for biomass estimation uses the spectral characteristics of vegetation by integrating regions such as red, near-infrared (NIR) and RE into VIs for analysing the correlation between biophysical parameters and these indices (Jin et al., 2014). In general, VIs enhances vegetation photosynthetic activity by suppressing the soil, and atmospheric background noise and, in turn, improves the estimation of the AGB in wetland and grasslands (Pia et al., 2007). Due to the sensitivity of optical sensors for detecting wetland AGB, numerous VIs has been successfully used as key input variables to estimate grassland and wetland AGB in several studies (Mutanga et al., 2012; Huang et al., 2016; Michez et al., 2019; Li et al., 2021). The Normalized Difference Vegetation Index (NDVI) has proven to be a proxy of AGB of wetland vegetation in many studies, attaining accuracy ranges of between R^2 = 0.31 to 0.84 (Adam and Mutanga, 2012; Mutanga et al., 2012; Wan et al., 2018). Li et al. (2021) showed that the Green Normalized Difference Vegetation Index (GNDVI) was among the most important VIs that were integrated into a random forest model scenario to estimate AGB in palustrine wetlands and obtained an accuracy of R^2 = 0.82 and RMSE = 135.91 $g.m^{-2}$. Nuthammachot et al. (2020) also found a strong correlation (R^2 = 0.86) between the Simple Ratio index and the AGB. Other studies have also investigated the correlation between field-measured biomass and Enhanced Vegetation Index (EVI) to precisely estimate CS in vegetation at a regional scale (Yang et al., 2009; Sjöström et al., 2011).

However, the shortcomings of using VIs, such as the NDVI, is saturation in locations with dense vegetation canopy (Mutanga and Skidmore, 2004, Adam et al., 2010; Hill, 2013; Li et al., 2016). Therefore, it is vital to investigate the applicability of other additional spectral indices to improve

vegetation biomass estimation, especially in wetland ecosystems with remote satellite data. VIs derived from the NIR, narrow NIR and RE bands can yield higher accuracy of AGB estimation and contribute to alleviating the saturation problem (Mutanga and Skidmore, 2004; Ramoelo et al., 2015; Sibanda et al., 2015). A series of studies indicated a strong correlation between vegetation biomass and indices derived from the RE and NIR regions exists (Sibanda et al., 2015; Naidoo et al., 2019; Guerini et al., 2020; Li et al., 2021). Guerini et al. (2020) estimated biomass in natural grasslands using five VIs derived from the Sentinel-2 dataset, and the models for biomass estimations which incorporated the NDVIRE showed a strong relationship between grass biomass and RE bands which improved accuracies from R^2 = 0.71 to 0.73 (Guerini et al., 2020). In Michez et al. (2019), the spectral biomass model, which included the Green-Red Vegetation Index (GRVI), GNDVI, and NDVIRE, showed improved accuracy with R^2 = 0.35 compared to Unmanned aerial systems (UASs) sward height biomass model (R^2 = 0.23) when mapping and monitoring biomass in pastures.

LAI is one of the most vital vegetation properties used to quantify the exchange of energy, carbon and water between vegetation and the atmosphere (Darvishzadeh et al., 2019). LAI defines the number of single-sided leaves per square metre of soil (Liang et al., 2015). LAI of vegetation quantifies the plant canopy and gives more details on how much vegetation there is, delineating all the active photosynthetic areas (Kamenova and Dimitrov, 2021). Furthermore, LAI is included as an input in AGB models as a vegetation parameter because it is considered a strong proxy for biomass. Dong et al. (2020) estimated the dry AGB of six crops using LAI derived from Landsat 8 and Sentinel-2 datasets. The results of the study suggested that crop biomass derived from LAI of the Sentinel-2 dataset had higher accuracies (R^2 = 0.80, RMSE = 136.7 g/m^2 and the normalized RMSE (nRMSE) = 38.3%) than from the assimilation of LAI from Landsat OLI (R^2 = 0.68, RMSE = 191.0 g/m^2, nRMSE = 53.5%). The significant contribution of LAI as an additional parameter in wetland AGB estimation models is not fully documented. The inclusion of LAI in AGB estimates could significantly improve the prediction of current and future wetland vegetation state and changes in vegetation canopy structure and thus help monitor wetland functionality and health.

2.6.1.2 Utilisation of radar data for estimating AGB in palustrine wetlands

SAR is an active sensor that transmits electromagnetic radio signals and collects information by recording backscattered signals from the target (Dabboor and Brisco, 2018). The total amount of SAR-reflected signals is influenced by polarisation, wavelength, moisture, incident angle and various land surface attributes, such as size, texture, and structure (Gallant, 2015; Sinha et al., 2015). SAR sensors mainly obtain data in horizontal (H) or vertical (V) polarisations; and can function in dual polarimetric mode (HH/HV, VH/VV or HH/VV) (i.e., Sentinel-1 and TerraSAR-X,) or in a full polarimetric mode (HH/HV/VH/VV) (i.e., RADARSAT-2 and ALOS-2). The SAR-recorded backscattering signals enable the provision of critical information on vegetation structure, including AGB, soil moisture and smooth water surfaces in wetlands depending on the sensor wavelength, incident angle and polarisation modes (Sinha et al., 2015; White et al., 2015). Sivasankar et al. (2019) estimated the AGB in a forest environment in Meghalaya and the backscatter variables HH and HV showed high accuracies with R^2 of 0.83 and 0.89, respectively while the combination of both HH and HV backscatter coefficients improved the accuracy of AGB estimation to $R^2 = 0.91$.

SAR systems emit energy at longer wavelengths than optical systems and can collect information from an object at any day or time without being affected by weather patterns (Sinha et al., 2015). Most importantly, SAR sensor wavelengths play distinct roles in wetland AGB monitoring (Guo et al., 2017; Dabboor and Brisco, 2018). For instance, the C-band and X-band have shorter wavelengths of 5.6 cm and 3.1 cm, respectively, and were found suitable for monitoring non-forested wetlands, preferably with herbaceous vegetation in Canada (Ghasemi et al., 2011). The L-band can penetrate through vegetation cover. It is more significant in monitoring forested wetlands and soil moisture because of their longer wavelength's (~24 cm) penetration ability (Lang et al., 2008). Currently, only a few L-band space-borne sensors are in operation, but access to this data is very limited because of their cost (Lang et al., 2008). The other limitation of the L-band such as the ALOS PALSAR/ALOS-2 sensor is that only a single mosaic image is made available yearly and free which limits seasonal studies. Also, most SAR sensors (i.e., TerraSAR-X and RADARSAT-2) have limited surface coverage (15 to 80 km), short life expectancy, longer revisit time of 11 to 46 days, very expensive and are not freely available for the public (Chen et al., 2020). Therefore, these sensors are less suitable for regional to global monitoring and reporting to global targets.

In 2014, ESA introduced Sentinel-1, which operates as a constellation of Sentinel-1A and Sentinel-1B and is the second most recent SAR sensor functioning with a C-band wavelength configuration (the first being Radarsat) (Torres et al., 2012; Filipponi, 2019). Sentinel-1A mission acquires data at different polarisations backscatter channels, for example, Vertical-Horizontal (VH), Vertical-Vertical (VV) and Horizontal-Horizontal (HH). This mission has a shorter revisit time of 6 to 12 days at the equator and a wide swath of approximately 250 km (Filipponi, 2019). Free and open access to C-band SAR data from the Sentinel-1 platform has allowed the application of temporal information from SAR data to efficiently map and monitor wetlands over larger spatial extents (Torres et al., 2012; Nuthammachot et al., 2020). Apart from being freely available, Sentinel-1 C-band wavelength is more suited to wetland herbaceous AGB estimation due to the low AGB ranges (i.e low risk of signal saturation) compared to forested AGB ranges and the ability to penetrate clouds. For this reason, Sentinel-1 SAR data can be used to monitor wetland vegetation biomass at a relatively higher temporal resolution during optimal periods (Ghasemi et al., 2011).

2.6.1.3 Estimation of wetland AGB using SAR image texture measurements

Image texture (Haralick et al., 1973) is a significant parameter that can be used to find features and a point of interest by increasing differentiation of spatial information independently of tone, horizontal structure, and relativity of grey values in an image (Kuplich et al., 2005; Kelsey and Neff, 2014). Texture measurements have the potential to explain how pixels are spatially correlated and to describe how vegetation structure varies, and this improves the estimation of AGB (Kelsey and Neff, 2014; Dube and Mutanga, 2015). Furthermore, texture variables are derived from both optical and radar images. The most basic image texture analysis methods are statistical methods which effectively describe texture based on analysing the distribution of grey levels in images. Examples of texture algorithms include sum and difference histograms (SADH), GLCMs, autocorrelation function (ACF) and local binary pattern (LBP) (Lu and Batistella, 2005). GLCMs textures are the most well-known and efficient statistical methods with strong texture analysis robustness (Argamosa et al., 2018). The computation of GLCMs also involves selecting essential factors such as window size or the number of image pixels considered in the analysis (Li et al., 2021).

Most studies that have applied texture measurements in biomass estimation have focused more on forest biomass using optical images (Kuplich et al., 2005; Kelsey and Neff, 2014; Dube and Mutanga, 2015). Other studies that have employed texture analysis in the estimation of AGB using SAR data concentrated more on the estimation of AGB in forest ecosystems (Kuplich et al., 2005; Sarker et al., 2011; Cutler et al., 2012). Less attention has been given to the application of textures in wetland AGB estimation (Li et al., 2021). SAR-derived textures can optimise the discrimination of spatial information in vegetation independently of tone (i.e., backscatter), increasing the saturation level and maximising the range of biomass estimated with SAR data (Kuplich et al., 2005). Sibanda et al. (2017) investigated the capability of using texture metrics from WorldView-3 images to estimate AGB of vegetation such as *Eragrostis plana, Heteropogon contortus, Panicum maximum, Setaria nigrirostrosis, Themeda triandra,* and *Tristachya leucothrix* within the Grassland biome in South Africa. This region was characterised by a subtropical climate of hot summers and cold winters. The outcomes of the study showed that textures enhanced the estimation of grass AGB and improved accuracy from an RMSE of 0.83 kg/m^2 to an RMSE of 0.35 kg/m^2. Furthermore, the study also indicated that using the combination of texture models and RE derivatives improved estimation accuracy to an RMSE of 0.2 kg/m^2.

Argamosa et al. (2018) derived texture derivatives from Sentinel-1 data to model AGB in mangrove forests, and their results showed high model accuracy with an R^2 = 0.79 and an RMSE = 0.44 Mg. The study proposed that the C-band of Sentinel-1 may be used to generate adequate AGB models, and therefore more studies on C-band texture are still lacking (Argamosa et al., 2018). There are no studies that have applied SAR textural features for estimating the AGB of palustrine wetland vegetation. However, although Rajngewerc et al. (2022) investigated the classification of wetland vegetation cover maps, multi-temporal C-band Sentinel-1 data GLCMs textures illustrated better classifications with summer attaining improved kappa values between 9% and 22% while the datasets for winter yielded improvements of up to 15%. Rajngewerc et al. (2022) highlighted that textures could offer supplementary information, particularly in dates and locations with high biomass, and winter was one of the most informative seasons in their findings. Mishra et al. (2019) demonstrated that combining SAR and GLCM texture features could significantly improve the classification of heterogeneous landscapes. Comparatively with the findings of Mishra et al. (2019)

and Rajngewerc et al. (2022), it can be pointed out that multi-temporal SAR texture measurements exhibit variations according to the phenological state of vegetation. Therefore, SAR textural features may provide information that improves multi-temporal backscatter AGB estimates in wetlands characterised by heterogeneous vegetation, such as palustrine wetlands.

2.6.1.4 Contribution of LiDAR data in estimating AGB of palustrine wetlands

LiDAR is a remote sensing system that uses a pulsed laser to obtain the distance between an object and the sensor (Rapinel et al., 2015). The sensor can produce topographical information about the earth's surface and a 3D representation of vegetation structure in both woody and herbaceous vegetation (Guo et al., 2017; Luo et al., 2017). For example, Fatoyinbo et al. (2018) the authors estimated wetland AGB using an airborne LiDAR dataset and attained an R^2 of 0.88 and an RMSE of 33%. Riegel et al. (2013) estimated carbon stocks of the AGB within Coastal Plain Wetland characterised by numerous vegetation types (i.e*., Baccharis halimifolia, Persea borbonia, Rhus copallinum, Salix nigra* and *Taxodium distichum*) using LiDAR. The study achieved R^2 values of 0.34 and 0.18 with RMSE of 0.14 Mg C/ha and 0.17 Mg C/ha, respectively (Riegel et al., 2013). Other studies have also successfully used LiDAR for estimating wetland biomass (Luo et al., 2017; de Almeida et al., 2019).

LiDAR data had higher estimation accuracy of R^2 = 0.59, RMSE = 180.22 g/m^2 and relRMSE = 22.26% compared to the hyperspectral data accuracy of R^2 = 0.48, RMSE = 200.98 g/m^2 and relRMSE = 24.84% for estimation of AGB in a wetland (Luo et al., 2017). However, the combined datasets achieved greater accuracies of R^2 = 0.65, RMSE = 167.55 g/m^2 and low relRMSE = 20.71% (Luo et al., 2017). Another study that combined LiDAR and hyperspectral data for estimating AGB in the Brazilian Amazon using different regression models showed higher accuracies of LiDAR with R^2 = 0.58, RMSE = 67.6 Mg. ha^{-1}, relRMSE% = 36%, while hyperspectral achieved R^2 = 0.58, RMSE = 68.1 Mg. ha^{-1}, relRMSE% = 36%, and both datasets had a more accurate AGB estimate of R^2 = 0.70, RMSE = 57.7 Mg. ha^{-1}, relRMSE% = 31% (de Almeida et al., 2019). LiDAR data has shown great capabilities for estimating biomass in forests, wetlands and grazing lands, with more application being focused or predominant in forest AGB estimation (Li et al., 2021). Despite the high

spatial resolution of LiDAR, it is expensive to acquire data using this type of sensor, suggesting its limited application in monitoring spatial and temporal changes in wetlands environments.

2.6.1.5 Combination of optical, radar and ancillary data improve the estimation of AGB of palustrine wetlands

Integration of SAR data and optical remotely sensed data provides an enhanced and reliable way to estimate the physical characteristics of wetland vegetation, including the AGB values, which can be quantified (Nuthammachot et al., 2019). For example, SAR backscatter signals can penetrate through vegetation structures (Naidoo et al., 2016; 2019) while optical generated VI and the RE bands enhanced the AGB estimates of wetland and terrestrial vegetation, reducing the saturation problem of certain VIs in higher AGB and dense canopies (Mutanga et al., 2012; Ramoelo et al., 2015; Sibanda et al., 2017). A complex nature characterises wetlands in terms of spatial and temporal distribution, requiring accurate and reliable techniques such as image fusion of remote sensing data. Backscatter, spectral reflectance, and derivatives (VIs and biophysical parameters) could improve the estimation of wetland vegetation AGB (Naidoo et al., 2019; Nuthammachot et al., 2020; David et al., 2022; Zhao et al., 2022).

Zhao et al. (2022) mapped the AGB of *Phragmites australis*, a wetland plant community in the Momoge wetland, using a combination of Sentinel-1 and Sentinel-2 images. The study posited that incorporating Sentinel-1 backscatter and 2 RE bands and radar features attained high accuracy of 89.13% when mapping *Phragmites australis* AGB. Although David et al. (2022) estimated AGB of dryland forests in Southern Africa, their study demonstrated that combining Sentinel-1and Sentinel-2 imagery increased accuracy, obtaining R^2 between 0.82 and 0.95 and RMSE of 0.45 Mg/ha and 0.25 Mg/ha. The integration of Sentinel-1 and Sentinel-2 for estimating the AGB was investigated by Nuthammachot et al. (2019). The results indicated that synergistic use of the two sensors improved accuracy to R^2= 0.84 compared to individual sensors with Sentinel-1 and 2 attaining R^2 of 0.34 and 0.82, respectively. Thus, the integration of both sensors can provide additional information that neither SAR nor optical data contains for sustainable monitoring of wetlands (Gosselin et al., 2014). In Addition, the synergistic use of remote sensing images obtained at different times or seasons holds great potential in attaining accurate mapping of wetlands and estimation of wetland

AGB compared to the evaluation done using single-date remote sensing images (Sinha et al., 2015; Mahdavi et al., 2017).

2.7 Remote sensing-based modelling techniques for estimating herbaceous AGB of wetlands.

This section gives a literature review on the remote sensing-based modelling techniques for estimating herbaceous AGB of wetlands. These techniques are categorised into biophysical-radiometric and empirical methods. The empirical techniques are further sub-divided into parametric and non-parametric algorithms. The following subsection (subsection 2.7.1) first provide a review on the types of biophysical methods and how they are used to estimate vegetation properties such AGB. Furthermore, the section will provide a review on the different types of empirical methods in subsection 2.7.2 and how they are incorporated with remote sensing data in order to improve the prediction of AGB in wetland.

2.7.1 Biophysical radiometric data-driven techniques

The literature has illustrated that biophysical-radiometric methods have used radiative transfer models (RTMs) to derive vegetation properties using physical principles (Verrelst et al., 2015). RTMs rely on sensor spectral and backscatter reflectance from the earth's surface (Darvishzadeh et al., 2008). The spectral reflectance attributes of vegetation provide vital information (as input variables) for physical-radiometric modelling (Jin et al., 2018). RTMs can accurately predict vegetation bio-geophysical parameters and canopy reflection (Darvishzadeh et al., 2008). However, extraction of vegetation parameters such as the LAI using biophysical-radiometric models is complex and not straightforward. As a result, LAI is calculated from canopy reflectance through the inversion of a model (Verrelst et al., 2015). The inversion technique determines a set of canopy biophysical factors from a set of spectral band reflectance so that the computed reflectance best match the remote sensing reflectance (Quan et al., 2017).

Various studies have applied RTMs, such as the PROSAIL model, which is an integration of both the PROSPECT model and SAIL model (Berger et al., 2018) in optical data to extract vegetation properties like LAI in grasslands (Darvishzadeh et al., 2008; Atzberger and Richter, 2012; Darvishzadeh et al., 2019; Schwieder et al., 2020). Also, RTMs have previously been used to retrieve and predict AGB in grasslands attaining accuracies of between $R^2 = 0.64$ and RMSE = 42.67 gm^{-2} and

R^2 = 0.48 and RMSE = 41.65 gm^{-2} (Quan et al., 2017). The application of RTM in wetland macrophytes and in extraction of vegetation biophysical parameter has been understudied due ill-posed nature of physical-radiometric techniques (Kganyago et al., 2021), limitations to correction of water column effect and complex parameterisation of RTMs for inland water application (Rowan et al., 2021; Kravitz et al., 2021). RTM-based methods (i.e., PROSAIL models) are used because of their feasibility, accuracy, and robustness in short or non-woody vegetation (Darvishzadeh et al., 2008; Berger et al., 2018). Another RTM approach includes the Water Cloud Model (WCM), commonly used in parametric models to explain the backscattered signal from the vegetation canopy in terms of scattering mechanisms (Attema and Ulaby, 1978). The WCM has been extensively used in numerous studies for woody forested AGB and stems volume retrieval (Svoray and Shoshany, 2002; Behera et al., 2016; Santoro et al., 2021). Interestingly, WCM has been modified to an extended water cloud model (EWCM) that demonstrated less reliance on field data to retrieve model parameters (Kumar et al., 2019). However, biophysical-radiometric approaches are characterised by complex data structures and may require intensive computation, for estimating vegetation properties, parameterisation and collecting reflectance or backscatter information and settings (i.e., incidence angle) in the field at the time of image acquisitions.

2.7.2 Empirical-statistical modelling techniques

The empirical approaches are statistical algorithms that employ predictor variables derived from remote sensing images and field-measured data to estimate AGB. For instance, these remote sensing predictor variables include VIs, spectral reflectance bands, and texture variables (Hall et al., 1997; Darvishzadeh et al., 2011). These algorithms allow for the detection of the most relevant remote sensing predictor variables to model AGB by correlating these variables with the field-observed grassland AGB (Chen et al., 2009; Jin et al., 2014). The empirical algorithms for estimating AGB with remote sensing are categorised as parametric and non-parametric (Verrelst et al., 2015). The following subsections discuss these empirical-statistical algorithms in more detail.

2.7.2.1 Parametric algorithms

Parametric algorithms are defined as methods that use distributional assumptions because they estimate the parameters of the distribution postulated for the data (Altman and Bland, 2009).

Stepwise Multiple linear regression (SMLR) and simple linear regression are an example of parametric methods that have been used to investigate the relationship between biomass and remotely sensed predictor variables (Grant et al., 2013; Rigge et al., 2013). Parametric algorithms are very easy to compute and have the ability produce satisfactory results in the estimation of vegetation biophysical parameters (Verrelst et al., 2015). However, parametric models tend to have difficulty in analysing high dimensionality and non-linear relationships of complex data between remote sensing variables and AGB (Verrelst et al., 2015; Lu et al., 2016). Chen et al. (2009) used the partial least regression algorithm to estimate AGB in grasslands of high vegetation cover with hyperspectral data and NDVI and attained accuracies between R^2 = 0.26 and 0.27. Mutanga et al. (2012) attained obtained an error of prediction of 0.5465 kg/m^2 when predicting the AGB of wetland vegetation with SLMR. The parametric methods are associated with model overfitting and yield lower accuracies when the sample size is small (Chen et al., 2009). Therefore, to improve the accuracy of modelling AGB in grasslands and wetlands advanced and more robust algorithms need to be implemented.

2.7.2.2 Non-parametric algorithms

Non-parametric methods are not based on the normal distributional assumptions of the data (Altman and Bland, 2009). These models have the advantage of being able to solve complicated non-linear patterns (Wan et al., 2018). Considering this, several efficient non-parametric machine-learning algorithms have become dominant for biomass estimation in wetlands and grasslands (Mutanga et al., 2012; Wan et al., 2018; Yang et al., 2018; Naidoo et al., 2019). Machine learning techniques such as ANNs, RF and SVM are part of non-parametric techniques that can be integrated with satellite data to estimate accurate AGB (Lu et al., 2016; Wan et al., 2018). Integrating non-parametric methods and satellite data help understand the complex relationship among spectral features and predict easily understood, interpreted, and visualised patterns.

For instance, Mutanga et al. (2012) showed that RF obtained reasonable estimation accuracies of 0.441 RMSEP within high-density AGB in wetland vegetation composed of *Cyperus papyrus L., Echinochloa pyramidalis, Phragmites australis* and *Thelypteris interrupta.* Wan et al. (2018) used SVM as regression method for modelling wetland AGB dominated by vegetation such as *Carex*

cinerascen, Miscanthus sacchariflorus and *Phalaris arundinacea.* According to their study, the SVM obtained a lowest error with a RMSE of 0.27 compared to simple linear regression method (RMSE = 0.31) and ANN (RMSE = 0.29) . However, the RF model was the overall best performing machine learning algorithm with an RMSE of 0.25 (Wan et al., 2018). Although non-parametric algorithms have shown significant results, they come with some drawbacks. Researchers have pointed out that the computation of algorithms such as the SVM and ANN are time-consuming and require considerable training data and extensive customisation compared to traditional parametric approaches (Mas and Flores, 2008). Also, the accuracy of the estimated AGB may be lower if the model hyper-parameters used are not adequately tuned (Mas and Flores, 2008). In addition, ANNs are complicated algorithms not easily interpretable by humans as they may not reveal the internal mechanism of the link between the dependent variables and the selected independent variables (Mas and Flores, 2008; Lu et al., 2014; Verrelst et al., 2015).

When compared to parametric methods, ML methods are unaffected by the normal distribution of data and are usable for large datasets from various sources (Barrett et al., 2014). For instance, Xie et al. (2009) conducted a comparative study and used Landsat data and spectral bands as input features to estimate grassland AGB using non-parametric ANNs and parametric MLR. According to their outcomes, ANN models produced an accuracy of $R^2 = 0.82$ compared to MLR models with $R^2 = 0.59$. Li et al. (2021) investigated the capability of spectral and texture features derived from the Sentinel-2 for modelling wetland grass AGB in Shengjin Lake using the RF algorithm. The results indicated that the RF models had a robust and efficient performance with RMSE of 126.57 $g \cdot m^2$ and R^2 of 0.84. Furthermore, the RF technique has also proven insensitive to noise and has produced satisfying results in several studies (Adam and Mutanga, 2012; Wan et al., 2018). Thus, non-parametric algorithms show great potential in accurately estimating herbaceous AGB in wetlands because they are very robust to missing values and model overfitting due to built-in variable importance criteria and bootstrapping, such as in the case of the RF algorithm. The variable importance criteria allows for selection of the predictor variable that yield to significantly higher and accurate predictions. The parametric algorithms have obtained less accuracies, like RMSEP of 0.55 kg/m^2, compared to the prediction of 0.44 kg/m^2 RF for grassland AGB estimation (Mutanga et al., 2012).

2.8 Conclusion

Chapter 2 presented the important overview of wetlands in the biodiversity and ecosystems. This include its essential role to the carbon sequestration process among other categories. Also carbon quantification arise in the vegetation biomass predictions. There are numerous methods that exist for biomass estimation in wetlands. However, the unprecedented and non-destructive remote sensing tools are ideal for large scale monitoring and assessments of wetland AGB. Therefore, integrating satellite data with RTMs, parametric and non-parametric algorithms have been successfully used for estimating AGB of wetlands. Hence, the following chapter provides the detailed information about the nature of the study area, datasets and methodological framework utilised for investigating research gaps associated with wetlands AGB in the current study.

CHAPTER 3: DATA AND METHODS

This chapter provide a general description of the selected study area and provides insights on why the area of interest was chosen. Secondly, the chapter gives a description of how the field data and the remote sensing data was collected and used to estimate terrestrial and wetland carbon from the AGB of palustrine wetland across the summer and winter seasons within the study area. Chapter 3 describes the machine learning methods that were used for the estimation of the wetland vegetation AGB, how the models were developed and validated, and how the developed models were employed for mapping the teal carbon across the investigated seasons within the study area. Therefore, the primary aim of this chapter is to provide a detailed explanation on the methodological approach in which this research project was conducted in this study.

3.1 General description of the study area

Section 3.1 provides the information and description of the study area site. The section describe the geographic setting of the study area, the type of vegetation that is found within the study site and the climatic conditions of the area. Furthermore, a map which shows the location of the study area in the catchment and within the Grassland Biome of South Africa is provided in this section.

3.1.1 Location and setting of the Tevredenpan study area

This study was conducted in Tevredenpan study area (26.2°S; 30.2°E) in the Grassland Biome of the Mpumalanga Province in South Africa (Figure 1: A). Tevredenpan site is found in the northern part of the Mpumalanga Lakes District (MLD) in the quaternary catchment W55A (Figure 1: B) (Van Deventer, 2020). The total extent of the W55A catchment is approximately 68 870 ha. The area experiences temperate weather with cold winters and warm summers, with mean annual rainfall of 600 to 800 mm (Middleton and Bailey, 2008) and a yearly mean annual evaporation of approximately 1 600 –1 800 mm (Schulze, 1997). The elevation of the study area is between 1700 - 1820 m above sea level and the geology is predominantly composed of Vryheid formation which is comparatively flat with coal mining taking place in the area. The MLD has wide range of different wetland types, including 416 depressions, a number of valley bottom and seeps wetlands (Van Deventer et al., 2020; 2022). Two river systems, the Mpuluzi River and Pearl stream, which are

situated in the north and south of the research area, respectively, are fed by wetlands in the MLD area (Naidoo et al., 2019).

The seeps wetlands and valley bottom wetlands found on hillslopes areas in the study area are temporary and seasonally saturated due to seasonal changes (Naidoo et al., 2019; Van Deventer et al., 2020). The western part of the study area consists of the largest depression (called Tevredenpan) (Figure 1: C) which contains a floating peat cap that supports wetland grass growth (Grundling et al., 2003). The accumulation or the presence of peat aids in regulating climate change by sequestering atmospheric carbon and storing it in vegetation and soils (McLaughlin and Packalen, 2021). In addition, it shows strong seasonality between summer and the winter seasons, making this part of the catchment a good case study for assessing teal carbon changes in palustrine wetlands. Moreover, serious threats posed by extensive agricultural activities such crop production, open cast coal mining applications, and cattle grazing have predominantly put wetlands in the area under pressure (Burgoyne et al., 2000; McCarthy et al., 2007; Fourie et al., 2015).

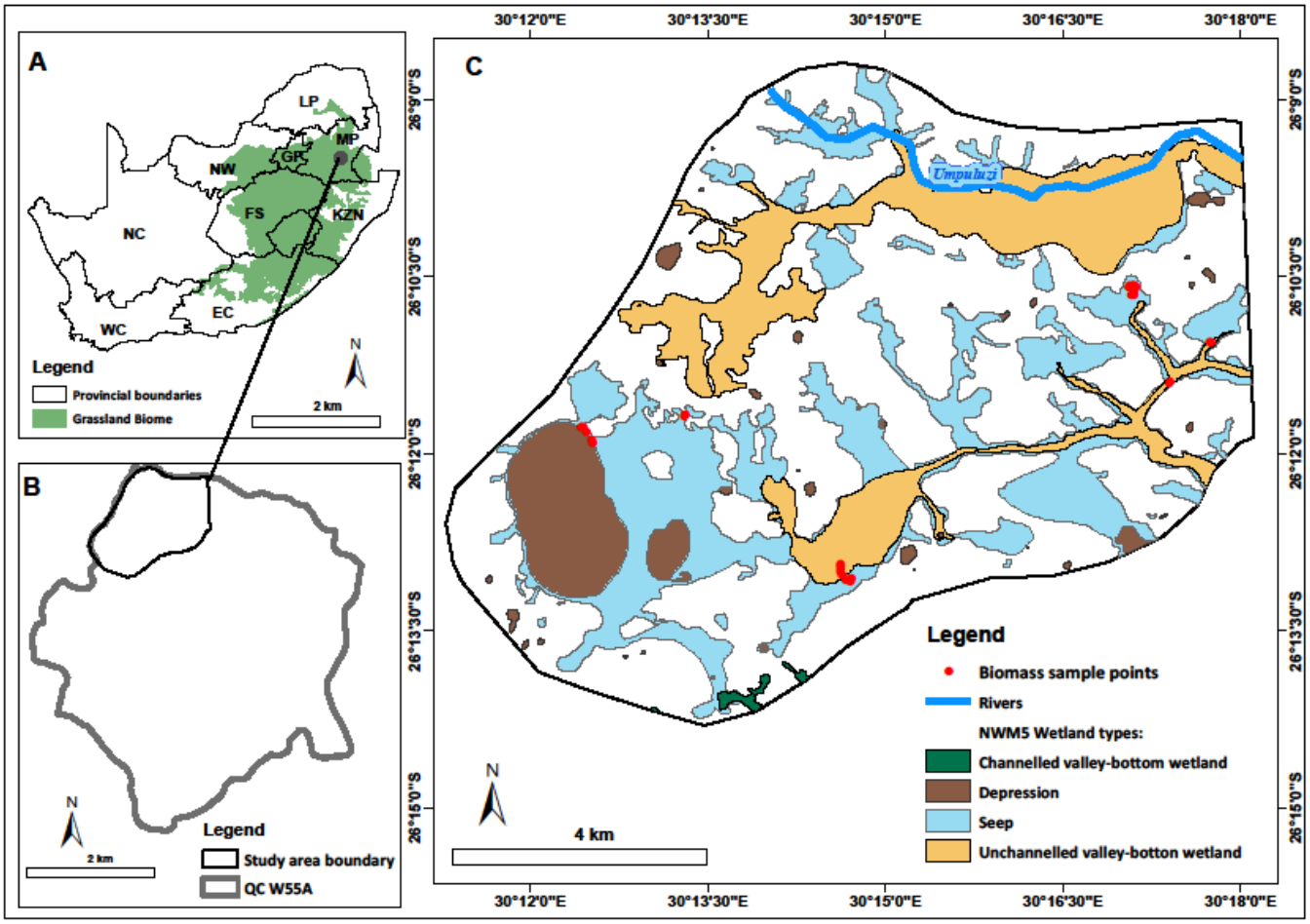

Figure 1: The map of the study area, indicating (**A**) extent of the Grassland Biome, within the Provinces of South Africa and location of study area in the Mpumalanga province; (**B)** the location of the study area in the northern part of the quaternary catchment (QC) W55A, considered the Mpumalanga Lakes District (MLD) of South Africa; and a map (**C**) showing the wetland types from the National Wetland Map version 5 (NWM5) and field sampling points of the Tevredenpan study area.

3.1.2 Vegetation communities in Tevredenpan study area

The vegetation type in the MLD catchment is described as the 'Eastern Highveld Grassland Biome' and is considered 'hardly protected' (Mucina and Rutherford, 2006). Wetlands in the catchment consists or are dominated by a diverse range of sedge and grass species (Sieben et al., 2014; Linström, 2015). The valley bottom wetlands within the area consists of prevalent patches of vegetation communities such as the *Carex acutiformis, Phragmites australis* and *Typha capensis*

(Naidoo et al., 2019; Van Deventer et al., 2022). The dense growth of *Phragmites australis* as well as floating microphytes are also predominant in Tevredenpan depression which is the largest depression in the study area (Grundling et al., 2003). Furthermore, the landscape of the Tevredenpan study area is characterised by nine dominant vegetation communities, eight are found in the wetland areas and one community within the terrestrial area (Table 1; Van Deventer et al., 2022).

Table 1: Wetland vegetation communities observed in the Tevredenpan study area

Wetland vegetation communities	**Location**
Aristida spp. (>50%)	Wetland
Arundinella nepalensis (>50%)	Wetland
Carex spp. (>70%)	Wetland
Eragrostis plana and Themeda triandra	Terrestrial
Grass-sedge communities	Wetland
Juncus effusus (>50%)	Wetland
Phragmites australis	Wetland
Sedge dominant (>20%)	Wetland
Wet-grass communities	Wetland

3.2 Methodological Framework

This section provides a flowchart (Figure 4) that summarises the methodological steps and processes that were conducted and implemented for achieving the research questions, aim, and objectives of this study. The framework involves remote sensing image acquisition, pre-processing of seasonal images and analyses. The implemented framework uses the integration of remote sensing imagery from two different seasons and field-measured biophysical parameters such as LAI into machine learning algorithms to develop season-specific models of AGB of wetlands. Chapter 3 describes in detail all the modelling procedures involved and summarised in this framework. The framework summarises all the steps conducted from section 3.3 to section 3.9

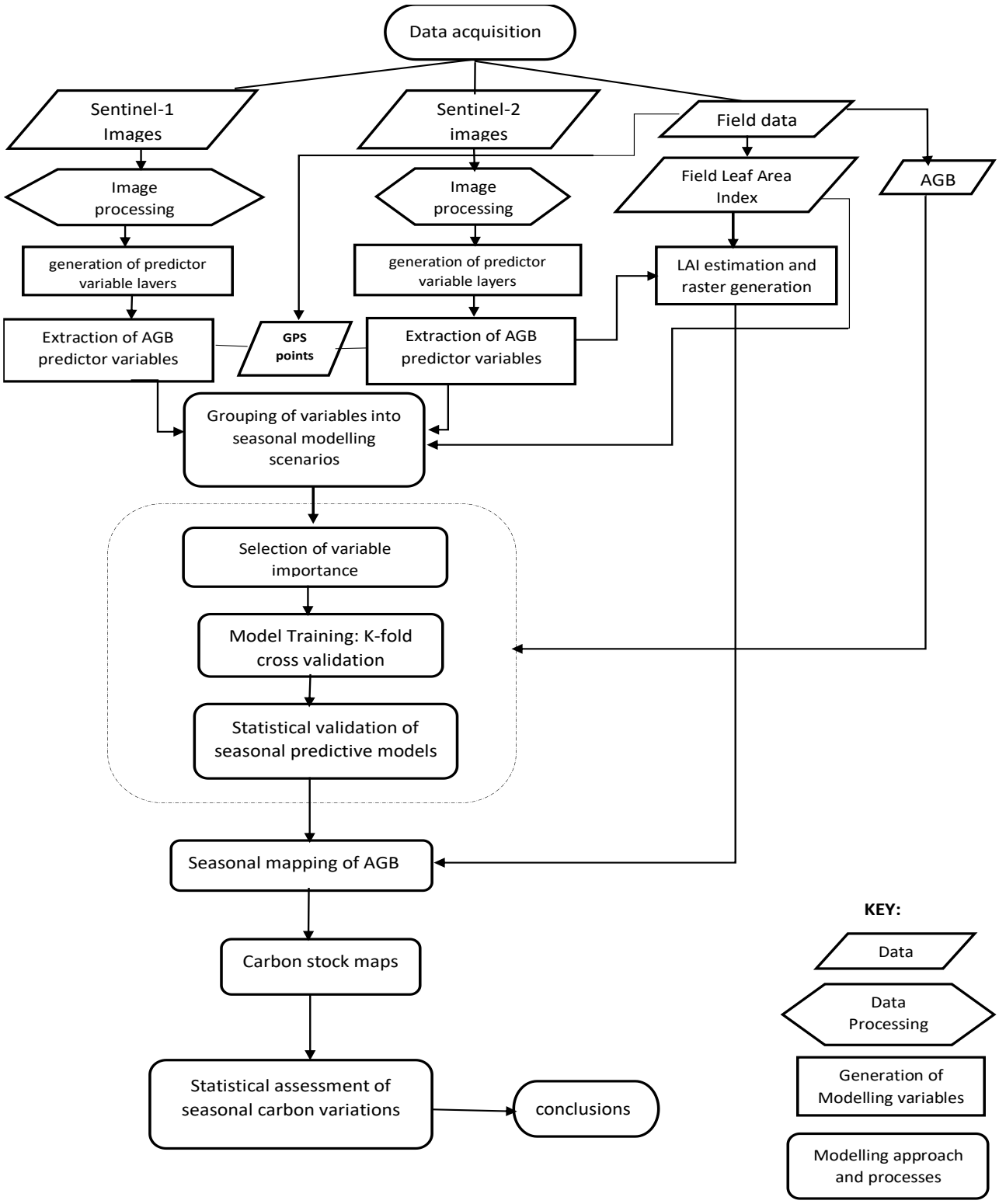

Figure 2: The methodological framework for estimation and assessment of carbon stock from the AGB of palustrine wetland vegetation in Tevredanpan study area between summer and winter seasons of 2017.

3.3 Data collection and Pre-processing methods

This section provide information about the field data sampling techniques, how the field data was collected including dates on when the sampling of the AGB and LAI took place. Furthermore, section 3.3 also provide information on the acquisition of remote sensing datasets that were used for estimating seasonal AGB. The characteristics and description of the remote sensing data used is also provide in this section.

3.3.1 Field data

3.3.1.1 Herbaceous AGB sampling

Field sampling took place across the summer and winter seasons of 2017 in the Tevredenpan study area. The summer visits were made in between 27 February 2017 and 2 March 2017 (Figure 2: A) and in winter they were made between 27 August 2017 and 1 September 2017 (Figure 2: B). The 2017 primary field data for the MLD was acquired by the Council for Scientific and Industrial Research (CSIR) (Naidoo et al., 2019; Van Deventer et al., 2020). Stratified random sampling method was implemented for the collection of AGB. The location of the sample plots was chosen based on homogeneity, dominant vegetation community as well as grass traits such as the canopy cover, community composition and height. A total of 32 wet herbaceous AGB of wetland vegetation samples were harvested for each season and from the collected samples, 26 samples were collected in the wetland sections and six samples from the terrestrial section. The collected samples contained the herbaceous grass AGB of wetland vegetation.

Sample plots of 6 m × 6 m were selected for sampling in both the summer and winter. In order to cover the representative range of variation in the AGB within each plot, three 0.5 m × 0.5 m quadrants were randomly positioned inside each plot of size 6 m × 6 m and the above ground vegetation within the quadrat was clipped. A Differential Global Positioning System (DGPS) (Trimble GEO 7X) with a horizontal error less than 50 cm was utilised to record the co-ordinates of the centre point of each plot for the summer season. During the winter sampling campaign, the Garmin 62s GPS was used again to locate the centre points of the sampling plots. The harvested AGB was later weighed, recorded, and the mean value was calculated for the three quadrants to get the average AGB for the entire plot. The AGB is a dry weight measure, thus the values of dry herbaceous AGB

per plot were then derived by drying the wet herbaceous AGB for 48 hours at a temperature of 80°C until the weight stabilised using an oven (Naidoo et al., 2019).

A **B**

Figure 3: Collection of the AGB of wetland vegetation in the Tevredenpan study area, indicating photographs of: (**A**) summer sampling and (**B**) winter sampling campaign.

3.3.1.2 *Leaf Area Index sampling*

To improve the AGB estimation accuracy, LAI was included as an additional input variable for estimating wetland AGB. The collection of the LAI values also took place in summer and winter during AGB sampling. The LAI Plant canopy Analyser (LiCOR LAI-2200C) was used to obtain observed LAI field values within the three 0.5 m × 0.5 m quadrant sub-plots prior to AGB harvesting (Figure 3: B). The LiCOR LAI-2200C measures the LAI from the vegetation canopy using the incoming light from the sun, hence objects (i.e human shadow) that could affect the analyser's optical sensor were avoided during LAI measurements in the field. To obtain the LAI values, the quadrant was randomly placed within the 6 m × 6 m plots in three locations and one measurement of the LAI was computed per quadrant the, one reading above the canopy and two measurements below vegetation canopy (Figure 3: A). The mean LAI value was calculated to represent an individual 0.5 m × 0.5 m quadrant. The final LAI value at each plot was the average of all the three 0.5 m × 0.5 m quadrants. The LAI measurements for the all the summer and winter points were recorded. LAI measurements were taken in the same plots and subplots as the AGB measurements prior to harvesting of AGB. Additionally, the LAI measurements were taken on a sunny day with a 25% sensor cap shroud to

avoid sensor saturation. Acquisition time was between 9am and 3pm to maximise exposure to the sun and the acquisition orientation was towards the sun to avoid the shadow effects.

A

B

Figure 4: Leaf Area Index collection, **(A)** recording of LAI values inside the quadrant, **(B)** depicts the quadrant and the LAI plant canopy analyser.

3.3.2 Remote sensing data acquisition

3.3.2.1 Acquisition of Sentinel radar images

The Sentinel-1 mission is a radar system that consists of two SAR satellite instruments (Sentinel-1A and 1B) that are operating at the C-band wavelength (5.405 GHz), allowing for the acquisition of imagery regardless of weather and illumination conditions (Torres et al., 2012). The bands of Sentinel-1 backscatter are made up of different polarisation signals that can be transferred to and retrieved from the targeted object (e.g., VV and VH). Sentinel-1 mission provide images every six to 12 days and have a large coverage of the land at about 250 km (Torres et al., 2012; Filipponi, 2019). With its active phased array antenna, the Sentinel-1 sensor obtain images at four distinct imaging modes with varying coverage and resolutions (Geudtner and Torres, 2012). For this study, high resolution Sentinel-1A Ground Range Detected (GRD) images for both winter and summer season were downloaded from the Alaska Satellite Facility website (https://search.asf.alaska.edu/#/). GRD products are composed of detected, multi-looked and projected to ground range SAR data using the WGS84 projection. The seasonal images were downloaded in an Interferometric Wide Swath (IW)

imaging mode which is an operational mode over land and has a pixel spacing of 10 m × 10 m. Additionally the images were acquired by taking into consideration the field sampling date (closest to the sampling dates) (Table 2).

Table 2: Sentinel-1A sensor specifications including image IDs and acquisition dates of the seasonal images

Downloaded Image IDs	Acquisition data and Season	Acquisition mode	Resolution (m)	Polarisation
S1A_IW_GRDH_1SDV_201701 25T163826_20170125T163851 _014990_0187A3_5A1F	25/01/2017 (Summer)	Interferometric Wide Swath (IW)	10 × 10	Dual: VV+VH
S1A_IW_GRDH_1SDV_201708 29T163834_20170829T163859 _018140_01E793_5489	29/08/2017 (Winter)	Interferometric Wide Swath (IW)	10 × 10	Dual: VV+VH

3.3.2.2 Sentinel-1A Pre-processing

Images of Sentinel-1A were pre-processed using the Sentinel Application Platform (SNAP) software version 8.0 developed by ESA (Zuhlke et al., 2015; SNAP Development Team, 2016). The pre-processing of these images included (1) radiometric calibration, (2) multi-looking (3) geometric correction (i.e., terrain correction) and (4) speckle filtering. The following subsections describe each of these steps in more detail.

3.3.2.2.1 Radiometric calibration of the radar images

Radiometric calibration is a method that is used for converting digital numbers (DN) to radiometrically calibrated or normalised radar cross section sigma nought (Sigma0) (Filipponi, 2019;

Braun and Veci, 2021). The Sentinel-1 GRD product already has the calibration equation information included within the calibration vector in the product metadata and this enables the image pixel values to be easily converted into sigma0 (Filipponi, 2019). Sentinel-1A images were radiometrically calibrated using the Radiometric Calibration Function which is found under the Radar Menu. Under the processing parameter tab, both the polarisations (VH and VV) were selected, and the output bands were kept at default as sigma0. The SNAP software automatically identifies what type of input products is opened and what corrections ought to be performed on the product by utilising the metadata of the product as the corrections that are performed during image calibration are mission specific based on the image's metadata (Braun and Veci, 2021). The subsequent output product was then kept in the native SNAP file format (BEAM-DIMAP). Radiometric calibrating of SAR images is important for quantitative applications of SAR data as this aids in better comparison of images obtained by the same sensor or different sensors (Braun and Veci, 2021). Thus, radiometric correction was done for both the summer and winter seasonal images of Sentinel-1A.

3..2.2.2.2 Multi-looking pre-processing of the radar images

Multi-looking is an averaging process that increases SAR image quality and reduces random noise, and this can be achieved by averaging the range and/or azimuth resolutions of the pixels thus improving the radiometric resolution (Cantalloube and Nahum, 2000; Braun and Veci, 2021). The multi-look process was performed to both the summer and winter Sentinel-1A images from the Radar menu under SAR Utilities in SNAP software. Therefore, the final multi-looked output images for this study had two range looks, two azimuth and the resulted mean ground range pixel or spatial resolution was 20 m.

3.2.2.2.3 Geometric correction of the radar images

To geometrically correct or orthorectify the Sentinel-1 images for this study the Range Doppler terrain correction was used (Small and Schubert, 2008). Range Doppler terrain correction is used to mitigate distortions caused by topography, such as foreshortening and shadows (Filipponi, 2019; Kumar, 2021). There are various other geometric correction algorithms on SNAP, however Range Doppler terrain correction was selected because it is simpler and quicker to compute (Kumar, 2021).

The images were acquired with the geometry of the sensor and the image pixels did not have the correct geographical coordinates. The tool allows for finding the correct location of the pixel values using a Digital Elevation Model (DEM) and also by changing the map projection (Filipponi, 2019). Therefore, in the processing parameters dialog both bands (VH and VV) were selected and a high-resolution DEM of the Shuttle Radar Topography Mission (SRTM 3 arc second) at 30 m pixel size was selected (Argamosa et al., 2018). Furthermore, under the map projection window the Custom Reference System (CRS) is by default set to the Universal Transverse Mercator (UTM) Zone 36 South and spheroid/datum of the World Geodetic System of 1984 (WGS 84). All the other processing parameters such the DEM resampling method and the input-output (I /O) Parameters tab was left at default. The geometrically corrected output image was then saved as a raster file (GeoTiff format).

3.2.2.2.4 Speckle filtering of the radar images

Speckle filtering is a procedure to increase image quality by reducing speckle but can result in reduced detail and blurred images. A number of studies have conducted a review and compared different speckle filters (Dong et al., 2000, Touzi et al., 2002; Lee et al., 2008; Rana and Suryanarayana, 2019). The speckle removal on seasonal images of Sentinel-1 was performed on the geometrically calibrated products in SNAP using the refined Lee filter (Argamosa et al., 2018). From the Radar menu, the Single Product Speckle filter which is found under Speckle filter was selected and under the processing dialog window, the Refined Lee speckle filter was then selected. The Refined Lee filter averages the image while preserving edges. It has no parameters to set, while others require the definition of a kernel size and other parameters.

3.3.2.3 Acquisition of the Sentinel-2 optical images

The Sentinel-2A MSI is an optical sensor which collects reflectance data from 13 spectral bands ranging from the visible to the short-wave infrared (SWIR) bands (Drusch et al., 2012). The Sentinel-2 mission provides two types of products: Level-1C which represents top of the atmosphere (TOA) reflectance and Level-2A which represents Bottom of the atmosphere (BOA) reflectance. For this study, two Sentinel-2A images for the summer (wet) and winter (dry) seasons were downloaded at the Level-1C processing level because BOA products (i.e. Sentinel-2 Level-2A) were not available for

the required dates from the United States Geological Survey website (https://earthexplorer.usgs.gov/). The spatial and spectral characteristics of Sentinel-2A MSI sensor are described in in Table 3.

Table 3: Characteristics and specifications of Sentinel-2A dataset with IDs of the acquired images for the summer and winter season

Acquisition date and Season	**Image ID**	**Spatial resolution (m)**	**Spectral band ID**	**Band name**	**Bandwidth (nm)**	**Centre Wavelength (nm)**
19/01/2017 (Summer, wet)	S2A_MSIL1C_20170119T074231_ N0204_R092_T36JTS_20170119T075734	10	Band 2	Blue	66	492
		10	Band 3	Red	36	560
		10	Band 4	Green	31	665
		10	Band 8	NIR	106	833
		20	Band 5	Red edge 1	15	705
30/08/2017 (Winter, dry)	S2A_MSIL1C_20170830T074611_ N0205_R135_T36JTS_20170830T081246	20	Band 6	Red edge 2	15	741
		20	Band 7	Red edge 3	20	783
		20	Band 8A	Narrow NIR	21	865
		20	Band 11	SWIR	91	1613.7
		20	Band 12	SWIR	175	2202.4

		60	Band 1	Coastal aerosol	21	442
		60	Band 9	Water vapour	20	945
		60	Band 10	SWIR-cirrus	31	1374

3.3.2.4 Pre-processing of Sentinel-2A

The pre-processing of the selected Sentinel-2 images included (1) atmospheric correction, (2) resampling of the images and (3) spatial and spectral bands sub-setting. All the pre-processing of Sentinel-2A images was done in in SNAP software (SNAP Development Team, 2016) and the steps are discussed in the following subsections.

3.2.2.4.1 Atmospheric correction of the Sentinel-2 optical images

Atmospheric correction is a technique that is used to correct and remove atmospheric effects from raw remote sensing data in order to establish accurate surface reflectance values (Themistocleous et al., 2008). The Sentinel-2A (Level-1C) images were converted from TOA to BOA using Sen2cor (v280). From the Optical menu in SNAP, the Sen2Cor (v280) processor, found within the Thematic Land Processor module, was selected. To run the algorithm, under the Sen2Cor popup tab the input product in the I/O Parameters for Sen2Cor was the original downloaded Level-1C product, and in the Processing Parameters tab the resolution was changed to "ALL". The atmospheric correction was applied to both the summer and winter images of Sentinel-2A.

3.2.2.4.2 Resampling of the optical images

Resampling is method that is mostly used to change the spatial resolution of a satellite image by changing the size of image pixels. In SNAP's toolbar in the Raster menu, the resample module was selected in order to open the Resampling operator in the Geometric Operation tool. The process of resampling the downloaded optical images involved using the atmospherically corrected image as

an input source product in the I/O Parameters. To get high spatial resolution for more accuracy in the prediction of the AGB, under the processing parameter tab, the spectral band 2 with high spatial resolution of 10m was used a reference band to define the geometric resolution of the final product. All the spectral bands for the summer and winter images of Sentinel-2 were resampled to a 10 m spatial resolution.

3.2.2.4.3 Spatial and Spectral band subset of the optical images

The subset function under the raster menu in SNAP allows to perform both spatial and spectral resampling by excluding irrelevant data such as selecting only the region of interest (ROI) and specific bands in order to reduce the volume of data. For focused research in this study, the spatial and band subset process involved creating a box around the ROI in the spatial subset parameter and in the spectral band sub-setting parameter tab only ten bands (band 2, band 3, band 4, band 5, band 6, band 7, band 8, band 8A, band 11, and band 12) out of the 13 acquired bands of Sentinel-2A were selected for estimation of AGB (Naidoo et al., 2019; Li et al., 2021). The other three bands (bands 1, 9 and 10) were not selected for further analysis as they related to or are mostly used for water and atmospheric elements (Li et al., 2021). The final resulting products for summer and winter images were saved and exported as a raster file (GeoTiff format) for the purpose of extracting predictor variables of AGB estimation of vegetation.

3.4 Remote sensing predictor variables for estimating seasonal AGB

Optical and SAR derived variables such as VIs, band ratios, reflectance bands, backscatter polarisation variables and texture variables have indicated strong correlation with vegetation biomass (Mutanga et al., 2012; Kelsey and Neff, 2014; Sibanda et al., 2017; Naidoo et al., 2019). The following sub-sections describe (1) the generation of the predictor variable from Sentinel-1A and Sentinel-2A imagery and (2) the processes that were undertaken for extracting the predictors in order to estimate the herbaceous AGB.

3.4.1 Generation of predictor variables

3.4.1.1 Calculation of predictor variables from Sentinel-1A imagery

For this study, predictor variables (textural metrics and SAR band ratio) were calculated from Sentinel-1A imagery. Textural features represent the spatial arrangements of image colours or intensities. In this study the efficiency of textures in estimating AGB of wetland vegetation for both summer and winter was based on the GLCM measurement technique, which has strong adaptability and robustness (Haralick et al., 1973). Thus, eight GLCM textural metrics (Haralick et al., 1973) derived from Sentinel-1A imagery were employed: dissimilarity (DIS), mean (MEA), homogeneity (HOM), variance (VAR), entropy (ENT), second angular moment (SAM), contrast (CON), and correlation (COR) to differentiate textural variety (Table 4).

To compute textures, the raster menu in SNAP's toolbar was selected in order to open the GLCM operator in the Image Analysis Operation tool, and the GLCMs textures were then derived using the final pre-processed raster product of Sentinel-1A seasonal images as the source product in the I/O parameter tab. Under the Processing parameter tab eight textures metrics were computed for both the polarisations bands (VH and VV) of the Sentinel-1A image. The selection of a suitable processing window size when deriving textural features is very crucial because using a larger window size may results to loss of important texture information while a smaller processing window may result to increased noise in the image pixel due to magnified image variations (Sarker and Nichol, 2011; Kelsey and Neff, 2014). Therefore, textures metrics in this study were calculated on one processing window size (9 × 9 pixels). The selected window size has been used in previous studies and have proven to have high correlation with biomass (Sarker and Nichol, 2011; Kelsey and Neff, 2014; Argamosa et al., 2018; Li et al., 2021). The polarisation ratio was used as a variable for modelling AGB (Naidoo et al., 2019). To generate SAR band ratio raster (VH/VV) in this study, the band maths tool in SNAP software was used to find the ratio between the dual-channel C-band SAR backscatter coefficients of Sentinel-1A imagery (VV and VH). Therefore, the output products of the derived textural metrics and the band ratio for both summer and winter were saved and exported as raster files for subsequent analysis in the study.

Table 4: Description and formulas of predictor variables derived from seasonal images of Sentinel-1A imagery for modelling AGB of palustrine wetland vegetation.

Sensor	**Remote sensing predictor variables**		**Variable Formula/name**	**Bands used**	**References**
Sentinel-1A	GLCM texture variables	DIS	$\sum_{i,j=0}^{N-1} iP_{i,j}\lvert i-j\rvert$	VH, VV	(Haralick *et al.,*1973)
		CON	$\sum_{i,j=0}^{N-1} iP_{i,j}(i-j)$		
		COR	$\sum_{i,j=0}^{N-1}\left(i\left(\sum_{i,j}^{N-1} ijP_{i,j}-\mu_i\mu_i\right)/\sigma_i^2\sigma_j^2\right)$		
		ENT	$\sum_{i,j=0}^{N-1} iP_{i,j}\ln P_{i,j}$		
		HOM	$\sum_{i,j=0}^{N-1} iP_{i,j}/(1+(i-j)^2)$		
		MEA	$\sum_{i,j=0}^{N-1} iP_{i,j}$		
		SAM	$\sum_{i,j=0}^{N-1} iP_{i,j}{}^2$		
		VAR	$\sum_{i,j=0}^{N-1} P_{i,j}(1-\mu_i)$		
	Backscatter channels			VH, VV	
	SAR band ratio		B1/B2	VH/VV	(Englhart,2011)

CON: Contrast; COR: Correlation; DIS: Dissimilarity; ENT: Entropy; HOM: Homogeneity; MEA: Mean; SAM: Second Angular Moment; VAR: Variance; VH and VV: cross and co-polarisations.

3.4.1.2 Calculation of spectral metrics from Sentinel-2 imagery

The wavelengths of EMS regions (green, red, RE, and NIR) have significant impact on the accuracy of AGB in wetland and grassland vegetation (Mutanga et al., 2012; Ramoelo et al., 2015; Li et al., 2021). In this regard, VIs and spectral band ratios derived from these spectral regions has indicated a correlation with the biomass of wetland vegetation and grasslands (Cho et al., 2007; Adam et al., 2010, Mutanga et al., 2012). For this study, eight VIs which were known to correlate well with AGB estimation, were calculated from the reflectance bands of Sentinel-2A. Four were traditional VIs (GNDVI, GRVI, NDVI, and SR) and the other four VIs were RE-based VIs (NDVIre5, NDVIre6, NDVIre7, SRre5). The traditional VIs were derived from three bands (B3, B4, B8) and the RE VIs from the NIR band (B8) and three RE bands (B5, B6, B7) of Sentinel-2A using the raster calculator in Quantum GIS (QGIS) version 3.18 (QGIS development Team, 2021). Thus, for this study Sentinel-2A variable for the estimation of AGB of wetland vegetation included 10 reflectance bands and eight VIs (Table 5). The calculated output products were saved and exported as raster files for extraction of modelling dataset.

Table 5 : Description and formulas of predictor variables derived from seasonal images of Sentinel-2A imagery for modelling AGB of palustrine wetland vegetation.

Sensor	Remote sensing predictor variables		Variable Formula/name	Bands used	References
	RE VIs	NDVIre5	$\frac{(NIR - RE)}{(NIR + RE)}$	$\frac{(Band\ 8 - Band\ 5)}{(Band\ 8 + band\ 5)}$	(Gitelson and Merzlyak 1994; Fernández-Manso et al., 2016)
		NDVIre6	$\frac{(NIR - RE)}{(NIR + RE)}$	$\frac{(Band\ 8 - Band\ 6)}{(Band\ 8 + Band\ 6)}$	
		NDVIre7	$\frac{(NIR - RE)}{(NIR + RE)}$	$\frac{(Band\ 8 - Band\ 7)}{(Band\ 8 + Band\ 7)}$	

Sentinel-2A		SRre5	$\frac{(NIR)}{(RE)}$	$\frac{(Band\ 8)}{(band\ 5)}$	(Sims and Gamon, 2002)
	Traditional VIs	GRVI	$\frac{(GREEN - RED)}{(GREEN + RED)}$	$\frac{(Band\ 3 - Band\ 4)}{(Band\ 3 + Band\ 4)}$	(Tucker, 1979. Falkowski et al., 2005; Motohka et al., 2010)
		NDVI	$\frac{(NIR - RED)}{(NIR + RED)}$	$\frac{(Band\ 8 - Band\ 4)}{(Band\ 8 + Band\ 4)}$	(Rouse et al., 1973; Tucker, 1979)
		GNDVI	$\frac{(NIR - GREEN)}{(NIR\ + GREEN)}$	$\frac{(Band\ 8 - Band\ 3)}{(Bamd\ 8 + Band\ 3)}$	(Gitelson and Merzlyak, 1998)
		SR	$\frac{(NIR)}{(RED)}$	$\frac{(Band\ 8)}{(Band\ 4)}$	(Chen, 1996)
	Reflectance bands			B2, B3, B4, B5, B6, B7, B8, B8A, B11, B12	(ESA, 2015)

GNDVI: Green Normalized Difference Vegetation Index; GRVI: Green Red Vegetation Index; NDVI: Normalized Difference Vegetation Index; NDVIre5: Normalized Difference Vegetation Index Red-edge 1; NDVIre6: Normalized Difference Vegetation Index Red-edge 2; NDVIre7: Normalized Difference Vegetation Index Red-edge 3; SR: Simple Ratio; SRre5: Simple Ratio Red-edge 1; and B; Bands.

3.4.1.3 Estimation of LAI as a significant parameter for modelling herbaceous wetland AGB

In this study, Stepwise Multiple Linear Regression (SMLR) (Breaux, 1967) was used to find the optimal model for predicting the LAI for the summer and winter season within the study area. For estimating the regional LAI layer, three modelling scenarios (Table 6) derived from the combination of the selected ten spectral bands, and eight VIs of Sentinel-2 (Table 5) were implemented in RStudio (v4.0.3). The Akaike Information Criterion (AIC) through the 'stepAIC' function implemented in the 'MASS' package in RStudio (Ripley et al., 2013) was used for variable selection and the model with lower AIC value was selected for modelling of LAI. The developed models were evaluated based on k-10-fold cross-validation. A model consisting of a combination of the variables with the lowest relative root-mean-square error (relRMSE) (Appendix A, Table A1) was selected for predicting the

LAI. Thus, scenario 3 (combination of both spectral bands and VIs) was the best performing model (Appendix A, Table A1) in both summer and winter season and was the used to predict the LAI with the study area. The upscaling modelling process to derive the regional LAI in this study was done to move from plot LAI measurements to a continuous regional layer for the mapping the AGB. LAI is a well-known proxy of AGB and has shown to have significant improved biomass estimates biomass (Van Wijk and Williams, 2005; Fan et al., 2009; Masemola et al., 2016; Naidoo et al., 2019) hence it was considered as important parameter in this study.

Table 6: Modelling scenarios implemented in the Stepwise Multiple Linear Regression for predicting Leaf Area Index, numbers in the brackets represent the total number of predictor variables in each scenario

Summer	Winter
Scenario 1: Spectral bands (10)	Scenario 1: Spectral bands (10)
Scenario 2: VIs (8)	Scenario 2: VIs (8)
Scenario 3: Spectral bands (10) + VIs (8)	Scenario 3: Spectral bands (10) + VIs (8)

3.4.2 Extraction of the modelling dataset from the remote sensing predictor variables

To investigate the ability and attributes of Sentinel-1A GRD derived variables for estimating seasonal AGB, this study selected Sentinel-1A derived variables included 16 GLCMs, VH and VV backscatter channels, and VH/VV band ratio making a total of 38 input variables (19 per season including the field measured LAI). Sentinel-2 MSI predictor variables for wetland vegetation AGB estimation in both summer and winter included ten reflectance bands and eight VIs totalling up to 38 variables (18 per season including field measured LAI). The raster layers of all the predictor variables derived from both Sentinel-1A and Sentinel-2A were later imported into ArcMap version 10.4.1 (ESRI, 2016) for further analysis. The extract multi-values to point tool in ArcMap was used and under the parameter tab, the shapefile with the centre co-ordinate of the biomass field sample points was selected as the input point feature to extract pixel values of reflectance bands,

backscatter values, VIs, ratios, and textures. The pixel values were exported and saved as excel file and used as the modelling dataset for wetland vegetation AGB estimation in RStudio software.

3.5 Different modelling scenarios for estimating herbaceous AGB

To optimise the modelling of AGB of wetland vegetation, different predictor variables of both Sentinel-1A and Sentinel-2A images for summer and winter were combined into modelling scenarios. Four modelling scenarios in each season were tested in RF and SVR machine learning algorithms to predict herbaceous AGB within the selected study area. All the modelling scenarios included the LAI field measured values as an additional predictor variable. The first four scenarios included the bands only for each season, namely the Summer Sentinel-1A (SS1), Winter Sentinel-1A (WS1), Summer Sentinel-2A (SS2), and Winter Sentinel-2 (WS2). Therefore, the following modelling scenarios (Table 7) were implemented in each season for the estimation of AGB using the algorithms explained in the below section (3.5).

Table 7: Modelling scenarios implemented in summer and winter seasons for estimating herbaceous AGB (all scenarios included LAI); Numbers in the brackets indicates total predictor variables.

Scenario (down) and Sensor (across)	**Sentinel-1A modelling scenarios**		**Sentinel-2A modelling scenarios**	
Seasons:	**Summer**	**Winter**	**Summer**	**Winter**
Scenario 1	GLCMs only (16) + LAI	GLCMs only (16) + LAI	Reflectance bands (10) +LAI	Reflectance bands (10) +LAI
Scenario 2:	Band ratio (1) + Backscatter (2) + LAI	Band ratio (1) + Backscatter (2) + LAI	Traditional VIs (4) +LAI	Traditional VIs (4) +LAI
Scenario 3:	Backscatter (2) + GLCMs only (16) + LAI	Backscatter (2) + GLCMs only (16) + LAI	RE indices (4) +LAI	RE indices (4) +LAI

Scenario 4:	Backscatter (2) + band ratio (1) + GLCMs (16) + LAI	Backscatter (2) + band ratio (1) + GLCMs (16) + LAI	Reflectance bands (10) + RE indices (4) + Traditional VIs (4) +LAI	Reflectance bands (10) + RE indices (4) + Traditional VIs (4) +LAI

3.6 Machine learning algorithms used for modelling seasonal herbaceous AGB

3.6.1 Random Forest

The RF algorithm, developed by Breiman (2001), is an efficient bagging-based ensemble learning method which improves on the regression and classification tree (CART) by combining multiple decision trees. The RF algorithm has been used for modelling AGB and analysing relationships between remote sensing variables and AGB (Schwieder et al., 2018; Li et al., 2021) and for estimating the AGB of wetland vegetation (Naidoo et al., 2019). RF is an approach with the advantages of being insensitive to noise, overtraining and producing accurate and precise predictive results (Mutanga et al., 2012). For this study, the RF algorithm was implemented using the "randomForest" package (Liaw, 2015) in RStudio software (v4.0.3). To assess the significant influence of different remote sensing variables and also to reduce the large number of predictor variables, the variable importance selection was implemented in modelling scenarios that had more than ten input predictor variables.

The VSURF function (Genuer et al., 2015) which is a RF-based important variable selection function was implemented. The R package "vsurf" (Genuer et al., 2015) returns two subsets of variables to address both regression and classification problems. The first subset is a subset containing significant variables that includes some duplication while the second subset is smaller, avoid duplications and subsequently corresponds more on the prediction variables. In order to train the RF models, the study implemented the repeated k-fold cross validation to adjust hyperparameters for more robust models. The k-fold cross validation is a method that is based on splitting the observations into k folds of equal size (Richter et al., 2012). Therefore, to improve robustness and model accuracy the study applied a repeated 10-fold cross validation resampling method as a trainControl function (repeated twice). Furthermore, two important parameters were

optimised in the RF models: (i) *ntree*, the tree number contained in the RF model, and (ii) *mtry*, the variable number used during node splitting of each tree. The selected value of *ntree* was set to a default value of 500. Thus, the final optimal models used for prediction of the AGB of wetland vegetation in the summer and winter season were selected where the value of the *mtry* had a minimised error. Furthermore, the mtry values in the study ranged between 2 and 12.

3.6.2 Support Vector Regression

SVM algorithm is a supervised machine learning method that can solve both classification and regression problems without considering the distribution of data (Cortes and Vapnik, 1995). The SVM method makes use of a high dimensional space, and it fundamentally converts the non-linear regression problems into linear form using kernel functions (Cortes and Vapnik, 1995). In this study, SVM was used as a regression method (SVR) to estimate herbaceous AGB for both the winter and summer season using the package "e1071" (Karatzoglou et al., 2006) which contains the SVM function in RStudio software (version 4.0.3). The SVR models employed Radial Basis Function (RBF) Kernel because it is efficient and at the same time it associated with fewer numeral difficulties such as computational time compared to other SVM kernels such as linear and polynomial kernels (Wan et al., 2018). To select the most significant predictor variables for training the SVR models, the recursive feature elimination (RFE) (Chen et al., 2007) was implemented in each modelling scenario that had more than ten predictors as input variables to reduce the large number of predictor variables and improve model performance.

RFE employs a backward selection process to find the optimal predictor features. It builds a model based on each attribute and then assesses the relative importance of each component inside the model (Guyon et al., 2002; Chen et al., 2007). The characteristics are then iteratively ranked in order of relevance, with the least important feature(s) being removed based on model assessment metrics (e.g., RMSE). RFE is effective at identifying important characteristics or variables that can be used to predict the target variable from a training dataset. To find the optimal values for tuning the SVR model, significant hyperparameters are required such as cost and sigma and these can be optimised using methods such as the gradient descent (Keerthi et al., 2007), grid search (Hsu et al., 2003), and meta-heuristics algorithms (Blum and Roli, 2003; Talbi, 2009). In this study, a grid search

function was then applied in each modelling scenario to tune the models by searching the optimal values for cost and sigma. The grid-search strategy is a viable method for hyper-parameter tuning as it exhaustively considers all possible parameter combinations and selects the pair of parameters with the lowest out-of-the-bag error (Kganyago et al., 2021). Therefore, the optimal trained model that was used to predict the target variable (herbaceous AGB) was trained using important variables selected by RFE and it was selected where cost had minimised error (RMSE), and sigma was kept constant at a default value.

3.7 Validating model accuracy

The accuracies of predictive models for both summer and winter models of RF and SVR were evaluated using three statistical "goodness-of-fit" measures recommended by Richter *et al.* (2012). These measures are the coefficient of determination or R^2 (Equation 1), the root mean square error or RMSE (Equation 2) and the relative root-mean square error (relRMSE, (Equation 3)). These equations are often used in the literature to assess accuracy of predictive models when estimating vegetation biophysical parameters (Richter et al., 2012; Naidoo et al., 2019; Kganyago et al., 2021; Li et al., 2021). R^2 is a statical measure with values ranging between 0 and 1 and it indicates the amount of variability explained by the predictive model, the RMSE indicates the magnitude of error in the units of the target variable and relRMSE is a dimensionless index expressed as percentage and it is suitable for comparisons between different variables or ranges (Richter et al., 2012). The resulting accuracies were recorded, and the optimal model was selected where the relRMSE was minimised. To facilitate comparison of model accuracies between different variables, the model accuracy is regarded as either excellent (RRMSE<10%), good (10%<RRMSE<20%), fair (20%<RRMSE<30%) or inadequate (RRMSE>30%) (Jamieson et al., 1991; Heinemann et al. 2012). The lower relRMSE the better the model's performance (Li et al., 2021) and more stable the replicability of the model. The evaluation of the accuracy was applied to both SVR and RF seasonal models in R statistical software.

$$R^2 = 1 - \frac{\sum_{i=1}^{n}(z_i - \hat{z}_i)^2}{\sum_{i=1}^{n}(z_i - \bar{z}_i)^2}$$

Equation 1: Coefficient of determination (Richter et al., 2012)

$$\text{RMSE} = \sqrt{\frac{1}{n}\sum_{i=1}^{n}(\hat{z}_i - z_i)^2}$$

Equation 2: Root mean square error (Richter et al., 2012)

$$\text{relRMSE} = \frac{RMSE}{\bar{Z}_i}$$

Equation 3: Relative root mean square error (Richter et al., 2012)

where Z_i and $\hat{Z}_i$ indicates the observed and predicted AGB values in the i^{th} plot sample respectively, $\bar{Z}_i$ denotes the mean of the observed AGB values, and *n* indicates the total number of samples (in the validation dataset).

3.8 Mapping of seasonal teal carbon

The seasonal maps of the AGB of wetland vegetation were created using the raster layers of the selected important variables of the optimal model per season. The LAI raster layer was used in the AGB mapping since it was one of the most important variables in all scenarios. The layers were stacked for the mapping procedure in R statistical software using packages: 'modelMap' (Freeman et al., 2018), 'raster' (Hijmans et al., 2015) and 'rgdal' (Bivand et al., 2015) and the most accurate modelling algorithm (i.e. RF or SVR). The scale for mapping both the summer and winter AGB was 20 m considering the resolution of Sentinel-1A image. The AGB maps for the summer and winter season were then converted into carbon stock maps by assuming that carbon is composed of 50% of the AGB content on average (Chave et al., 2005). A Scaling Factor (SF) of 0.5 was applied to the resulting estimated AGB raster map in ArcGIS (version 10.4.1) to convert it to carbon stock using

equation 4. The equation has been proven to be efficient in converting the AGB to carbon stock (Otukei and Emanuel, 2015; Behera et al., 2016; Shen et al., 2020). Therefore, the conversion equation is given as:

$$\mathrm{C} = \mathrm{AGB} \times SF$$

Equation 4: Conversion of the wetland AGB to carbon stock (Penman et al., 2003)

Where: C= Carbon stock (g C/m^2 DM), AGB=above ground biomass (g/m^2), and SF= 0.5.

3.9 Assessment of seasonal variations in carbon stocks between the summer and winter

3.9.1 Statistical significance between summer and winter using the National Wetland Map version 5 boundaries.

In order to assess the seasonal variations in the amount of carbon stored within the AGB in the selected study area, the points were stratified into wetland hydrogeomorphic (HGM) types and terrestrial systems to distinguish between teal and green carbon. The stratification of points was done based on the NWM5 wetland polygons (Van Deventer et al., 2020). All the points outside the NWM5 polygons were considered to be terrestrial points, while points falling within or inside the polygons were considered wetlands. The Random Points Inside Layer Bounds tool found under Research Tools in QGIS (v3.18) used to generate random points inside the HGM layers. Therefore, both the terrestrial and wetland layers in this study had 176 random points each. The points were generated for both the summer and winter seasons to facilitate a comparative analysis between the two investigated seasons. Additionally, the generated random points were used to extract estimated carbon values for each season from the estimated carbon maps using the extract multi-values to points tool in ArcMap for seasonal variation analysis.

Statistical measures of variability such as mean, standard deviation (SD) and coefficient of variation (COV%) computed in RStudio software was used to assess seasonal differences in the extracted carbon values of wetlands and terrestrial areas across the summer and winter seasons. The COV is an amount of relative variability that shows how values are distributed in a dataset

relative to the mean. It is calculated as the ratio of the standard deviation to the mean. Independent unpaired Welch T-test was also computed at 95% confidence interval to ascertain if values are statistically different between summer and winter seasons and between the HGM types (terrestrial-wetland). Also, to visualise the seasonal variability of carbon, a box and whisker plot was plotted in R software.

3.9.2 Seasonal differences in carbon across wetland vegetation communities in the Tevredenpan study area

Vegetation in wetlands plays a crucial role in storing carbon either in the AGB and subsequently facilitates the process of carbon sequestration. Seasonal variations were further determined between the vegetation types found in the study site. The classification boundaries of wetland vegetation communities of Van Deventer et al. (2022) were used for the Tevredenpan study area. Thus, for this study, nine wetland vegetation communities were considered for analysis of seasonal variations namely, *Aristida* spp., *Arundinella nepalensis*, *Carex* spp., grass-sedge, *Eragrostis plana*, *Juncus effuses*, *Phragmites australis*, Sedge dominant, *Themeda triandra* and Wet-grass. The shapefiles of each vegetation type were used to generate random points in QGIS using the Random Points Inside Layer Bounds tool in QGIS. For each vegetation type, 76 random points were generated inside the boundary layers using the Random Points Inside Layer Bounds tool in QGIS (v3.18). The outputs were exported as point shapefiles for further comparative analysis. The points shapefiles for each wetland vegetation type were later used to extract carbon values from the estimated carbon maps of the summer and winter seasons, respectively, in ArcMap using the Spatial Analyst tool “extract multi-values to points”. Additionally, a t-test was computed to determine if the variation in carbon stock were statistically significant between the summer and winter. The t-test was computed for each wetland vegetation type in RStudio software. Statistical significance was tested at a confidence interval of 95%.

3.10 Conclusion

Chapter 3 emphasised the important background and features of Tevredenpan study area description with its associated vegetation communities. The vegetation communities varied from *Aristida* spp., *Arundinella nepalensis*, *Carex* spp., grass-sedge, *Eragrostis plana*, *Juncus effuses*,

Phragmites australis, Sedge dominant, *Themeda triandra* and Wet-grass. This study used wet summer and dry winter in-situ herbaceous biomass with Sentinel-1 and sentinel-2 derived variables for wetland biomass estimation. The GLCM textures, backscatter channels, SAR band ratio, reflectance bands, both RE and traditional VIs were used as predictor variables in the current study. The remote sensing derived predictor variables were grouped into different modelling scenarios to estimate AGB of wetland vegetation Accordingly, LAI was the significant parameter for the modelling of herbaceous wetland AGB. The above applications were necessary to improve monitoring procedures of wetland AGB carbon distribution protection. However, in the following chapter, the study explain the results in detail and discuss the meaning of the findings for estimation of herbaceous wetland AGB.

CHAPTER 4: RESULTS AND ANALYSIS

This chapter provides the results of the research project in relation to the methods used in this study. It first highlights the significant predictor variables and their influence towards the estimation of wetland vegetation AGB and teal carbon. Secondly it provides the accuracies of all the modelling scenarios obtained using different machine learning algorithms as well as the optical and SAR sensors. A detailed representation and observations on the spatial distribution of the predicted teal carbon maps are documented. Furthermore, the chapter also provides a statistical analysis on variations or differences that observed between the investigated seasons within the selected study area of interest. The results presented in this chapter addressed the aim, objectives, and the research questions of this study.

4.1 Variable importance in Sentinel-1A and Sentinel-2A predictors

The results in Tables 8 and 9 illustrate the varying influence of predictor variables derived from Sentinel-1 and Sentinel-2 imagery, respectively, coupled with different modelling scenarios that had more than ten input variables for estimating AGB of wetland vegetation across the summer and winter seasons. The results in both Tables 8 and 9, indicate that the selection of important variables by VSURF and RFE was not entirely consistent in both the RF and SVR models throughout the investigated seasons. According to Table 8, for Sentinel-1 models in both summer and winter, the LAI appeared in all the models (RF and SVR) indicating that it was one of the most important AGB predictor variable. VH backscatter and the textures derived from VH (vhMEAN and vhVariance) also appeared to have influence when AGB of wetland vegetation within the study area in both seasons. Comparatively, VV only indicated to be more important for prediction of herbaceous AGB during the winter season in Scenario 3 and Scenario 4. Additionally, when observing the trend of input variables in Scenario 4 (Backscatter, band ratio, GLCMs, and LAI), the ratio between VH and VV didn't appear to be an important predictor in the estimation of both summer and winter herbaceous AGB in the study.

Table 8: Variable importance of RF and SVR models with more than 10 input predictor variables derived from Sentinel-1 imagery.

Sentinel-1	**SS1**		**WS1**	
	RF_VSURF	**SVR_RFE**	**RF_VSURF**	**SVR_RFE**
Scenario 1: GLCMs (16) +LAI	LAI, vhMEAN	LAI, vhMEAN, vhVariance	vhVariance, LAI	LAI, vhMEAN, vhVariance, vvMEAN, vvVariance
Scenario 3: Backscatter (2) + GLCMs only (16) +LAI	LAI, vhMEAN, VH	LAI, vhMEAN, vhVariance	VH, LAI, vhVariance	VH, LAI, vhVariance, vhMEAN, VV
Scenario 4: Backscatter (2) + Band ratio (1) + GLCMs (16) +LAI	LAI, vhMEAN, vhVariance, VH	LAI, vhVariance, vhMEAN, VH, vvCorrelat	VH, LAI, vhVariance	VH, LAI, vhVariance, vhMEAN, VV

SS1: Summer Sentinel-1; WS1: Winter Sentinel-1

When examining the influence of input variables in Table 9 in Sentinel-2 modelling scenarios for both summer and winter, the LAI showed to be the most important predictor variable in Scenario 1 and Scenario 4 across the summer and winter seasons. In both the RF and SVR models, the RE bands (B5, B6), the red (B4) and green (B3) were selected as most important AGB predictors compared to other input bands (B2, B7, B8, B8A, B11 and B12) for the summer season. However, in the winter season the SWIR band (B12) was the only important reflectance band for estimating the AGB of wetland vegetation than other bands. Moreover, it is worth noting that traditional indices such as NDVI and SR were important variables when incorporating all the variables in RF and SVR (Scenario 4) for both the winter and summer. VIs derived from the RE region (NDVIre5, SRre5) appeared to be important predictors of the AGB of wetland vegetation.

Table 9: Variable importance of RF and SVR models with more than 10 input predictor variables derived from Sentinel-2A.

Implementation of variable importance Sentinel-2	SS2		WS2	
	RF_VSURF	**SVR_RFE**	**RF_VSURF**	**SVR_RFE**
Scenario 1: Reflectance bands (10) +LAI	LAI, B4, B3, B6, B8	LAI, B4, B5, B3, B7	LAI, B12	LAI, B12
Scenario 4: Reflectance bands (10) + RE indices (4) + Traditional VIs (4) +LAI	LAI, SR, NDVI, B4, B3, GNDVI, B5	LAI, SR, B8, NDVI, B5, B4	LAI, NDVI, SRre5, NDVIre5, B12	LAI, SR, B12, SRre5, NDVI, NDVIre5

SS2: Summer Sentinel-2; WS2: Winter Sentinel-2

4.2 Accuracy of modelling scenarios for predicting wetland AGB for the summer and winter season

The results in Table 10 presented the statistical description of four modelling scenarios for estimation of the AGB of palustrine wetland vegetation for both summer and winter seasons and for Sentinel-1 and Sentinel-2 comparisons using the RF and SVR algorithms, respectively. When comparing the results obtained by different Sentinel-1 modelling scenarios for the summer, Scenario 3 which incorporated GLCMS textures, backscatter channel, and LAI was the best performing model for estimating the AGB of wetland vegetation with a R^2 = 0.735, RMSE = 39.848 g·m^{-2}, relRMSE = 17.286% compared to Scenario 1 which attained R^2 = 0.709, RMSE = 40.919 g·m^{-2}, and relRMSE = 17.538%, Scenario 2 (R^2 = 0.699, RMSE = 44.005 g·m^{-2}, relRMSE = 17.546%), and Scenario 4 (R^2 = 0.697, RMSE = 44.278 g·m^{-2}, relRMSE = 17.796%) for the same season. However, the difference between the models was minimal when considering the relRMSE. For the winter season, a combination of GLCMs and LAI in Scenario 1 yielded higher accuracy in estimating AGB (R^2 = 0.785, RMSE = 67.582 g·m^{-2}, relRMSE = 20.885%) than the combination of backscatter channels and GLCMs (R^2 = 0.805, RMSE = 67.063 g·m^{-2}, relRMSE = 21.371%), or that of band ratio and backscatter (R^2 = 0.736, RMSE = 72.944 g·m^{-2}, relRMSE = 21.53 %), and when all the variables (backscatter channels, band ratio, GLCMs, and LAI) were combined (R^2 = 0.777, RMSE = 68.778 g·m^{-2}, relRMSE = 21.774%).

Incorporation of all the variables (spectral bands, traditional VIs and RE VIs) of the Sentinel-2 models, yield higher accuracies for estimating wetland vegetation AGB in the summer with an accuracy of R^2 = 0.753, RMSE = 52.856 g·m^{-2}, relRMSE = 20.009%, compared to individual spectral bands (R^2 = 0.644, RMSE = 67.063 g·m^{-2}, relRMSE = 19.610 %) or VIs (R^2 = 0.665, RMSE = 52.865 g·m^{-2}, relRMSE = 22.051%) for the same season (Table 10). Similarly, the estimation of AGB in winter also improved when all the variables (spectral bands, traditional VIs, and RE VIs) were combined (R^2 = 0.749, RMSE = 69.634 g·m^{-2}, relRMSE = 21.248%) compared to the use of traditional VIs (R^2 = 0.658, RMSE = 76.079 g·m^{-2}, relRMSE = 24.512%) or reflectance bands. However, the difference between the combination of all the variables (reflectance bands, traditional VIs, and RE VIs) was minimal in both the summer and winter models (Scenario 4) in comparison to the accuracy obtained by scenario 3 (RE bands).

It is worth noting that in terms of algorithm performance when looking at the predicted model validation accuracy of the relRMSE, the results suggest that RF models performed better than SVR. This can be attributed to the fact that the relRMSE of the SVR scenarios is twice the RF obtained relRMSE values. Furthermore, when examining the overall performance of the sensors or that of the best performing models in terms of the lowest relRMSE, the SAR C-band obtained high accuracies when looking at the results in the summer (relRMSE = 17.286%) compared to the optical sensor (relRMSE= 20.009%) for the same season. Similar trend of results is evident in winter, Sentinel-1 illustrated a better performance (relRMSE = 20.885%) when compared to Sentinel-2 (relRMSE = 21.248%) in estimating AGB within the Tevredenpan study site. Thus, the combination of SAR GLCMs, C-band backscatter and LAI (Scenario 3) was applied for mapping summer AGB while in winter Scenario 1 (SAR GLCMs textures and LAI) was used for mapping winter AGB.

Table 10: RF and SVR model accuracies of Sentinel-1 and Sentinel-2 derived modelling scenarios for estimation of wetland AGB with 10-fold cross validation across summer and winter.

	Summer						Winter					
Sentinel-1A	**RF**			**SVR**			**RF**			**SVR**		
All scenarios (LAI included)	**R^2**	**RMSE ($g.m^{-2}$)**	**relRMSE (%)**	**R^2**	**RMSE ($g.m^{-2}$)**	**relRMSE (%)**	**R^2**	**RMSE ($g.m^{-2}$)**	**relRMSE (%)**	**R^2**	**RMSE ($g.m^{-2}$)**	**relRMSE (%)**
Scenario 1: GLCMs	0.709	40.919	17.538	0.723	46.861	38.328	0.785	67.582	20.885	0.795	64.209	35.206
Scenario 2: Band ratio + Backscatter	0.699	44.005	17.546	0.716	44.794	36.568	0.736	72.944	21.53	0.763	64.953	39.682
Scenario 3: GCLMs + Backscatter	0.735	39.848	17.286	0.708	44.188	36.753	0.805	67.063	21.371	0.852	59.887	33.287
Scenario 4: GLCMs+ backscatter+ band ratio	0.697	44.278	17.796	0.726	44.294	36.719	0.777	68.778	21.774	0.773	65.442	37.773
Sentinel-2A	**RF**			**SVR**			**RF**			**SVR**		
All scenarios (LAI included)	**R^2**	**RMSE ($g.m^{-2}$)**	**relRMSE (%)**	**R^2**	**RMSE ($g.m^{-2}$)**	**relRMSE (%)**	**R^2**	**RMSE ($g.m^{-2}$)**	**relRMSE (%)**	**R^2**	**RMSE ($g.m^{-2}$)**	**relRMSE (%)**
Scenario 1: Reflectance bands	0.644	52.856	19.610	0.651	51.071	37.891	0.671	78.961	21.293	0.644	73.267	40.726
Scenario 2: Traditional VIs	0.665	52.865	22.051	0.643	48.890	38.674	0.658	76.079	24.512	0.691	68.911	46.198
Scenario 3: RE VIs	0.629	50.352	21.918	0.702	52.937	41.983	0.673	67.798	22.663	0.640	69.775	43.839
Scenario 4: Reflectance bands traditional Vis +RE VIs	0.753	49.269	20.009	0.652	50.595	40.374	0.749	69.634	21.248	0.768	65.699	38.447

To analyse the modelling accuracy, the scatterplots illustrated in Figure 5 (A-D) below were constructed based on the performance of RF and SVR models to find correlation between the observed and predicted AGB in relation to the line of best fit in the study area. An estimation from the RF models showed the best agreement along the 1:1 line compared to the SVR models. The goodness of fit was measured and found to be 0.735 and 0.726 for the RF and SVR models in summer, respectively. However, for the winter season the SVR model showed a strong correlation between the observed and predicted wetland vegetation AGB obtaining a $R^2 = 0.852$.

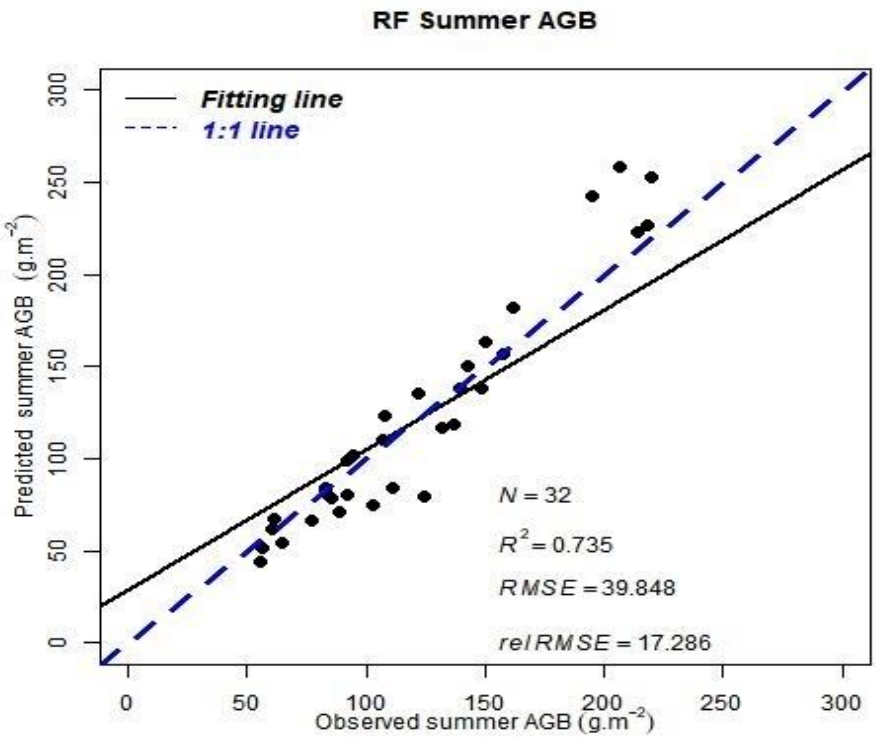
RF Summer AGB
Fitting line
1:1 line
N = 32
R^2 = 0.735
RMSE = 39.848
relRMSE = 17.286
Predicted summer AGB (g.m^{-2})
Observed summer AGB (g.m^{-2})
0
50
100
150
200
250
300

(**A**)

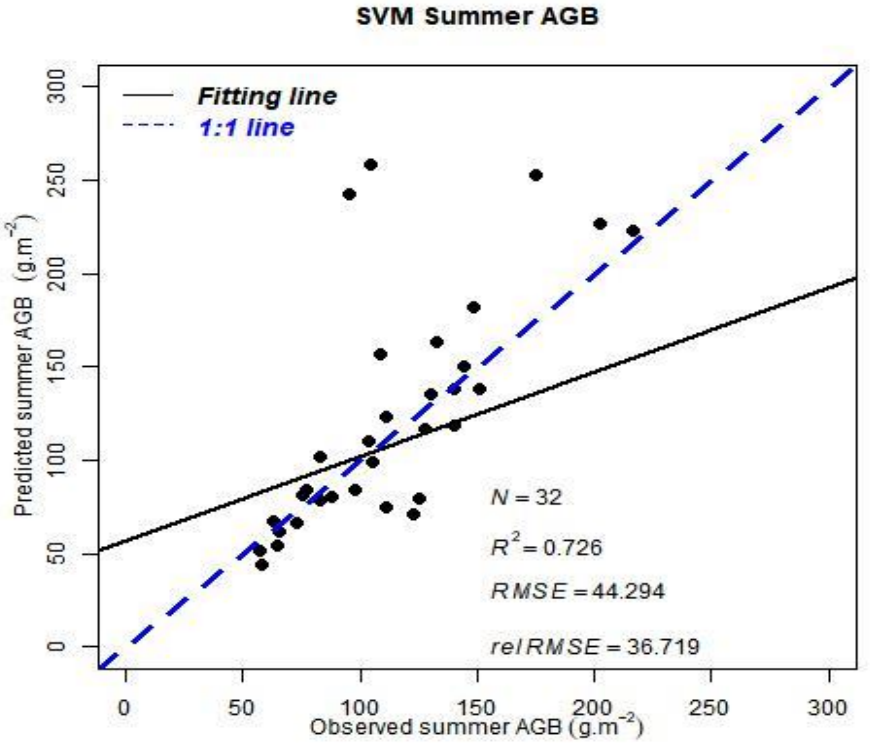
SVM Summer AGB
Fitting line
1:1 line
N = 32
R^2 = 0.726
RMSE = 44.294
relRMSE = 36.719
Predicted summer AGB (g.m^{-2})
Observed summer AGB (g.m^{-2})
0
50
100
150
200
250
300

(**B**)

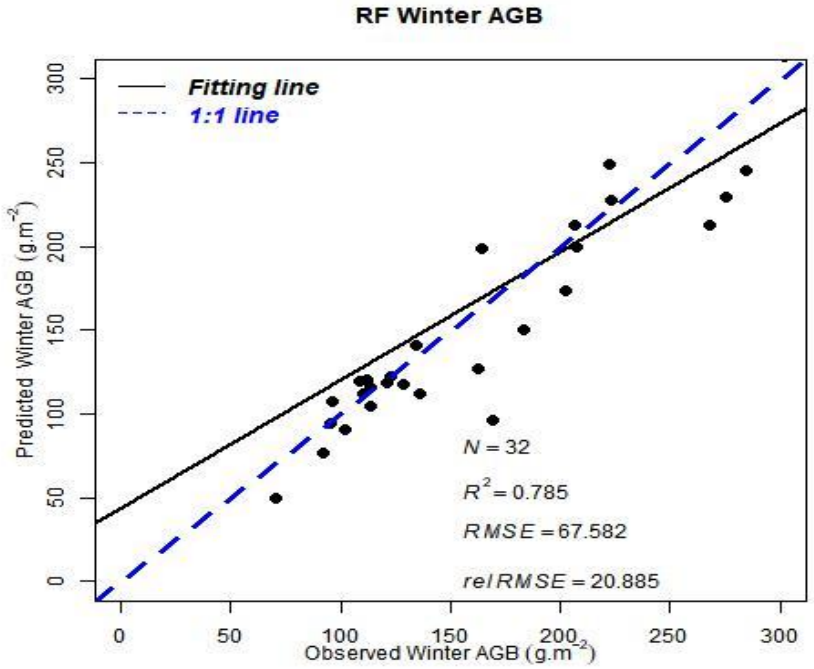

(C)

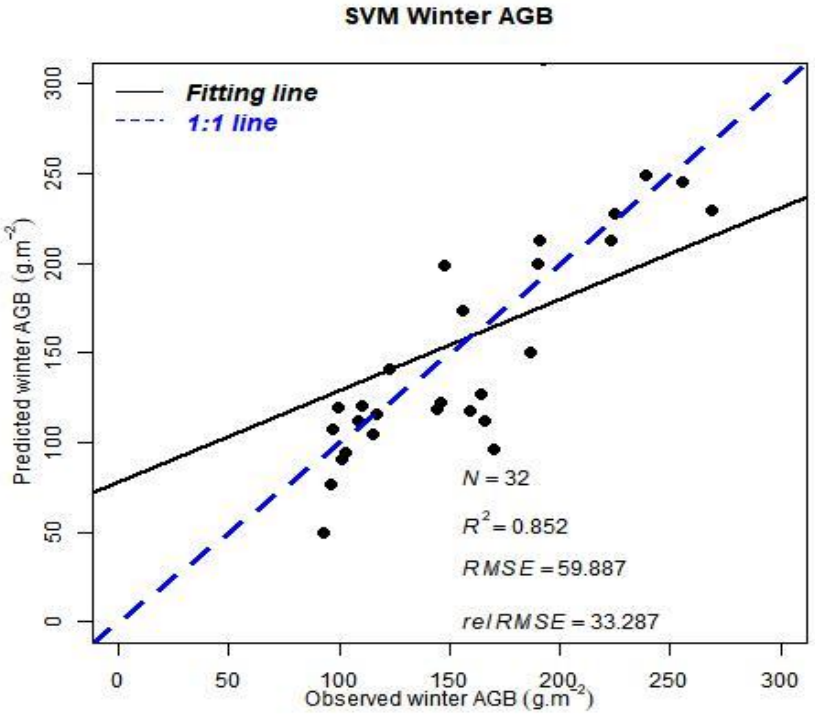

(D)

Figure 5: Seasonal accuracies of observed versus predicted AGB density scatterplots across seasons using the RF and SVR models after 10-fold cross validation. (**A**) RF summer model ; (**B)** SVR summer model; (**C**) RF winter model; (**D**) SVR winter model and dotted blue line=1:1 trend line.

4.3 Spatial patterns in carbon of AGB of wetland vegetation in Tevredenpan

In this study, carbon maps within the selected study area were generated by converting the AGB maps into carbon using a factor of 0.50. Figure 6 and Figure 7 shows the spatial patterns of the estimated wetlands and terrestrial carbon stock in the Tevredenpan study area. The spatial distribution trends of terrestrial and wetland carbon varied across the summer (Figure 6) and winter (Figure 8) indicating patterns of low to high carbon ranges throughout the study area. In both the summer and winter carbon maps, the green areas exhibit high carbon content ranges i.e. 190 g C/m^{-2} DM to 300 g C/m^{-2} stored in the AGB of wetland and terrestrial vegetation. The yellow areas illustrated moderate carbon stocks that ranged between 160 g C/m^{-2} DM and 190 g C/m^{-2} followed by the brown zones which had relatively lower wetland and terrestrial carbon stock below 160 g C/m^{-2} DM per pixel compared to the above mentioned green and yellow areas.

Along the seasonal seep wetlands i.e. D-2 moderate ranges of carbon stock between 160 – 180 g C/m^{-2} DM were evident in the summer season in Figure 6, whereas during winter season in Figure 8 the seasonal or temporal seep wetlands (E-2) illustrated lower ranges of carbon <160 g C/m^{-2} DM. In the south-western part of the study site, a high-density range between 205 to 280 g C/m^{-2} DM of teal carbon was observed over the Tevredenpan depression in D-1 during summer and similar high ranges were also evident in the same depression in E-1 during the winter season (Figure 7). The Tevredenpan is mostly dominated by a dense growth of *Phragmites australis* species which contains a floating peat cap. The agricultural fields (D-4) also showed high ranges of carbon ranging from 190 to 220 g C/m^{-2}DM in summer. However, the amount of carbon in the AGB gradually decreased and the range was <160 g C/m^{-2} DM) over the agricultural fields (E-4) during the winter season. Moreover, the channelled valley-bottom wetland in the northern eastern part of the study area showed high range of teal carbon values in both the summer (Figure 6, D-3) and winter season (Figure 8, E-3). The *Phragmites australis* and *Typha capensis* species prevail along these channels i.e. D-1 and E-3.

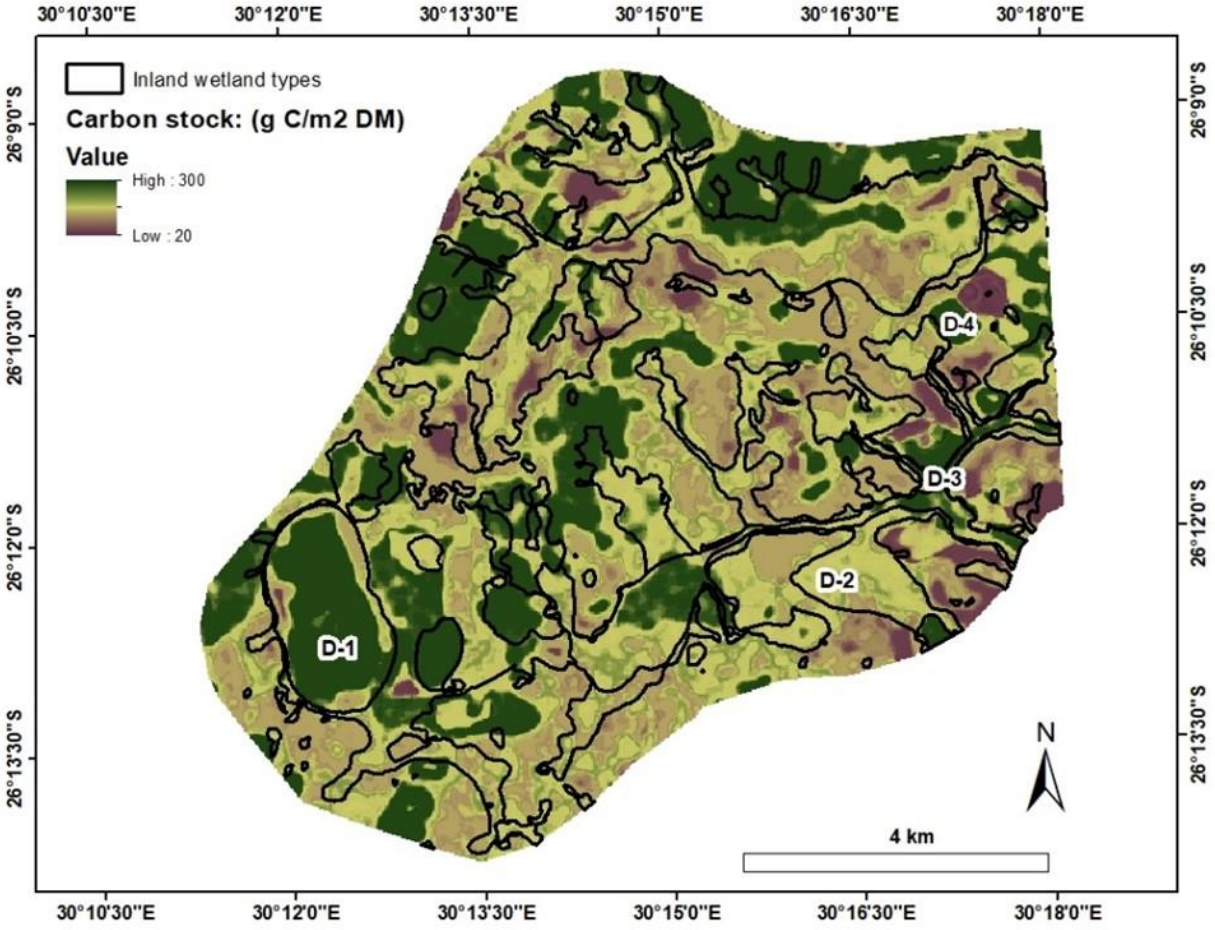

Figure 6: Spatial distribution of estimated teal carbon across the summer season of 2017 in Tevredenpan study area.

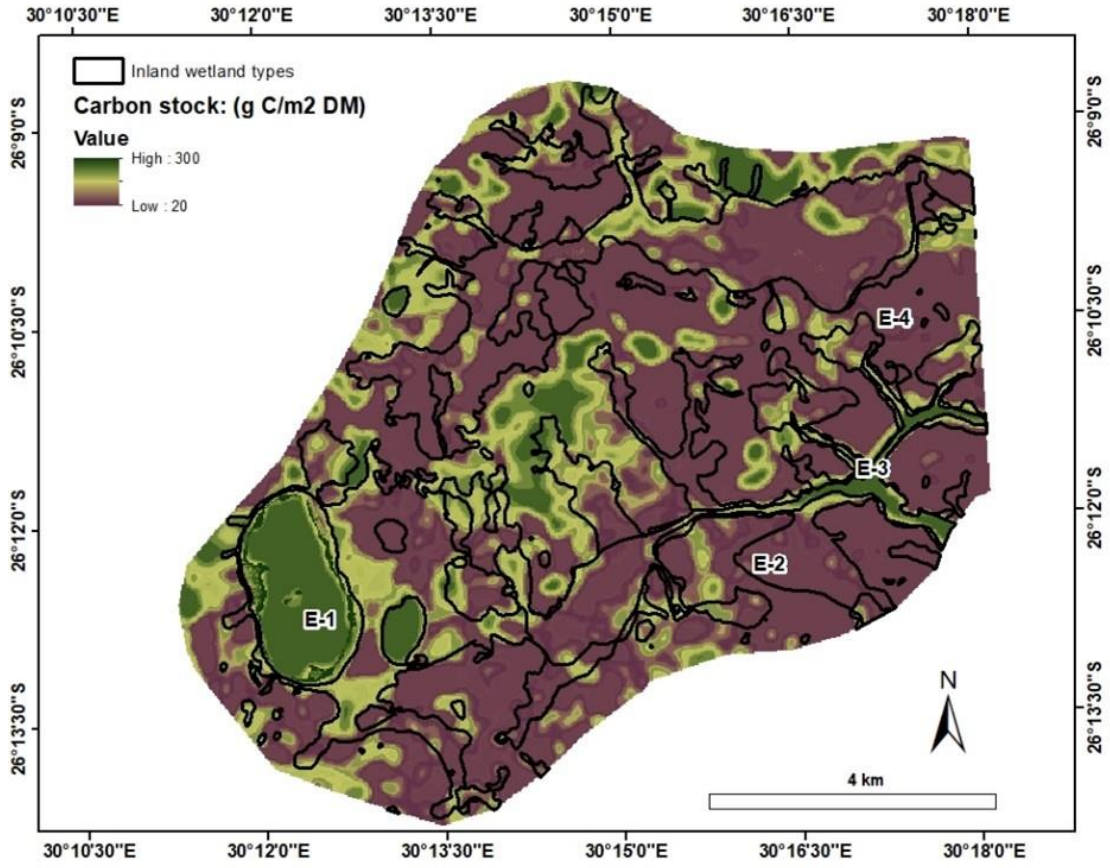

Figure 7: Spatial pattern of the predicted wetland teal carbon across the winter season of 2017 in the Tevredenpan study area

4.4 Seasonal variations in estimated carbon stocks in the Tevredenpan study area

In Figure 8 and Table 11, the predicted teal carbon of wetlands between the seasons, illustrated highest carbon stock in summer than in the winter season within the study site. The estimated carbon stock in wetland areas in the Tevredenpan study area ranged from 33.460 g C/m^{-2} DM to 109.100 g C/m^{-2} DM, with a standard deviation (SD) of 20.066 g C/m^{-2} DM for the summer season (Figure 8, Table 11). For the winter season, teal carbon stock in the study area varied from 38.630 g C/m^{-2} DM to 98.539 g C/m^{-2} DM, with a SD of 20.672 g C/m^{-2} DM (Figure 8, Table 11). The mean teal carbon (i.e. wetland grass and sedges) values were significantly high in the summer i.e. 78.288 g

C/m^{-2} DM than in the winter season i.e. 58.599 g C/m^{-2} DM. When looking at the green carbon (i.e. terrestrial grasses), Tevredenpan study area depicted high range of green carbon in the summer season compared to the winter season in Figure 8 and Table 11. These carbon values ranged between 31.310 g C/m^{-2} DM and 112.650 g C/m^{-2} DM in summer with a mean of 76.767 g C/m^{-2} DM and SD of 21.490 g C/m^{-2} DM. However, in the winter season the range of green carbon was between 39.596 g C/m^2 DM to 96.611 g C/m^{-2} DM with a mean and SD of 57.250 g C/m^{-2} DM and 18.602 g C/m^{-2} DM, respectively.

Although the green carbon was slightly greater i.e. 112.650 g C/m^{-2} than the teal carbon (109.100 g C/m^{-2} DM) in summer (Figure 8), mean values in Table 11 between the teal carbon and green carbon showed no significant difference (<2% difference, $p > 0.05$) in summer. Similar pattern of results was evident in winter between the mean carbon values of terrestrial and wetland indicating no significant difference for this season (<1% difference, $p > 0.05$) (Table 11). However, wetlands contained a marginal higher carbon content of 98.539 g C/m^{-2} DM than terrestrial i.e. 96.611 g C/m^{-2} DM for this season (Figure 8). High coefficient of variation (COV %) of carbon stock in the terrestrial area (27.994%) reflects a substantial spatial variability, showing the heterogeneity of the carbon in the study area when compared to the teal carbon (COV = 25.630%) in summer (Table 11). Contrary, in the winter season high COV in wetland teal carbon (35.278%) illustrated the high degree of variation to the mean in carbon stock while lower variability was observed in the estimated green carbon (32.494%) (Table 11).

Table 11: Descriptive statistical table with variations in predicted carbon maps across summer and winter season in Tevredenpan study site. COV= co-efficient of variation, SD= standard deviation, N= total number of random points per season, min =minimum, and max= maximum.

Season	HGM Type	N	Min	Mean (g C/m^{-2})	Max	SD	COV	p-value
Summer	Wetland	175	33.460	78.288	109.100	20.066	25.630	0.4941
	Terrestrial	175	31.310	76.767	112.650	21.490	27.994	
Winter	Wetland	175	38.630	58.599	98.539	20.672	35.278	0.5236
	Terrestrial	175	39.596	57.250	96.611	18.602	32.494	

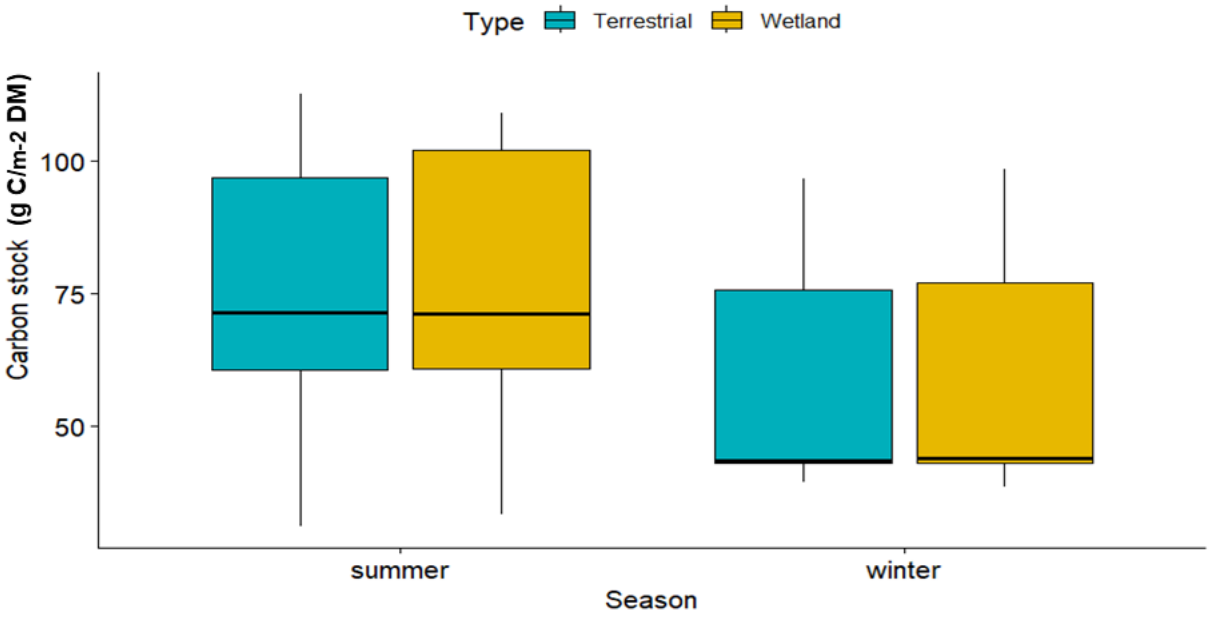

Figure 8: Seasonal variations in the predicted teal carbon for Tevredenpan study area across the summer and winter seasons for the year 2017.

The means in groups (Group one: summer-winter) illustrated higher mean of carbon stocks (77.527 g C/m^{-2}) in summer when compared to the means in groups for the winter season (57.918 g C/m^{-2}). Thus, significant statistical difference ($p < 0.05$) between the summer and winter season was observed when looking at the mean in groups of the estimated carbon of both terrestrial and wetland across the seasons in Group one (Table 12).

Table 12: Statistical differences in mean in groups across the seasons for the year 2017 in the Tevredanpan.

Differences in groups	**Means in groups (g C/m^{-2})**	**p-value < 0.05**
One: Summer - Winter	Summer: 77.527 Winter: 57.918	Yes

According to Table 13 the analysis of carbon stock in the vegetation communities found within the Tevredenpan study area varied between the summer and winter season. The results indicated that all the wetland vegetation communities of the study area had high mean values of carbon in the summer season compared to the winter season (Table 13). For example, *Juncus effusus* a wetland species contained high carbon content in the AGB with a mean of 86.690 g C/m^{-2} DM in summer and a mean of 70.355 g C/m^{-2} DM in the winter season. Similarly, terrestrial vegetation community i.e. *Eragrostis* spp. and *Themeda* spp. had high mean carbon content of 72.275 g C/m^{-2} DM in the AGB during the summer season while in winter it was lower 57.148 g C/m^{-2} DM indicating a statistical significance between the two seasons ($p < 0.05$). Therefore, at 95% confidence interval the carbon stock in the wetland vegetation types illustrated to be significantly different between the summer and winter in all the nine vegetation communities of the Tevredenpan study site ($p < 0.05$).

Table 13: Seasonal differences in the estimated carbon between wetland vegetation communities of the Tevredenpan study area; n represents the number of random points.

Vegetation type	N	Location	Means in groups (g C/m^{-2})		p-value < 0.05
			Summer	Winter	
Arundinella nepalensis	76	Wetland	74.432	55.662	Yes
Aristida spp.	76	Wetland	75.964	59.203	Yes
Carex spp.	76	Wetland	84.978	60.074	Yes
Eragrostis spp. and *Themeda* spp.	76	Terrestrial	72.275	57.148	Yes
Grass-sedge communities	76	Wetland	79.631	63.079	Yes
Juncus effusus	76	Wetland	86.690	70.355	Yes
Phragmites australis	76	Wetland	75.290	58.904	Yes
Sedge dominant	76	Wetland	72.123	60.128	Yes
Wet-grass community	76	Wetland	74.621	57.523	Yes

4.5 Conclusion

The study showed the feasibility of integrating satellite dataset and non-parametric algorithms for seasonal AGB of wetland vegetation estimation. In general, RF outperformed the SVR algorithm for estimating seasonal AGB of wetland vegetation with lower relRMSE. The variations in the spatial pattern of the predicted wetland teal carbon between winter and summer season were expected due to different climate variability. Despite, the overall high values of the predicted carbon stocks in most vegetation communities of the study area in summer than winter, vegetation abundance contributed to the observed seasonal variations. The next chapter focus is to provide justification of the current study findings and link the findings with existing literature.

CHAPTER 5: DISCUSSION

This study aimed to assess seasonal variations in carbon derived from the AGB of palustrine wetland vegetation across the summer and winter seasons in the Grassland Biome of Mpumalanga, South Africa. The study integrated different remote sensing variables derived from the Sentinel-1A and Sentinel-2A imagery and arranged them into modelling scenarios for predicting wetland AGB using RF and SVR algorithms. The study showed the seasonal variation of carbon stock and its distribution across the summer and winter and within the wetland vegetation communities in the Tevredenpan study area. Machine learning algorithms implemented in this study illustrated a varying performance of important input variables selected, with the RF algorithm yielding a better performance for predicting AGB. Assessing seasonal variations using Sentinel-1 and Sentinel-2 seasonal datasets and their derivatives could help to know how wetland vegetation influences CS and how it varies between seasons.

5.1 Selection of important variables for estimating wetland herbaceous AGB

The results of important variable selection in Sentinel-1 variables showed that VH polarisation was a more prominent predictor variable than VV polarisation (Table 8). The importance of VH in mapping and estimated AGB are consistent in previous studies (Sinha et al., 2015; Castillo et al., 2017; Crabbe et al., 2019). Castillo et al. (2017) demonstrated that the cross-polarisation (VH) was more efficient in estimating the AGB of mangroves than that of the VV co-polarisation. In a grassland environment, Crabbe et al. (2019) observed that VH backscatter yielded better estimates of pasture AGB (R^2 = 0.71) than VV co-polarisation band. These observations may be due to the fact that VH backscatter results from volumetric scattering, which is more evident in vegetation which displays volumetric architecture (e.g., grasses) than in co-polarised backscatter which is often affected by surface roughness (Laurin et al., 2018). This study found that GLCMs textures of VH, particularly the vhMEAN and VhVariance were important predictor variables for modelling AGB of wetland vegetation within the grasslands. Selection of important textural features for biomass estimation

however may differ based on the window size utilised, spectral wavelengths, and different vegetation types.

In line with the finding of this study, the importance of SAR-based GLCMs texture variables as important predictor variables for estimating AGB is also evident in previous studies though they estimated AGB in forested environments (Zhao et al., 2016; Argamosa et al., 2018; Chen et al., 2018). For example, Argamosa et al. (2018) demonstrated that VH textures (Variance and contrast) calculated from 9 × 9 window size were selected as important predictors for mangrove AGB estimation, significantly improving model performance (R^2 = 0.79). Application of SAR textural features in retrieving AGB of wetland and grassland vegetation is poorly documented in the literature. However, some studies applied SAR textures in the classification of wetland vegetation, the results demonstrated improved classification of wetland vegetation between summer (9% to 22%) and winter (up to 15%) (Rajngewerc et al., 2022) and also that of heterogeneous wetland terrains (Mishra et al., 2019). Therefore, C-Band Sentinel-1 data GLCMs textures are significant variables for wetland AGB estimation due to their ability to provide and characterise vegetation structure required for precise AGB models.

Analysis of important predictor variables for Sentinel-2 derived variables in this study showed that bands centred around the 704- 782 nm (RE), 665nm (red), 833 nm (NIR), and 559 nm (green) spectral regions were selected as necessary for predicting biomass, particularly during the summer season. The selected bands in this study B4, B3, B6, B5, B7 and B8 (Table 9) fall within the wavelengths of EMS regions that have previously been found to strongly link or relate to the biomass of wetland and grassland vegetation by numerous studies (Mutanga et al., 2012; Ramoelo et al., 2015; Sibanda et al., 2015; Li et al., 2021). Interestingly both the RF and SVR importance variable selection demonstrated that the SWIR band (2202 nm) was the most critical spectral band compared to other bands in winter. These findings are supported by Ramoelo and Cho (2014), who state that the SWIR region is a significant wavelength for estimating biomass in the dry or winter season because the vegetation is photosynthetically inactive and dead. Similar findings were presented by Xu et al. (2014), who found a correlation between the Normalized Difference Water Index (NDWI)

derived from the SWIR and dead vegetation cover. The use of SWIR band (B12) as a prominent input variable for modelling winter AGB in this study thus further confirms the significant influence of the SWIR region in AGB modelling, particularly in the dry season.

VIs reduces the soil background and environment noise effect and overcome the saturation problem when estimating biomass (Mutanga and Skidmore, 2004; Adam et al., 2014). In this study, traditional VIs (GNDVI, NDVI, SR) and RE VIs (NDVIre5, SRre5) were among the important selected spectral indices for estimating the AGB of wetland vegetation across the summer and winter seasons (Table 9). Previous studies have proved that the VIs calculated from the NIR, red, and red-edge bands significantly yield greater accuracies for estimation of wetland and grassland AGB (Ramoelo et al., 2015; Sibanda et al., 2016; Naidoo et al., 2019; Li et al., 2021). LAI illustrated to be the most important variable amongst Sentinel-1A and Sentinel-2A predictor variables in all the investigated seasons. Earlier studies have also documented the significance of LAI in modelling the AGB (Van Wijk and Williams, 2005; Fan et al., 2009; Masemola et al., 2016; Naidoo et al., 2019). The LAI is a good indicator of vegetation status and a strong proxy of biomass because it greatly influences the spectral reflectance of vegetation canopies and therefore has a crucial role in vegetation ecosystem processes (Darvishzadeh et al., 2008). Thus, LAI is a good indicator of growth and productivity in the vegetation of grasslands and wetlands and has improved the estimation of AGB for this study.

5.2 Performance of Sentinel-1 and Sentinel-2 AGB modelling scenarios across summer and winter

For this study, the accuracy of Sentinel-1 and Sentinel-2 seasonal modelling scenarios (Table 10) revealed that a combination of SAR GLCMs texture variables and backscatter performed better in predicting summer wetland AGB (R^2 = 0.735, RMSE = 39.848 g·m^{-2} and relRMSE = 17.286%) than a combination of reflectance bands, VIs and RE bands (R^2 = 0.753, RMSE= 49.268 g·m^{-2} and relRMSE = 20.009%). SAR-derived scenarios obtained higher accuracies across the winter regardless of the incorporation of GLCMs only (R^2 = 0.785, 67.582 g·m^{-2}, 20.885%) compared to the combination of reflectance bands, VIs and RE bands of optical data (R^2 = 0.749, RMSE = 69.634 g·m^{-2} and relRMSE = 21.248%). These results suggest that the SAR C-band variable had a stronger correlation with the

herbaceous AGB of palustrine in our study compared to modelling scenarios of the optical sensor. The findings of this study are in contrast to the results obtained by earlier studies (Naidoo et al., 2019; Nuthammachot et al., 2020). Nuthammachot et al. (2020) found that Sentinel-1 variables obtained lower accuracy (R^2 = 0.34) compared to Sentinel-2 variables (R^2 = 0.82) in a forest environment. However, studies documented that SAR C-band is saturated in high biomass areas such as forests and could attain lower AGB accuracies (Imhoff et al., 1995; Huang et al., 2018). As such C-band is more suitable for monitoring low herbaceous vegetation (Ghasemi et al., 2011), as in the case of this study.

Consistently with the successful application of SAR in retrieving wetland AGB in grasslands for the present study, studies of Wang et al. (2019) and Crabbe et al. (2019) have also demonstrated the suitability of using Sentinel-1 datasets in estimating AGB in grasslands. Furthermore, previous comparative studies that found Sentinel-1 to perform better than Sentinel-2 stated that the inclusion of SAR GLCMs textural information improved the modelling of AGB (Chen et al., 2018; Navarro et al., 2019). However, some studies found that the optical derived models performed better than SAR modelling data for modelling AGB (Zhao et al., 2016; Forkuor et al., 2020). Fourker et al. (2020) reckoned that the poor performance of Sentinel-1 to Sentinel-2 in their study could be influenced by the exclusion of textural features. Consequently, the performance of remote sensing sensors in estimating AGB vary with different regional factors such as climate, vegetation types, and landscape.

The high penetration capability of SAR as a result of enhanced backscatter or double bounce scattering between water, emergent, and flooded vegetation in wetlands allows for extensive information extraction of the structural parameters of plants not contained within the spectral signature of vegetation to improve biomass estimation (Dabboor and Brisco, 2019). This supports the better performance of SAR-derived modelling scenarios for estimating AGB of palustrine wetlands compared to the performance of optical modelling scenarios in this study. Integrating SAR texture variables and SAR backscatter in models retrieves crucial structural information, decreases the influence of environmental background to some extent, and subsequently improves the

capability of the models for measuring the AGB of palustrine wetlands. However, the potential to track the seasonal dynamics of grassland and wetland vegetation with Sentinel-1 and Sentinel-2 derived variables is not fully known. Our results also demonstrated that the Sentinel-1 backscatter data (under all-weather conditions) and Sentinel-2 data can track the seasonality of carbon changes in the AGB of wetland vegetation in grasslands.

5.3 Machine learning algorithms in modelling seasonal AGB of wetland vegetation

Comparative analysis between the machine learning algorithms in this study showed that the RF model performed better (relRMSE = 17.286%) than the SVR machine learning algorithm (relRMSE = 36.719%) (Table 10). RF modelling approach is very robust, has variable importance selection, minimises overfitting, multi-collinearity, and has been implemented independently of the data distribution (Mutanga et al. 2012). The lower accuracies with the SVR may be associated with the absence of a basic method to optimise and tune the model hyperparameters (Cherkassky and Ma 2004; Siegmann and Jarmer, 2015; Wan et al., 2018). The findings of Chen et al. (2018) however posited that SVR performed better than RF and ANN in forest AGB estimation which contradicts the findings of this study. Comparative analysis in some previous studies discovered that the there was no significant difference between the SVR and RF machine learning algorithms (Adam et al., 2014).

The improved performance of results in RF in this study agrees with previous studies in wetland AGB estimation (Wan et al., 2018; Naidoo et al., 2019) and in forest biomass retrieval (Chen et al., 2019). Wan et al. (2018) indicated that the RF was the best-performing machine learning algorithm with an RMSE of 250 g m^{-2} than SVR (RMSE = 270 g m^{-2}) for modelling the AGB of a wetland. Naidoo et al. (2019) successfully demonstrated the robustness of the RF algorithm in estimating palustrine wetland herbaceous AGB. However, the previous studies of Wan et al. (2018) and Naidoo et al. (2019) did not apply or assess the performance of these machine learning algorithms at different seasons (i.e. wet and dry seasons). Therefore, the results of this study further revealed that machine learning algorithms have the capacity to identify non-linear relations between relevant biophysical parameters and satellite-based predictor variables of different seasons

5.4 Spatial mapping of seasonal carbon changes from the AGB in palustrine wetland

The predicted carbon maps of terrestrial and wetland vegetation had a range of carbon stock between 30 g C/m^{-2} DM to 300 g C/m^{-2} DM across the seasons (Figures 6 and 7) . The seasonal seep wetlands demonstrated moderate ranges of carbon stock (160 – 180 g C/m^{-2} DM) in the summer season. In contrast, during the winter season, lower ranges of carbon (<160 g C/m^{-2} DM) were evident in these wetlands. Salimi et al. (2021) state that during the winter season, monitoring may yield different results in ephemeral/temporal wetlands, and the dynamics of nutrient cycles and carbon dynamics from wetlands may vary. The influence or presence of vegetation communities such as the *Phragmites australis* and *Typha capensis* in the Tevredenpan study site resulted in high spatial patterns of carbon stock along the valley-bottom wetlands and depression in both summer and winter. Naidoo et al. (2019) also reported that the Tevredenpan study sites illustrated signs of cattle grazing along the seasonal and temporal valley-bottom and seeps wetlands. However, the inundation and saturation in seasons prohibit cattle from moving around through certain wetland types; thus macrophytes like *Phragmites australis* are less likely to experience grazing. Hence the high accumulation of carbon in these wetland types. Literature also indicates that these wetland vegetation types tend to store large quantities of biomass or carbon (Mutanga et al., 2012; Lolu et al., 2019).

5.5 Seasonal variation in carbon stock between the summer and winter season

The assessment of seasonal variations using the NWM5 polygons to extract the predicted carbon stock values from the predicted maps indicated differences between the terrestrial and wetland carbon. The results illustrated that the green carbon was slightly greater (112.650 g C/m^{-2}) than the teal carbon (109.100 g C/m^{-2} DM) in summer, and during the winter season, wetlands contained a marginal higher teal carbon content of 98.539 g C/m^{-2} DM than green carbon i.e. 96.611 g C/m^{-2} DM. The results indicated slightly higher carbon in terrestrial areas in summer compared to winter, which could be associated with the impacts of fires in grasslands during the winter. The current study did not evaluate the impact of fire and Naidoo et al. (2019) indicated that the Tevredanpan study area did not illustrate any apparent effects of fires. Disturbances from activities such as fires,

agriculture practices, and cattle ranging affect the composition of vegetation and decreases the AGB, resulting in low carbon in the above-ground vegetation (Matayaya et al., 2017). Furthermore, though the grazing pressure component was also not evaluated in this study, in summer the grass is in abundance, and during the winter plant growth is significantly reduced because vegetation is photosynthetically inactive (Ramoelo and Cho, 2014); so there is less grass available and the little grass that is available is heavily grazed, this could affect the process of carbon sequestration by the AGB vegetation.

The findings of this study indicated that there were no significant differences ($p > 0.05$) between terrestrial and wetland carbon in the summer and that for the winter season in this study (Table 11). Thus, wetlands have great potential for maintaining expected ranges of AGB carbon stock comparable to terrestrial vegetation. The findings of this study also suggested that overall carbon differences in seasons were statistically significant ($p < 0.05$), with means of green and teal carbon illustrating higher mean of carbon stocks (77.527 g C/m^{-2} DM) in summer than mean of teal and green carbon for the winter season (57.918 g C/m^{-2} DM). These results are consistent and comparable to previous studies that have also recorded high mean carbon stock values in summer compared to the winter season (Costa and Henry 2010; Lolu et al., 2019). Lolu et al. (2019) found that the above ground carbon stock in wetland macrophytes in Hokersar wetland , to have an average of 244.86 g C/m^{-2} in the summer season and an average of 188.790 g C/m^{-2} in the winter season. In contrast, Costa and Henry (2010) documented a carbon range of 114.3 g C/m^{-2} in summer to 203 g C/m^{-2} in winter in the lakes of Brazil. Therefore, based on the varying results of this study as well as of the previous studies, the primary productivity of wetland ecosystems differs due to the influence of geographic setting or location, climate condition, and the type of vegetation. Furthermore, at different seasons the natural ecosystems undergo seasonal changes due to their natural cycles (UN, 2017). Hence the observed significant differences in the results of carbon stocks between summer and winter.

This study also illustrated that wetland vegetation communities within the Tevredenpan study area contained significant carbon content in summer compared to the winter (Table 13), indicating

significant variation between the summer and winter season ($p < 0.05$). This study further revealed that the taller, evergreen, and sturdier species (i.e., *Juncus effusus*) were significant sinks of AGB carbon storing about 70.355 g C/m^{-2} DM in winter to 86.690 g C/m^{-2} DM in summer. These results have been observed by other studies in the literature (Tang et al., 2011; Gagnon et al., 2012; Means et al., 2016). The range of carbon stock in the AGB of *Juncus effusus* in this study however is lower compared to the findings of Means et al. (2016), who found that the same species in a created wetland contained 703 g C/m^2 of above ground carbon. Some earlier studies implied that climatic conditions during the growing season or wet season may enhance photosynthetic rate in vegetation species and results in increased AGB in grasslands (Piao et al., 2003; Piao et al., 2008; Zeng et al., 2019). Hence the high carbon content in the AGB vegetation of wetland during summer in this study. Due to vegetation dying out and being photosynthetically inactive in winter, this could explain the low mean carbon stocks observed during winter compared to the summer in our study. Therefore, the carbon content and balance of wetlands is likely to fluctuate significantly because of factors such as climate and land-use practices that alter water-table dynamics, temperatures, and vegetation communities. Furthermore, the addition of BGB however, which was not quantified in this study would have likely displayed a more complete view on the overall biomass stored in all the palustrine wetland vegetation species. Assessment of seasonal carbon changes in various natural ecosystems is therefore a crucial factor for the development of sustainable climate change strategies, protection of wetlands and better understanding of CS.

CHAPTER 6: CONCLUSION

This chapter provides a summary of the current study key findings and shows the importance of remote sensing techniques in temporal monitoring of palustrine wetland ecosystems at regional scales in arid and semi-arid areas. The chapter provides the limitations of the current study and further proposes recommendations in order to improve on the seasonal monitoring of AGB of wetland vegetation. The recommendations and key findings stipulated in this chapter could help in understanding the role of wetland particularly vegetated wetland in the changing climate to facilitate conservation and monitoring of these ecosystems.

6.1 General summary and conclusion

Wetland ecosystems are essential for providing ecosystem services related to global climate change (Were et al., 2019). However, intensive water extraction for agriculture, deforestation, industrial expansion, reservoir construction, increasing sea levels and altered climate patterns are threats to wetlands. (Schmitt and Brisco, 2013; Salimi et al., 2021). Furthermore, the impacts of anthropogenic pressures and global climatic changes are projected to result in changes in the functioning and integrity of most ecosystems. Biomass of wetland vegetation is a significant component of wetland vegetation that plays a crucial role in CS. Due to the dynamic nature of wetlands, assessment of temporal changes and estimating carbon stock in the AGB can aid in conserving grasslands and wetlands and notably help to understand the carbon changes in wetland vegetation leading to more accurate future predictions of global climate change. This study aimed to use seasonal derived AGB of palustrine herbaceous vegetation to determine the differences in teal carbon, using active and passive remote sensing data across the summer and winter seasons. The current study investigated three objectives to address specific research questions. The objectives of the study were to : (i) Derive and test different season-specific modelling scenarios from Sentinel-1 and Sentinel-2 imagery to assess the optimal model for estimating AGB of palustrine wetland vegetation for the summer and winter seasons, (ii) Assess the performance of RF and SVR algorithms in predicting seasonal AGB of palustrine wetland vegetation, (iii) Map the spatial

distribution of wetland vegetation carbon stock for the summer and winter seasons and, (iv) Assess the seasonal variations and if there is a statistical difference in teal carbon derived from wetland herbaceous AGB in the summer and winter seasons for the year 2017.

To address and answer the current study research questions and objectives, this study integrated machine learning techniques, i.e. RF and SVR, with different combinations of predictor variables from Sentinel-1A GRD and Sentinel-2A MSI imagery, to assess and map seasonal variations in teal carbon derived from the herbaceous AGB of palustrine wetland. The study was carried out in the Tevredenpan study area in the Grassland biome of the Mpumalanga province, South Africa. The results of the investigated objectives of the study showed that palustrine wetland vegetation plays a significant role in storing carbon in the AGB. However, the amount of carbon stored in the above-ground wetland vegetation significantly differs between seasons and across wetland vegetation communities. This study highlighted that summer had significantly high values of carbon stored in the AGB of wetland vegetation. Furthermore, inclusion of the dry season in AGB monitoring studies could provide a substantial understanding of the seasonal functioning of the AGB of wetland and grassland vegetation and its role in CS at a regional scale.

The predicted carbon maps illustrated significant differences in the spatial distribution of green and teal carbon across the summer and winter seasons. These seasonal differences could be linked to the grassland vegetation communities' sensitivity to seasonality and land utilisation for agriculture, grazing, mining, and grass fires. This study further illustrated the importance of a hybrid methodological approach for enhancing the estimation, mapping and monitoring of AGB of wetland vegetation. Incorporating texture measurements derived from SAR improved the estimation of wetland AGB in this study. Sentinel-1 SAR C-band performed better in estimating herbaceous AGB of palustrine wetlands than Sentinel-2 due to the volumetric information from the VH polarisation and capability of penetrating through vegetation canopy structures. Furthermore, the results revealed that the RF regression machine algorithm offers better modelling performance compared to the SVR algorithm in prediction models and therefore is potentially a good contender for seasonal teal AGB estimates. Therefore, the results of the current study have imperative contributions for

the long-term monitoring of wetlands functioning in arid and semi-arid regions in response to climate change

6.2 Limitations of the study

Despite the satisfactory modelling accuracies achieved in this study, the number of samples collected could have influenced the accuracy of the predictive models. According to Korhonen et al. (2017) and Morais et al. (2021) one of the general problems that affects the accuracy of predictive biomass models is the limited number of field-collected sample points that are used for model validation and calibration. Furthermore, the integration of LAI raster layers which were derived using the stepwise multiple linear regression into the models for mapping AGB could have influenced the mapping of wetland and terrestrial carbon spatial distribution across the studied seasons. These algorithms are associated with model overfitting and yield lower accuracies when the sample size is small (Chen et al., 2009). Furthermore, empirical models are seldom transferrable. For example, there is minimal to no chance for these models to effectively work elsewhere or be in a different site – without additional field measurements from that particular site.

6.3 Recommendations for future research

The RF algorithm yielded better results compared to the SVR model and was able to identify non-linear relations between AGB and predictor variables of different seasons in this study. However, the current study recommends that these seasonal models should be tested in a different location and environment to further validate the model transferability of machine learning techniques as well as their prediction accuracy. The current study only tested a single window (9 × 9) when extracting the SAR GLCM features and this may have influenced the accuracy of the results in the AGB models. Larger window size may omit significant information while smaller window size may result to pixel noise (Sarker and Nichol, 2011; Kelsey and Neff, 2014). Thus, current study recommends that future studies should use or test multiple moving window sizes for calculating the GLCMs feature in order to determine if there are significant improvements in seasonal AGB accuracies. Future studies should explore the combination of RTMs and ensemble algorithms for

mapping LAI at different seasons to improve the accuracy of LAI maps to be integrated in biomass mapping. Potential future work should also evaluate other approaches for tuning hyper-parameters of machine learning algorithms especially in SVR models to improve prediction accuracy. Further investigation on the influence of vegetation heterogeneity in the canopy (Dang et al., 2019; Li et al., 2019) particularly in smaller wetlands needs to be considered for estimating the AGB of wetland vegetation in grasslands. Although individual sensors had good performance in this study, the synergy of multiple remote sensing data or the combination of predictor variables for different seasons from both optical and radar should also be explored in future work to determine if there are significant improvements in the differences of seasonal above ground carbon stock of palustrine wetland vegetation.

REFERENCES

Adam, E., Mutanga, O. and Rugege, D., 2010. Multispectral and hyperspectral remote sensing for identification and mapping of wetland vegetation: a review. Wetlands ecology and management, 18, pp.281-296.

Adam, E., Mutanga, O., Odindi, J. and Abdel-Rahman, E.M., 2014. Land-use/cover classification in a heterogeneous coastal landscape using RapidEye imagery: evaluating the performance of random forest and support vector machines classifiers. International Journal of Remote Sensing, 35(10), pp.3440-3458.

Adam, E.M. and Mutanga, O., 2012, October. Estimation of high-density wetland biomass: combining regression model with vegetation index developed from Worldview-2 imagery. In Remote sensing for agriculture, ecosystems, and hydrology XIV (Vol. 8531, pp. 198-206). SPIE.

Altman, D.G. and Bland, J.M., 2009. Parametric v non-parametric methods for data analysis. Bmj, 338.

Argamosa, R.J.L., Blanco, A.C., Baloloy, A.B., Candido, C.G., Dumalag, J.B.L.C., DImapilis, L.L.C. and Paringit, E.C., 2018. Modelling above ground biomass of mangrove forest using sentinel-1 imagery. ISPRS Annals of Photogrammetry, Remote Sensing & Spatial Information Sciences, 4(3).

Attema, E.P.W. and Ulaby, F.T., 1978. Vegetation modelled as a water cloud. Radio science, 13(2), pp.357-364.

Atzberger, C. and Richter, K., 2012. Spatially constrained inversion of radiative transfer models for improved LAI mapping from future Sentinel-2 imagery. Remote Sensing of Environment, 120, pp.208-218.

Barrachina, M., Cristóbal, J. and Tulla, A.F., 2015. Estimating above-ground biomass on mountain meadows and pastures through remote sensing. International Journal of Applied Earth Observation and Geoinformation, 38, pp.184-192.

Barrett, B., Nitze, I., Green, S. and Cawkwell, F., 2014. Assessment of multi-temporal, multi-sensor radar and ancillary spatial data for grasslands monitoring in Ireland using machine learning approaches. Remote sensing of environment, 152, pp.109-124.

Barrett, T., 2014. Storage and flux of carbon in live trees, snags, and logs in the Chugach and Tongass National Forests. Gen. Tech. Rep. PNW-GTR-889. Portland, OR: US Department of Agriculture, Forest Service, Pacific Northwest Research Station. 44 p., 889.

Behera, M.D., Tripathi, P., Mishra, B., Kumar, S., Chitale, V.S. and Behera, S.K., 2016. Above-ground biomass and carbon estimates of Shorea robusta and Tectona grandis forests using QuadPOL ALOS PALSAR data. Advances in Space Research, 57(2), pp.552-561.

Berger, K., Atzberger, C., Danner, M., D'Urso, G., Mauser, W., Vuolo, F. and Hank, T., 2018. Evaluation of the PROSAIL model capabilities for future hyperspectral model environments: A review study. Remote Sensing, 10(1), p.85.

Berry, S., Keith, H., Mackey, B., Brookhouse, M. and Jonson, J., 2010. Green Carbon Part 2.: The role of natural forests in carbon storage (p. 124). ANU Press.

Bivand, R., Keitt, T., Rowlingson, B., Pebesma, E., Sumner, M., Hijmans, R., Rouault, E. and Bivand, M.R., 2015. Package 'rgdal'. Bindings for the Geospatial Data Abstraction Library. Available online: https://cran. r-project. org/web/packages/rgdal/index. html (accessed on 15 October 2017), p.172.

Blum, C. and Roli, A., 2003. Metaheuristics in combinatorial optimization: Overview and conceptual comparison. ACM computing surveys (CSUR), 35(3), pp.268-308.

Braun, A. and Veci, L., 2021. TOPS Interferometry Tutorial. Sentinel-1 Toolbox.

Breaux, H.J., 1967. On stepwise multiple linear regression. Army Ballistic Research Lab Aberdeen Proving Ground MD.

Breiman, L., 2001. Random forests. Machine learning, 45, pp.5-32.

Brisco, B., Kapfer, M., Hirose, T., Tedford, B. and Liu, J., 2011. Evaluation of C-band polarization diversity and polarimetry for wetland mapping. Canadian Journal of Remote Sensing, 37(1), pp.82-92.

Burgoyne, B.M., Bredenkamp, G.J. and Van Rooyen, N., 2000. Wetland vegetation in the North-eastern Sandy Highveld, Mpumalanga, South Africa. Bothalia, 30(2), pp.187-200.

Campbell, J.B. and Wynne, R.H., 2011. Introduction to remote sensing. Guilford Press.

Cantalloube, H. and Nahum, C., 2000. How to compute a multi-look SAR image. European Space Agency-Publications-Esa Sp, 450, pp.635-640.

Carrington, D.P., Gallimore, R.G. and Kutzbach, J.E., 2001. Climate sensitivity to wetlands and wetland vegetation in mid-Holocene North Africa. Climate Dynamics, 17(2), pp.151-157.

Castillo, J.A.A., Apan, A.A., Maraseni, T.N. and Salmo III, S.G., 2017. Estimation and mapping of above-ground biomass of mangrove forests and their replacement land uses in the Philippines using Sentinel imagery. ISPRS Journal of Photogrammetry and Remote Sensing, 134, pp.70-85.

Chamaillé-Jammes, S. and Bond, W.J., 2010. Will global change improve grazing quality of grasslands? A call for a deeper understanding of the effects of shifts from C4 to C3 grasses for large herbivores. Oikos, 119(12), pp.1857-1861.

Chang, J. and Shoshany, M., 2016, July. Mediterranean shrublands biomass estimation using Sentinel-1 and Sentinel-2. In 2016 IEEE International Geoscience and Remote Sensing Symposium (IGARSS) (pp. 5300-5303).

Chave, J., Andalo, C., Brown, S., Cairns, M.A., Chambers, J.Q., Eamus, D., Fölster, H., Fromard, F., Higuchi, N., Kira, T. and Lescure, J.P., 2005. Tree allometry and improved estimation of carbon stocks and balance in tropical forests. Oecologia, 145(1), pp.87-99.

Chave, J., Réjou-Méchain, M., Búrquez, A., Chidumayo, E., Colgan, M.S., Delitti, W.B., Duque, A., Eid, T., Fearnside, P.M., Goodman, R.C. and Henry, M., 2014. Improved allometric models to estimate the aboveground biomass of tropical trees. Global change biology, 20(10), pp.3177-3190.

Chen, J., Gu, S., Shen, M., Tang, Y. and Matsushita, B., 2009. Estimating aboveground biomass of grassland having a high canopy cover: an exploratory analysis of in situ hyperspectral data. International Journal of Remote Sensing, 30(24), pp.6497-6517.

Chen, J.M., 1996. Evaluation of vegetation indices and a modified simple ratio for boreal applications. Canadian Journal of Remote Sensing, 22(3), pp.229-242.

Chen, L., Ren, C., Zhang, B., Wang, Z. and Xi, Y., 2018. Estimation of forest above-ground biomass by geographically weighted regression and machine learning with sentinel imagery. Forests, 9(10), p.582.

Chen, L., Wang, Y., Ren, C., Zhang, B. and Wang, Z., 2019. Optimal combination of predictors and algorithms for forest above-ground biomass mapping from Sentinel and SRTM data. Remote Sensing, 11(4), p.414.

Chen, X.W. and Jeong, J.C., 2007, December. Enhanced recursive feature elimination. In Sixth international conference on machine learning and applications (ICMLA 2007) (pp. 429-435). IEEE.

Chen, Y., Qiao, S., Zhang, G., Xu, Y.J., Chen, L. and Wu, L., 2020. Investigating the potential use of Sentinel-1 data for monitoring wetland water level changes in China's Momoge National Nature Reserve. PeerJ, 8, p.e8616.

Cherkassky, V. and Ma, Y., 2004. Practical selection of SVM parameters and noise estimation for SVM regression. Neural networks, 17(1), pp.113-126.

Cho, M.A. and Skidmore, A.K., 2006. A new technique for extracting the red edge position from hyperspectral data: The linear extrapolation method. Remote sensing of environment, 101(2), pp.181-193.

Cho, M.A., Skidmore, A., Corsi, F., Van Wieren, S.E. and Sobhan, I., 2007. Estimation of green grass/herb biomass from airborne hyperspectral imagery using spectral indices and partial least squares regression. International journal of applied Earth observation and geoinformation, 9(4), pp.414-424.

Collen, B., Whitton, F., Dyer, E.E., Baillie, J.E., Cumberlidge, N., Darwall, W.R., Pollock, C., Richman, N.I., Soulsby, A.M. and Böhm, M., 2014. Global patterns of freshwater species diversity, threat and endemism. Global ecology and Biogeography, 23(1), pp.40-51.

Cortes, C. and Vapnik, V., 1995. Support-vector networks. Machine learning, 20, pp.273-297.

Costa, M.L.R. and Henry, R., 2010. Phosphorus, nitrogen, and carbon contents of macrophytes in lakes lateral to a tropical river (Paranapanema River, São Paulo, Brazil). Acta Limnologica Brasiliensia, 22, pp.122-132.

Cowan, G.I. (Ed.). 1995: Wetlands of South Africa. Pretoria: Department of Environmental Affairs and Tourism.

Crabbe, R.A., Lamb, D.W. and Edwards, C., 2021. Investigating the potential of Sentinel-1 to detect varying spatial heterogeneity in pasture cover in grasslands. International Journal of Remote Sensing, 42(1), pp.274-285.

Cutler, M.E.J., Boyd, D.S., Foody, G.M. and Vetrivel, A., 2012. Estimating tropical forest biomass with a combination of SAR image texture and Landsat TM data: An assessment of predictions between regions. ISPRS Journal of Photogrammetry and Remote Sensing, 70, pp.66-77.

Dabboor, M. and Brisco, B., 2018. Wetland monitoring and mapping using synthetic aperture radar. Wetl. Manag., 1, p.13.

Dabboor, M. and Brisco, B., 2018. Wetland monitoring and mapping using synthetic aperture radar. Wetland Management Assessment Risk Sustainability Solution, 1, p.13.

Dahy, B., Issa, S., Ksiksi, T. and Saleous, N., 2020, July. Geospatial Technology Methods for Carbon Stock Assessment: A Comprehensive Review. In IOP Conference Series: Earth and Environmental Science (Vol. 540, No. 1, p. 012036). IOP Publishing.

Dai, X., Yang, G., Liu, D. and Wan, R., 2020. Vegetation Carbon Sequestration Mapping in Herbaceous Wetlands by Using a MODIS EVI Time-Series Data Set: A Case in Poyang Lake Wetland, China. Remote Sensing, 12(18), p.3000.

Dang, A.T.N., Nandy, S., Srinet, R., Luong, N.V., Ghosh, S. and Kumar, A.S., 2019. Forest aboveground biomass estimation using machine learning regression algorithm in Yok Don National Park, Vietnam. Ecological Informatics, 50, pp.24-32.

Darvishzadeh, R., Atzberger, C., Skidmore, A. and Schlerf, M., 2011. Mapping grassland leaf area index with airborne hyperspectral imagery: A comparison study of statistical approaches and inversion of radiative transfer models. ISPRS Journal of Photogrammetry and Remote Sensing, 66(6), pp.894-906.

Darvishzadeh, R., Skidmore, A., Schlerf, M. and Atzberger, C., 2008. Inversion of a radiative transfer model for estimating vegetation LAI and chlorophyll in a heterogeneous grassland. Remote sensing of environment, 112(5), pp.2592-2604.

Darvishzadeh, R., Wang, T., Skidmore, A., Vrieling, A., O'Connor, B., Gara, T.W., Ens, B.J. and Paganini, M., 2019. Analysis of Sentinel-2 and RapidEye for retrieval of leaf area index in a saltmarsh using a radiative transfer model. Remote sensing, 11(6), p.671.

David, R.M., Rosser, N.J. and Donoghue, D.N., 2022. Improving above ground biomass estimates of Southern Africa dryland forests by combining Sentinel-1 SAR and Sentinel-2 multispectral imagery. Remote Sensing of Environment, 282, p.113232.

Dayathilake, D.D.T.L., Lokupitiya, E. and Wijeratne, V.P.I.S., 2020. Estimation of aboveground and belowground carbon stocks in urban freshwater wetlands of Sri Lanka. Carbon Balance and Management, 15(1), pp.1-10.

de Almeida, C.T., Galvao, L.S., Ometto, J.P.H.B., Jacon, A.D., de Souza Pereira, F.R., Sato, L.Y., Lopes, A.P., de Alencastro Graça, P.M.L., de Jesus Silva, C.V., Ferreira-Ferreira, J. and Longo, M., 2019. Combining LiDAR and hyperspectral data for aboveground biomass modeling in the Brazilian Amazon using different regression algorithms. Remote Sensing of Environment, 232, p.111323.

Diouf, A.A., Brandt, M., Verger, A., El Jarroudi, M., Djaby, B., Fensholt, R., Ndione, J.A. and Tychon, B., 2015. Fodder biomass monitoring in Sahelian rangelands using phenological metrics from FAPAR time series. Remote Sensing, 7(7), pp.9122-9148.

Dong, Y., Milne, A.K. and Forster, B.C., 2000, July. A review of SAR speckle filters: texture restoration and preservation. In IGARSS 2000. IEEE 2000 International Geoscience and Remote Sensing Symposium. Taking the Pulse of the Planet: The Role of Remote Sensing in Managing the Environment. Proceedings (Cat. No. 00CH37120) (Vol. 2, pp. 633-635).

Drusch, M., Del Bello, U., Carlier, S., Colin, O., Fernandez, V., Gascon, F., Hoersch, B., Isola, C., Laberinti, P., Martimort, P. and Meygret, A., 2012. Sentinel-2: ESA's optical high-resolution mission for GMES operational services. Remote sensing of Environment, 120, pp.25-36.

Dube, T. and Mutanga, O., 2015. Evaluating the utility of the medium-spatial resolution Landsat 8 multispectral sensor in quantifying aboveground biomass in uMngeni catchment, South Africa. ISPRS Journal of Photogrammetry and Remote Sensing, 101, pp.36-46.

Dube, T. and Mutanga, O., 2015. Investigating the robustness of the new Landsat-8 Operational Land Imager derived texture metrics in estimating plantation forest aboveground biomass in resource constrained areas. ISPRS Journal of Photogrammetry and Remote sensing, 108, pp.12-32.

Eastman, J.R., Sangermano, F., Machado, E.A., Rogan, J. and Anyamba, A., 2013. Global trends in seasonality of normalized difference vegetation index (NDVI), 1982–2011. Remote Sensing, 5(10), pp.4799-4818.

Eggleston, S., Buendia, L., Miwa, K., Nagara, T., Tanabe, K., 2006. IPCC guidelines for national greenhouse gas inventories. Volume 4-Agriculture, Forestry and Other Land Use. IGES, Japan.

Emerton, L., 2005. The economic value of Africa's wetlands. Freshwater Ecoregions of Africa and Madagascar: A Conservation Assessment, p.11.

Englhart, S., Keuck, V. and Siegert, F., 2011. Aboveground biomass retrieval in tropical forests—The potential of combined X-and L-band SAR data use. Remote sensing of environment, 115(5), pp.1260-1271.

Environmental Systems Research Institute. 2016. "ArcGIS Desktop: Release 10.4." Redlands: ESRI.

Erwin, K.L., 2009. Wetlands and global climate change: the role of wetland restoration in a changing world. Wetlands Ecology and management, 17(1), pp.71-84.

European Space Agency. 2015. Sentinel-2 User Handbook, ESA Standard Document; European Space Agency: Paris, France.

Falkowski, M.J., Gessler, P.E., Morgan, P., Hudak, A.T. and Smith, A.M., 2005. Characterizing and mapping forest fire fuels using ASTER imagery and gradient modeling. Forest ecology and management, 217(2-3), pp.129-146.

Fan, L.Y., Gao, Y.Z., Brück, H.E.B.C. and Bernhofer, C., 2009. Investigating the relationship between NDVI and LAI in semi-arid grassland in Inner Mongolia using in-situ measurements. Theoretical and applied climatology, 95, pp.151-156.

Fatoyinbo, T., Feliciano, E.A., Lagomasino, D., Lee, S.K. and Trettin, C., 2018. Estimating mangrove aboveground biomass from airborne LiDAR data: a case study from the Zambezi River delta. Environmental Research Letters, 13(2), p.025012.

Feret, J.B., François, C., Asner, G.P., Gitelson, A.A., Martin, R.E., Bidel, L.P., Ustin, S.L., Le Maire, G. and Jacquemoud, S., 2008. PROSPECT-4 and 5: Advances in the leaf optical properties model separating photosynthetic pigments. Remote sensing of environment, 112(6), pp.3030-3043.

Fernández-Manso, A., Fernández-Manso, O. and Quintano, C., 2016. Sentinel-2A red-edge spectral indices suitability for discriminating burn severity. International journal of applied earth observation and geoinformation, 50, pp.170-175.

Filipponi, F., 2019. Sentinel-1 GRD preprocessing workflow. Multidisciplinary digital publishing institute proceedings, 18(1), p.11.

Forkel, M., Carvalhais, N., Verbesselt, J., Mahecha, M.D., Neigh, C.S. and Reichstein, M., 2013. Trend change detection in NDVI time series: Effects of inter-annual variability and methodology. Remote Sensing, 5(5), pp.2113-2144.

Forkuor, G., Zoungrana, J.B.B., Dimobe, K., Ouattara, B., Vadrevu, K.P. and Tondoh, J.E., 2020. Above-ground biomass mapping in West African dryland forest using Sentinel-1 and 2 datasets-A case study. Remote Sensing of Environment, 236, p.111496.

Fourie, L., Rouget, M. and Lötter, M., 2015. Landscape connectivity of the grassland biome in M pumalanga, South Africa. Austral Ecology, 40(1), pp.67-76.

Freeman, E.A., Frescino, T.S. and Moisen, G.G., 2018. ModelMap: an R package for model creation and map production. R package version, 4, pp.6-12.

Fussell, J., Rundquist, D. and Harrington, J.A., 1986. On defining remote sensing. Photogrammetric Engineering and Remote Sensing, 52(9), pp.1507-1511.

Gagnon, V., Chazarenc, F., Kõiv, M. and Brisson, J., 2012. Effect of plant species on water quality at the outlet of a sludge treatment wetland. Water research, 46(16), pp.5305-5315.

Gallant, A.L., 2015. The challenges of remote monitoring of wetlands. Remote Sensing, 7(8), pp.10938-10950.

García, M., Riaño, D., Chuvieco, E. and Danson, F.M., 2010. Estimating biomass carbon stocks for a Mediterranean forest in central Spain using LiDAR height and intensity data. Remote Sensing of Environment, 114(4), pp.816-830.

Gasparri, N.I., Parmuchi, M.G., Bono, J., Karszenbaum, H. and Montenegro, C.L., 2010. Assessing multi-temporal Landsat 7 ETM+ images for estimating above-ground biomass in subtropical dry forests of Argentina. Journal of Arid Environments, 74(10), pp.1262-1270.

Genuer, R., Poggi, J.M. and Tuleau-Malot, C., 2015. VSURF: an R package for variable selection using random forests. The R Journal, 7(2), pp.19-33.

Geudtner, D. and Torres, R., 2012, July. Sentinel-1 system overview and performance. In 2012 IEEE International Geoscience and Remote Sensing Symposium (pp. 1719-1721). IEEE.

Ghasemi, N., Sahebi, M.R. and Mohammadzadeh, A., 2011. A review on biomass estimation methods using synthetic aperture radar data. International Journal of Geomatics and Geosciences, 1(4), p.776.

Gitelson, A. and Merzlyak, M.N., 1994. Spectral reflectance changes associated with autumn senescence of Aesculus hippocastanum L. and Acer platanoides L. leaves. Spectral features and relation to chlorophyll estimation. Journal of plant physiology, 143(3), pp.286-292.

Gitelson, A.A. and Merzlyak, M.N., 1998. Remote sensing of chlorophyll concentration in higher plant leaves. Advances in Space Research, 22(5), pp.689-692.

Grant, K.M., Johnson, D.L., Hildebrand, D.V. and Peddle, D.R., 2013. Quantifying biomass production on rangeland in southern Alberta using SPOT imagery. Canadian Journal of Remote Sensing, 38(6), pp.695-708.

Grundling, P., Linström, A., Grobler, R. and Engelbrecht, J., 2003. The Tevredenpan peatland complex of the Mpumalanga Lakes District. International Mire Conservation Group Newsletter, (2007/3).

Grundling, P.L., 2015. Genesis and hydrological function of an African mire: understanding the role of peatlands in providing ecosystem services in semi-arid climates.

Guerini Filho, M., Kuplich, T.M. and Quadros, F.L.D., 2020. Estimating natural grassland biomass by vegetation indices using Sentinel 2 remote sensing data. International Journal of Remote Sensing, 41(8), pp.2861-2876.

Guo, M., Li, J., Sheng, C., Xu, J. and Wu, L., 2017. A review of wetland remote sensing. Sensors, 17(4), p.777.

Guo, X., Coops, N.C., Tompalski, P., Nielsen, S.E., Bater, C.W. and Stadt, J.J., 2017. Regional mapping of vegetation structure for biodiversity monitoring using airborne lidar data. Ecological informatics, 38, pp.50-61.

Guyon, I., Weston, J., Barnhill, S. and Vapnik, V., 2002. Gene selection for cancer classification using support vector machines. Machine learning, 46, pp.389-422.

Hall, F.G., Knapp, D.E. and Huemmrich, K.F., 1997. Physically based classification and satellite mapping of biophysical characteristics in the southern boreal forest. Journal of Geophysical Research: Atmospheres, 102(D24), pp.29567-29580.

Han, L., Yang, G., Dai, H., Xu, B., Yang, H., Feng, H., Li, Z. and Yang, X., 2019. Modeling maize above-ground biomass based on machine learning approaches using UAV remote-sensing data. Plant methods, 15(1), pp.1-19.

Haralick, R.M., Shanmugam, K. and Dinstein, I.H., 1973. Textural features for image classification. IEEE Transactions on systems, man, and cybernetics, (6), pp.610-621.

Heinemann, A.B., Van Oort, P.A., Fernandes, D.S. and Maia, A.D.H.N., 2012. Sensitivity of APSIM/ORYZA model due to estimation errors in solar radiation. Bragantia, 71, pp.572-582.

Hemes, K.S., Chamberlain, S.D., Eichelmann, E., Anthony, T., Valach, A., Kasak, K., Szutu, D., Verfaillie, J., Silver, W.L. and Baldocchi, D.D., 2019. Assessing the carbon and climate benefit of restoring degraded agricultural peat soils to managed wetlands. Agricultural and Forest Meteorology, 268, pp.202-214.

Hijmans, R.J., Van Etten, J., Cheng, J., Mattiuzzi, M., Sumner, M., Greenberg, J.A., Lamigueiro, O.P., Bevan, A., Racine, E.B., Shortridge, A. and Hijmans, M.R.J., 2015. Package 'raster'. R package, 734, p.473.

Hill, M.J., 2013. Vegetation index suites as indicators of vegetation state in grassland and savanna: An analysis with simulated Sentinel-2 data for a North American transect. Remote Sensing of Environment, 137, pp.94-111.

Houghton, R.A., Hall, F. and Goetz, S.J., 2009. Importance of biomass in the global carbon cycle. Journal of Geophysical Research: Biogeosciences, 114(G2).

Houghton, R.A., Lawrence, K.T., Hackler, J.L. and Brown, S., 2001. The spatial distribution of forest biomass in the Brazilian Amazon: a comparison of estimates. Global Change Biology, 7(7), pp.731-746.

Hsu, C.W., Chang, C.C. and Lin, C.J., 2003. A practical guide to support vector classification.

Huang, C., Ye, X., Deng, C., Zhang, Z. and Wan, Z., 2016. Mapping above-ground biomass by integrating optical and SAR imagery: a case study of Xixi National Wetland Park, China. Remote Sensing, 8(8), p.647.

Imhoff, M.L., 1995. Radar backscatter and biomass saturation: Ramifications for global biomass inventory. IEEE Transactions on Geoscience and Remote Sensing, 33(2), pp.511-518.

IPCC (2006). Eggleston, S., Buendia, L., Miwa, K., Ngara, T. and Tanabe, K., 2006. IPCC guidelines for national greenhouse gas inventories.

IPCC, 2014. Impacts, adaptation, and vulnerability. Part A: global and sectoral aspects. Contribution of working group II to the fifth assessment report of the intergovernmental Panel on Climate Change, 1132.

Jamieson, P.D., Porter, J.R. and Wilson, D.R., 1991. A test of the computer simulation model ARCWHEAT1 on wheat crops grown in New Zealand. *Field crops research*, *27*(4), pp.337-350.

Jin, X., Kumar, L., Li, Z., Feng, H., Xu, X., Yang, G. and Wang, J., 2018. A review of data assimilation of remote sensing and crop models. European Journal of Agronomy, 92, pp.141-152.

Jin, Y., Yang, X., Qiu, J., Li, J., Gao, T., Wu, Q., Zhao, F., Ma, H., Yu, H. and Xu, B., 2014. Remote sensing-based biomass estimation and its spatio-temporal variations in temperate grassland, Northern China. Remote Sensing, 6(2), pp.1496-1513.

Kamenova, I. and Dimitrov, P., 2021. Evaluation of Sentinel-2 vegetation indices for prediction of LAI, fAPAR and fCover of winter wheat in Bulgaria. European Journal of Remote Sensing, 54(sup1), pp.89-108.

Kang, L., Han, X., Zhang, Z. and Sun, O.J., 2007. Grassland ecosystems in China: review of current knowledge and research advancement. Philosophical transactions of the royal society B: Biological Sciences, 362(1482), pp.997-1008.

Kaplan, G. and Avdan, U., 2018. Monthly analysis of wetlands dynamics using remote sensing data. ISPRS International Journal of Geo-Information, 7(10), p.411.

Karatzoglou, A., Meyer, D. and Hornik, K., 2006. Support vector machines in R. Journal of statistical software, 15, pp.1-28.

Keerthi, S., Sindwhani, V. and Chapelle, O., 2007. An efficient method for gradient-based adaptation of hyperparameters in SVM models in Advances in Neural Information Processing Systems19, eds Schölkopf B., Platt JC, Hoffman T.

Keith, D.A., Ferrer, J.R., Nicholson, E., Bishop, M.J., Polidoro, B.A., Ramirez-Llodra, E., Tozer, M.G., Nel, J.L., Mac Nally, R., Gregr, E.J. and Watermeyer, K.E., 2020. The IUCN global ecosystem typology v1. 01: Descriptive profiles for biomes and ecosystem functional groups.

Kelsey, K.C. and Neff, J.C., 2014. Estimates of aboveground biomass from texture analysis of Landsat imagery. Remote Sensing, 6(7), pp.6407-6422.

Kganyago, M., Mhangara, P. and Adjorlolo, C., 2021. Estimating crop biophysical parameters using machine learning algorithms and Sentinel-2 imagery. Remote Sensing, 13(21), p.4314.

King, E., 2014. Southern Africa's Dryland Forests and Climate Change Adaptation. A policy briefing prepared for Governance of Africa's Resources Programme.

Knapp, N., Fischer, R., Cazcarra-Bes, V. and Huth, A., 2020. Structure metrics to generalize biomass estimation from lidar across forest types from different continents. Remote Sensing of Environment, 237, p.111597.

Knox, N.M., Skidmore, A.K., Prins, H.H., Asner, G.P., van der Werff, H.M., de Boer, W.F., van der Waal, C., de Knegt, H.J., Kohi, E.M., Slotow, R. and Grant, R.C., 2011. Dry season mapping of savanna forage quality, using the hyperspectral Carnegie Airborne Observatory sensor. Remote sensing of environment, 115(6), pp.1478-1488.

Kokaly, R.F., Asner, G.P., Ollinger, S.V., Martin, M.E. and Wessman, C.A., 2009. Characterizing canopy biochemistry from imaging spectroscopy and its application to ecosystem studies. Remote sensing of environment, 113, pp. S78-S91.

Kravitz, J., Matthews, M., Lain, L., Fawcett, S. and Bernard, S., 2021. Potential for high fidelity global mapping of common inland water quality products at high spatial and temporal resolutions based on a synthetic data and machine learning approach. Frontiers in Environmental Science, 9, p.587660.

Kumar, D., 2021. Urban objects detection from C-band synthetic aperture radar (SAR) satellite images through simulating filter properties. Scientific Reports, 11(1), p.6241.

Kumar, L. and Mutanga, O., 2017. Remote sensing of above-ground biomass. Remote Sensing, 9(9), p.935.

Kumar, S., Garg, R.D., Govil, H. and Kushwaha, S.P., 2019. PolSAR-decomposition-based extended water cloud modeling for forest aboveground biomass estimation. Remote Sensing, 11(19), p.2287.

Kuplich, T.M., Curran, P.J., Atkinson, P.M., 2005. Relating SAR image texture to biomass of regenerating tropical forests. International Journal of Remote Sensing 26 (21), 4829–4854.

Lal, R., 2008. Carbon sequestration. Philosophical Transactions of the Royal Society B: Biological Sciences, 363(1492), pp.815-830.

Lang, M.W. and Kasischke, E.S., 2008. Using C-band synthetic aperture radar data to monitor forested wetland hydrology in Maryland's coastal plain, USA. IEEE Transactions on Geoscience and Remote Sensing, 46(2), pp.535-546.

Lang, M.W., Kasischke, E.S., Prince, S.D. and Pittman, K.W., 2008. Assessment of C-band synthetic aperture radar data for mapping and monitoring Coastal Plain forested wetlands in the Mid-Atlantic Region, USA. Remote Sensing of Environment, 112(11), pp.4120-4130.

LaRocque, A., Phiri, C., Leblon, B., Pirotti, F., Connor, K. and Hanson, A., 2020. Wetland Mapping with Landsat 8 OLI, Sentinel-1, ALOS-1 PALSAR, and LiDAR Data in Southern New Brunswick, Canada. Remote Sensing, 12(13), p.2095.

Lauck, M. and Benscoter, B., 2015. Non-destructive estimation of aboveground biomass in sawgrass communities of the Florida Everglades. Wetlands, 35(1), pp.207-210.

Laurin, G.V., Balling, J., Corona, P., Mattioli, W., Papale, D., Puletti, N., Rizzo, M., Truckenbrodt, J. and Urban, M., 2018. Above-ground biomass prediction by Sentinel-1 multitemporal data in central Italy with integration of ALOS2 and Sentinel-2 data. Journal of Applied Remote Sensing, 12(1), pp.016008-016008.

Lee, J.S., Wen, J.H., Ainsworth, T.L., Chen, K.S. and Chen, A.J., 2008. Improved sigma filter for speckle filtering of SAR imagery. IEEE Transactions on Geoscience and Remote Sensing, 47(1), pp.202-213.

Li, C., Zhou, L. and Xu, W., 2021. Estimating aboveground biomass using Sentinel-2 MSI data and ensemble algorithms for grassland in the Shengjin Lake Wetland, China. Remote Sensing, 13(8), p.1595.

Li, F., Zeng, Y., Luo, J., Ma, R. and Wu, B., 2016. Modeling grassland aboveground biomass using a pure vegetation index. Ecological Indicators, 62, pp.279-288.

Li, Y., Li, C., Li, M. and Liu, Z., 2019. Influence of variable selection and forest type on forest aboveground biomass estimation using machine learning algorithms. Forests, 10(12), p.1073.

Liaw, A., 2006. Package randomForest: Breiman and Cutler's Random Forest for Classification and Regression. CRAN Repository.

Linström, A., 2015. Wetland status Quo report: Chrissiesmeer project. Tevredenpan Wetland W55A (Wetlands W55A - 05 to 07). In: Lowies, M. (Ed.), SANBI Rehabilitation Plan for the Chrissiesmeer Wetland Project, Mpumalanga Province: Planning Year 2015/2016. Prepared by Margaret Lowies, Aurecon South Africa (Pty) Ltd as Part of the Planning Phase for the Working for Wetlands Rehabilitation Programme. Report No. 109664/9589, South African National Biodiversity Institute (SANBI). Pretoria, South Africa.

Lolu, A.J., Ahluwalia, A.S., Sidhu, M.C. and Reshi, Z.A., 2019. Carbon sequestration potential of macrophytes and seasonal carbon input assessment into the Hokersar wetland, Kashmir. Wetlands, 39(3), pp.453-472.

Lu, D., Batistella, M., 2005. Exploring TM image texture and its relationships with biomass estimation in Rondônia, Brazilian Amazon. Acta Amazonica 35, 249–257.

Lu, D., Chen, Q., Wang, G., Liu, L., Li, G. and Moran, E., 2016. A survey of remote sensing-based aboveground biomass estimation methods in forest ecosystems. International Journal of Digital Earth, 9(1), pp.63-105.

Luo, J., Duan, H., Ma, R., Jin, X., Li, F., Hu, W., Shi, K. and Huang, W., 2017. Mapping species of submerged aquatic vegetation with multi-seasonal satellite images and considering life history information. International journal of applied earth observation and geoinformation, 57, pp.154-165.

Luo, S., Wang, C., Xi, X., Pan, F., Qian, M., Peng, D., Nie, S., Qin, H. and Lin, Y., 2017. Retrieving aboveground biomass of wetland *Phragmites australis* (common reed) using a combination of airborne discrete-return LiDAR and hyperspectral data. International journal of applied earth observation and geoinformation, 58, pp.107-117.

Macreadie, P.I., Anton, A., Raven, J.A., Beaumont, N., Connolly, R.M., Friess, D.A., Kelleway, J.J., Kennedy, H., Kuwae, T., Lavery, P.S. and Lovelock, C.E., 2019. The future of Blue Carbon science. Nature communications, 10(1), pp.1-13.

Mahdavi, S., Salehi, B., Granger, J., Amani, M., Brisco, B. and Huang, W., 2018. Remote sensing for wetland classification: A comprehensive review. GIScience & Remote Sensing, 55(5), pp.623-658.

Mas, J.F. and Flores, J.J., 2008. The application of artificial neural networks to the analysis of remotely sensed data. International Journal of Remote Sensing, 29(3), pp.617-663.

Masemola, C., Cho, M.A. and Ramoelo, A., 2016. Comparison of Landsat 8 OLI and Landsat 7 ETM+ for estimating grassland LAI using model inversion and spectral indices: case study of Mpumalanga, South Africa. International Journal of Remote Sensing, 37(18), pp.4401-4419.

Matayaya, G., Wuta, M. and Nyamadzawo, G., 2017. Effects of different disturbance regimes on grass and herbaceous plant diversity and biomass in Zimbabwean dambo systems. International Journal of Biodiversity Science, Ecosystem Services & Management, 13(1), pp.181-190.

Mathieu, R., Naidoo, L., Cho, M.A., Leblon, B., Main, R., Wessels, K., Asner, G.P., Buckley, J., Van Aardt, J., Erasmus, B.F. and Smit, I.P., 2013. Toward structural assessment of semi-arid African savannahs and woodlands: The potential of multitemporal polarimetric RADARSAT-2 fine beam images. Remote Sensing of Environment, 138, pp.215-231.

Matthews, G.V.T., 1993, March. The Ramsar Convention on Wetlands: its history and development. Gland: Ramsar Convention Bureau.

McCarthy, T., Cairncross, B., Huizenga, J., Batchelor, A., 2007. Conservation of the Mpumalanga Lakes District. Technical Report. School of Geosciences, University of the Witwatersrand, Johannesburg and Wetland Consulting Services (Pty) Ltd, South Africa.

McLaughlin, J.W. and Packalen, M.S., 2021. Peat carbon vulnerability to projected climate warming in the Hudson Bay Lowlands, Canada: A decision support tool for land use planning in peatland dominated landscapes. Frontiers in Earth Science, 9, p.650662.

Means, M.M., Ahn, C., Korol, A.R. and Williams, L.D., 2016. Carbon storage potential by four macrophytes as affected by planting diversity in a created wetland. Journal of environmental management, 165, pp.133-139.

Melton, J.R., Wania, R., Hodson, E.L., Poulter, B., Ringeval, B., Spahni, R., Bohn, T., Avis, C.A., Beerling, D.J., Chen, G. and Eliseev, A.V., 2013. Present state of global wetland extent and wetland methane modelling: conclusions from a model inter-comparison project (WETCHIMP). Biogeosciences, 10(2), pp.753-788.

Michez, A., Lejeune, P., Bauwens, S., Herinaina, A.A.L., Blaise, Y., Castro Muñoz, E., Lebeau, F. and Bindelle, J., 2019. Mapping and monitoring of biomass and grazing in pasture with an unmanned aerial system. *Remote Sensing*, *11*(5), p.473.

Middleton, B.J. and Bailey, A.K., 2008. Water resources of South Africa, 2005 study (WR2005). Water Research Commission Report No. TT, 381(08).

Mishra, V.N., Prasad, R., Rai, P.K., Vishwakarma, A.K. and Arora, A., 2019. Performance evaluation of textural features in improving land use/land cover classification accuracy of heterogeneous landscape using multi-sensor remote sensing data. Earth Science Informatics, 12(1), pp.71-86.

Mitch, W.J. and Gosselink, J.G., 2007. Wetlands. Hoboken, New Jersey: Wiley, 574p.

Mitchell, S.A., 2013. The status of wetlands, threats and the predicted effect of global climate change: the situation in Sub-Saharan Africa. Aquatic sciences, 75(1), pp.95-112.

Mitsch, W.J., Bernal, B., Nahlik, A.M., Mander, Ü., Zhang, L., Anderson, C.J., Jørgensen, S.E. and Brix, H., 2013. Wetlands, carbon, and climate change. Landscape Ecology, 28(4), pp.583-597.

Moncrieff, G.R., Scheiter, S., Slingsby, J.A. and Higgins, S.I., 2015. Understanding global change impacts on South African biomes using Dynamic Vegetation Models. South African Journal of Botany, 101, pp.16-23.

Moomaw, W.R., Chmura, G.L., Davies, G.T., Finlayson, C.M., Middleton, B.A., Natali, S.M., Perry, J.E., Roulet, N. and Sutton-Grier, A.E., 2018. Wetlands in a changing climate: science, policy and management. Wetlands, 38(2), pp.183-205.

Morais, T.G., Teixeira, R.F., Figueiredo, M. and Domingos, T., 2021. The use of machine learning methods to estimate aboveground biomass of grasslands: A review. Ecological Indicators, 130, p.108081.

Motohka, T., Nasahara, K.N., Oguma, H. and Tsuchida, S., 2010. Applicability of green-red vegetation index for remote sensing of vegetation phenology. Remote Sensing, 2(10), pp.2369-2387.

Mucina, L. and Rutherford, M.C., 2006. The vegetation of South Africa, Lesotho and Swaziland. South African National Biodiversity Institute.

Munyati, C., 2022. Detecting the distribution of grass aboveground biomass on a rangeland using Sentinel-2 MSI vegetation indices. Advances in Space Research, 69(2), pp.1130-1145.

Mutanga, O. and Skidmore, A.K., 2004. Narrow band vegetation indices overcome the saturation problem in biomass estimation. International journal of remote sensing, 25(19), pp.3999-4014.

Mutanga, O., Adam, E. and Cho, M.A., 2012. High density biomass estimation for wetland vegetation using WorldView-2 imagery and random forest regression algorithm. International Journal of Applied Earth Observation and Geoinformation, 18, pp.399-406.

Nahlik, A.M. and Fennessy, M.S., 2016. Carbon storage in US wetlands. Nature Communications, 7(1), pp.1-9.

Naidoo, L., Mathieu, R., Main, R., Kleynhans, W., Wessels, K., Asner, G. and Leblon, B., 2015. Savannah woody structure modelling and mapping using multi-frequency (X-, C-and L-band) Synthetic Aperture Radar data. ISPRS Journal of Photogrammetry and Remote Sensing, 105, pp.234-250.

Naidoo, L., Mathieu, R., Main, R., Wessels, K., Asner, G.P., 2016. L-band Synthetic Aperture Radar imagery performs better than optical datasets at retrieving woody fractional cover in deciduous, dry savannahs. Int. J. Appl. Earth Obs. Geoinf. 52, 54–64.

Naidoo, L., Van Deventer, H., Ramoelo, A., Mathieu, R., Nondlazi, B. and Gangat, R., 2019. Estimating above ground biomass as an indicator of carbon storage in vegetated wetlands of the grassland biome of South Africa. International Journal of Applied Earth Observation and Geoinformation, 78, pp.118-129.

Navarro, J.A., Algeet, N., Fernández-Landa, A., Esteban, J., Rodríguez-Noriega, P. and Guillén-Climent, M.L., 2019. Integration of UAV, Sentinel-1, and Sentinel-2 data for mangrove plantation aboveground biomass monitoring in Senegal. Remote Sensing, 11(1), p.77.

Nuthammachot, N., Askar, A., Stratoulias, D. and Wicaksono, P., 2022. Combined use of Sentinel-1 and Sentinel-2 data for improving above-ground biomass estimation. Geocarto International, 37(2), pp.366-376.

Osborn, D., Cutter, A. and Ullah, F., 2015. Universal sustainable development goals. Understanding the Transformational Challenge for Developed Countries.

Otukei, J.R. and Emanuel, M., 2015. Estimation and mapping of above ground biomass and carbon of Bwindi impenetrable National Park using ALOS PALSAR data. South African Journal of Geomatics, 4(1), pp.1-13.

Pachauri RK, Allen MR, Barros VR, Broome J, Cramer W, Christ R et al (2014) Climate change 2014: synthesis report. Contribution of Working Groups I, II and III to the fifth assessment report of the Intergovernmental Panel on Climate Change. IPCC, Geneva, p 151.

Pang, H., Zhang, A., Kang, X., He, N. and Dong, G., 2020. Estimation of the Grassland Aboveground Biomass of the Inner Mongolia Plateau Using the Simulated Spectra of Sentinel-2 Images. Remote Sensing, 12(24), p.4155.

Pant, H.K., Rechcigl, J.E. and Adjei, M.B., 2003. Carbon sequestration in wetlands: concept and estimation. Food, Agriculture and Environment, 1(2), pp.308-313.

Penman, J., Gytarsky, M., Hiraishi, T., Krug, T., Kruger, D., Pipatti, R., Buendia, L., Miwa, K., Ngara, T., Tanabe, K. and Wagner, F., 2003. Good practice guidance for land use, land-use change and forestry. Good practice guidance for land use, land-use change and forestry.

Pereira, H.M., Ferrier, S., Walters, M., Geller, G.N., Jongman, R.H.G., Scholes, R.J., Bruford, M.W., Brummitt, N., Butchart, S.H.M., Cardoso, A.C. and Coops, N.C., 2013. Essential biodiversity variables. Science, 339(6117), pp.277-278.

Piao, S., Ciais, P., Friedlingstein, P., Peylin, P., Reichstein, M., Luyssaert, S., Margolis, H., Fang, J., Barr, A., Chen, A. and Grelle, A., 2008. Net carbon dioxide losses of northern ecosystems in response to autumn warming. Nature, 451(7174), pp.49-52.

Piao, S., Fang, J., Zhou, L., Guo, Q., Henderson, M., Ji, W., Li, Y. and Tao, S., 2003. Interannual variations of monthly and seasonal normalized difference vegetation index (NDVI) in China from 1982 to 1999. Journal of Geophysical Research: Atmospheres, 108(D14).

Powell, S.L., Cohen, W.B., Healey, S.P., Kennedy, R.E., Moisen, G.G., Pierce, K.B. and Ohmann, J.L., 2010. Quantification of live aboveground forest biomass dynamics with Landsat time-series and field inventory data: A comparison of empirical modeling approaches. Remote Sensing of Environment, 114(5), pp.1053-1068.

Programme, W.W.A. The United Nations World Water Development Report 2015; United Nations Educational, Scientific and Cultural Organization: Paris, France, 2015.

Quan, X., He, B., Yebra, M., Yin, C., Liao, Z., Zhang, X., & Li, X. (2017). A radiative transfer model-based method for the estimation of grassland aboveground biomass. International Journal of Applied Earth Observation and Geoinformation, 54, 159-168.

Quantum GIS Development Team, 2021. Quantum GIS Geographic Information System 2009.

Rajngewerc, M., Grimson, R., Bali, L., Minotti, P. and Kandus, P., 2022. Cover classifications in wetlands using Sentinel-1 data (Band C): a case study in the Parana River delta, Argentina. Revista de Teledetección, (60), pp.29-46.

Ramoelo, A. and Cho, M.A. 2014. Dry season biomass estimation as an indicator of rangeland quantity using multi-scale remote sensing data. In: 10th International Conference on African Association of Remote Sensing of Environment (AARSE) 2014, University of Johannesburg, 27-31 October 2014.

Ramoelo, A., Cho, M., Mathieu, R. and Skidmore, A.K., 2015. Potential of Sentinel-2 spectral configuration to assess rangeland quality. Journal of applied remote sensing, 9(1), p.094096.

Ramoelo, A., Cho, M.A., Mathieu, R., Madonsela, S., Van De Kerchove, R., Kaszta, Z. and Wolff, E., 2015. Monitoring grass nutrients and biomass as indicators of rangeland quality and quantity using random forest modelling and WorldView-2 data. International journal of applied earth observation and geoinformation, 43, pp.43-54.

Ramoelo, A., Cho, M.A., Mathieu, R.S., Skidmore, A.K., Schlerf, M. and Heitkönig, I.M.A., 2012. Estimating grass nutrients and biomass as an indicator of rangeland (forage) quality and quantity using remote sensing in Savanna ecosystems.

Ramoelo, A., Skidmore, A.K., Cho, M.A., Schlerf, M., Mathieu, R. and Heitkönig, I.M., 2012. Regional estimation of savanna grass nitrogen using the red-edge band of the spaceborne RapidEye sensor. International Journal of Applied Earth Observation and Geoinformation, 19, pp.151-162.

Rana, V.K. and Suryanarayana, T.M.V., 2019. Evaluation of SAR speckle filter technique for inundation mapping. Remote Sensing Applications: Society and Environment, 16, p.100271.

Rapinel, Sébastien, Laurence Hubert-Moy, and Bernard Clément. "Combined use of LiDAR data and multispectral earth observation imagery for wetland habitat mapping." International journal of applied earth observation and geoinformation 37 (2015): 56-64.

Republic Of South Africa (RSA), 1998. National Water Act (NWA), Act 36 of 1998. Government Printers, Pretoria, South Africa.

Ribeiro, K., Pacheco, F.S., Ferreira, J.W., de Sousa-Neto, E.R., Hastie, A., Krieger Filho, G.C., Alvalá, P.C., Forti, M.C. and Ometto, J.P., 2021. Tropical peatlands and their contribution to the global carbon cycle and climate change. Global Change Biology, 27(3), pp.489-505.

Richter, K., Atzberger, C., Hank, T.B. and Mauser, W., 2012. Derivation of biophysical variables from Earth observation data: validation and statistical measures. Journal of Applied Remote Sensing, 6(1), pp.063557-063557.

Riegel, J.B., Bernhardt, E. and Swenson, J., 2013. Estimating above-ground carbon biomass in a newly restored coastal plain wetland using remote sensing. Plos one, 8(6), p.e68251.

Rigge, M., Smart, A., Wylie, B., Gilmanov, T. and Johnson, P., 2013. Linking phenology and biomass productivity in South Dakota mixed-grass prairie. Rangeland Ecology & Management, 66(5), pp.579-587.

Ripley, B., Venables, B., Bates, D.M., Hornik, K., Gebhardt, A., Firth, D. and Ripley, M.B., 2013. Package 'mass.' Cran r, 538, pp.113-120.

Rouse, J.W., Haas, R.H., Schell, J.A. and Deering, D.W., 1974. Monitoring vegetation systems in the Great Plains with ERTS. NASA Spec. Publ, 351(1), p.309.

Rowan, G. S., & Kalacska, M. (2021). A review of remote sensing of submerged aquatic vegetation for non-specialists. Remote Sensing, 13(4), 623.

Salas Macias, C.A., Alegre Orihuela, J.C. and Iglesias Abad, S., 2017. Estimation of above-ground live biomass and carbon stocks in different plant formations and in the soil of dry forests of the Ecuadorian coast. Food and Energy Security, 6(4), p.e00115.

Salimi, S., Almuktar, S.A. and Scholz, M., 2021. Impact of climate change on wetland ecosystems: A critical review of experimental wetlands. Journal of Environmental Management, 286, p.112160.

Santoro, M., Cartus, O. and Fransson, J.E., 2021. Integration of allometric equations in the water cloud model towards an improved retrieval of forest stem volume with L-band SAR data in Sweden. Remote Sensing of Environment, 253, p.112235.

Sarker, L.R. and Nichol, J.E., 2011. Improved forest biomass estimates using ALOS AVNIR-2 texture indices. Remote Sensing of Environment, 115(4), pp.968-977.

Sawadogo, L., Savadogo, P., Tiveau, D., Dayamba, S.D., Zida, D., Nouvellet, Y., Oden, P.C. and Guinko, S., 2010. Allometric prediction of above-ground biomass of eleven woody tree species in the Sudanian savanna-woodland of West Africa. Journal of Forestry Research, 21(4), pp.475-481.

Schmitt, A. and Brisco, B., 2013. Wetland monitoring using the curvelet-based change detection method on polarimetric SAR imagery. Water, 5(3), pp.1036-1051

Schulze, R.E., 1997. South African Atlas of Agrohydrology and Climatology. Water Research Commission, Pretoria, South Africa. Report TT82/96.

Schwieder, M., Buddeberg, M., Kowalski, K., Pfoch, K., Bartsch, J., Bach, H., Pickert, J. and Hostert, P., 2020. Estimating grassland parameters from Sentinel-2: A model comparison study. PFG–Journal of Photogrammetry, Remote Sensing and Geoinformation Science, 88(5), pp.379-390.

Schwieder, M., Leitão, P.J., Pinto, J.R.R., Teixeira, A.M.C., Pedroni, F., Sanchez, M., Bustamante, M.M. and Hostert, P., 2018. Landsat phenological metrics and their relation to aboveground carbon in the Brazilian Savanna. Carbon balance and management, 13(1), pp.1-15.

Shen, G., Wang, Z., Liu, C. and Han, Y., 2020. Mapping aboveground biomass and carbon in Shanghai's urban forest using Landsat ETM+ and inventory data. Urban Forestry & Urban Greening, 51, p.126655.

Shoko, C. and Mutanga, O., 2017. Examining the strength of the newly-launched Sentinel 2 MSI sensor in detecting and discriminating subtle differences between C3 and C4 grass species. ISPRS journal of photogrammetry and remote sensing, 129, pp.32-40.

Shoko, C., Mutanga, O. and Dube, T., 2016. Progress in the remote sensing of C3 and C4 grass species aboveground biomass over time and space. ISPRS Journal of Photogrammetry and Remote Sensing, 120, pp.13-24.

Sibanda, M., Mutanga, O. and Rouget, M., 2015. Examining the potential of Sentinel-2 MSI spectral resolution in quantifying above ground biomass across different fertilizer treatments. ISPRS Journal of Photogrammetry and Remote Sensing, 110, pp.55-65.

Sibanda, M., Mutanga, O., Rouget, M. and Kumar, L., 2017. Estimating biomass of native grass grown under complex management treatments using worldview-3 spectral derivatives. Remote Sensing, 9(1), p.55.

Sieben, E.J.J., Mtshali, H., Janks, M., 2014. National Wetland Vegetation Database: classification and analysis of wetland vegetation types for conservation planning and monitoring. In: Water Research Commission (WRC). WRC, Pretoria, South Africa, p. 241. Report No. K5/1980.

Siegmann, B. and Jarmer, T., 2015. Comparison of different regression models and validation techniques for the assessment of wheat leaf area index from hyperspectral data. International journal of remote sensing, 36(18), pp.4519-4534.

Silva, T.S., Costa, M.P., Melack, J.M. and Novo, E.M., 2008. Remote sensing of aquatic vegetation: theory and applications. Environmental monitoring and assessment, 140(1), pp.131-145.

Sims, D.A. and Gamon, J.A., 2002. Relationships between leaf pigment content and spectral reflectance across a wide range of species, leaf structures and developmental stages. Remote sensing of environment, 81(2-3), pp.337-354.

Sinha, S., Jeganathan, C., Sharma, L.K. and Nathawat, M.S., 2015. A review of radar remote sensing for biomass estimation. International Journal of Environmental Science and Technology, 12(5), pp.1779-1792.

Sinha, S., Jeganathan, C., Sharma, L.K. and Nathawat, M.S., 2015. A review of radar remote sensing for biomass estimation. International Journal of Environmental Science and Technology, 12, pp.1779-1792.

Sivasankar, T., Lone, J.M., Sarma, K.K., Qadirº, A. and Raju, P.L.N., 2019. Estimation of above ground biomass using support vector. Vietnam Journal of Earth Sciences, 41(2), pp.95-104.

Sjöström, M., Ardö, J., Arneth, A., Boulain, N., Cappelaere, B., Eklundh, L., De Grandcourt, A., Kutsch, W.L., Merbold, L., Nouvellon, Y. and Scholes, R.J., 2011. Exploring the potential of MODIS EVI for modeling gross primary production across African ecosystems. Remote sensing of environment, 115(4), pp.1081-1089.

Skowno, A., Raimondo, D., Powrie, L., Hoffman, M.T., Van der Merwe, S., Hlahane, K., Fizzoti, B., Varaiwa, T., 2019. Chapter 3: Pressures and Threats. South African National Biodiversity Assessment 2018: Technical Report. In: Terrestrial Environment, vol. 1. South African National Biodiversity Institute (SANBI), Pretoria, South Africa.

Small, D. and Schubert, A., 2008. Guide to ASAR geocoding. ESA-ESRIN Technical Note RSL-ASAR-GC-AD, 1, p.36.

SNAP Development Team, 2016. S1TBX. SNAP - ESA Sentinel Application Platform v2.0.2, http://step.esa.int

Solomon, S., Qin, D., Manning, M., Averyt, K. and Marquis, M. eds., 2007. Climate change 2007-the physical science basis: Working group I contribution to the fourth assessment report of the IPCC (Vol. 4). Cambridge university press.

Stephenson, P.J., Ntiamoa-Baidu, Y. and Simaika, J.P., 2020. The use of traditional and modern tools for monitoring wetlands biodiversity in Africa: challenges and opportunities. Frontiers in Environmental Science, 8, p.61.

Stratoulias, D., Balzter, H., Sykioti, O., Zlinszky, A. and Tóth, V.R., 2015. Evaluating sentinel-2 for lakeshore habitat mapping based on airborne hyperspectral data. Sensors, 15(9), pp.22956-22969.

Sundquist E, Burruss R, Faulkner S, Gleason RA, Harden JW, Kharaka YK et al (2008) Carbon sequestration to mitigate climate change. US Geological Survey, Fact Sheet 2008–3097.

Svoray, T. and Shoshany, M., 2002. SAR-based estimation of areal aboveground biomass (AAB) of herbaceous vegetation in the semi-arid zone: A modification of the water-cloud model. International Journal of Remote Sensing, 23(19), pp.4089-4100.

Taddeo, S., Dronova, I. and Depsky, N., 2019. Spectral vegetation indices of wetland greenness: Responses to vegetation structure, composition, and spatial distribution. Remote sensing of Environment, 234, p.111467.

Talbi, E.G., 2009. Metaheuristics: from design to implementation. John Wiley & Sons.

Tang, Y.S., Wang, L., Jia, J.W., Fu, X.H., Le, Y.Q., Chen, X.Z. and Sun, Y., 2011. Response of soil microbial community in Jiuduansha wetland to different successional stages and its implications for soil microbial respiration and carbon turnover. Soil Biology and Biochemistry, 43(3), pp.638-646.

Tavasoli, N. and Arefi, H., 2020. Comparison of capability of SAR and optical data in mapping forest above ground biomass based on machine learning. Environmental Sciences Proceedings, 5(1), p.13.

Themistocleous, K., Hadjimitsis, D., Hadjimitsis, D.G. and Themistocleous, K., 2008, October. The importance of considering atmospheric correction in the pre-processing of satellite remote sensing data intended for the management and detection of cultural sites: a case study of the Cyprus area. In Conference Paper:14th International Conference on Virtual Systems and Multimedia (dedicated to culture heritage). VSMM, Limmasol, Turkey.

Torres, R., Snoeij, P., Geudtner, D., Bibby, D., Davidson, M., Attema, E., Potin, P., Rommen, B., Floury, N., Brown, M. and Traver, I.N., 2012. GMES Sentinel-1 mission. Remote sensing of environment, 120, pp.9-24.

Touzi, R., 2002. A review of speckle filtering in the context of estimation theory. IEEE Transactions on Geoscience and Remote Sensing, 40(11), pp.2392-2404.

Tucker, C.J., 1979. Red and photographic infrared linear combinations for monitoring vegetation. Remote sensing of Environment, 8(2), pp.127-150.

Turak, E., Harrison, I., Dudgeon, D., Abell, R., Bush, A., Darwall, W., Finlayson, C.M., Ferrier, S., Freyhof, J., Hermoso, V. and Juffe-Bignoli, D., 2017. Essential Biodiversity Variables for measuring change in global freshwater biodiversity. Biological Conservation, 213, pp.272-279.

United Nations (UN), 2017. Integrated Monitoring Guide for SDG 6: Step-by-step Monitoring Methodology for Indicator 6.6.1 on Water-Related Ecosystems. Version 20 January 2017

Urbazaev, M., Thiel, C., Mathieu, R., Naidoo, L., Levick, S.R., Smit, I.P., Asner, G.P. and Schmullius, C., 2015. Assessment of the mapping of fractional woody cover in southern African savannas using multi-temporal and polarimetric ALOS PALSAR L-band images. Remote Sensing of Environment, 166, pp.138-153.

Van Deventer, H., Linström, A., Naidoo, L., Job, N., Sieben, E.J.J. and Cho, M.A., 2022. Comparison between Sentinel-2 and WorldView-3 sensors in mapping wetland vegetation communities of the Grassland Biome of South Africa, for monitoring under climate change. Remote Sensing Applications: Society and Environment, 28, p.100875.

Van Deventer, H., Van Niekerk, L., Adams, J., Dinala, M.K., Gangat, R., Lamberth, S.J., Lötter, M., Mbona, N., MacKay, F., Nel, J.L. and Ramjukadh, C.L., 2020. National Wetland Map 5: An improved spatial extent and representation of inland aquatic and estuarine ecosystems in South Africa. Water SA, 46(1), pp.66-79.

Van Wijk, M.T. and Williams, M., 2005. Optical instruments for measuring leaf area index in low vegetation: application in arctic ecosystems. Ecological Applications, 15(4), pp.1462-1470.

Verrelst, J., Camps-Valls, G., Muñoz-Marí, J., Rivera, J.P., Veroustraete, F., Clevers, J.G. and Moreno, J., 2015. Optical remote sensing and the retrieval of terrestrial vegetation bio-geophysical properties–A review. ISPRS Journal of Photogrammetry and Remote Sensing, 108, pp.273-290.

Villa, J.A. and Bernal, B., 2018. Carbon sequestration in wetlands, from science to practice: An overview of the biogeochemical process, measurement methods, and policy framework. Ecological Engineering, 114, pp.115-128.

Wan, R., Wang, P., Wang, X., Yao, X. and Dai, X., 2018. Modeling wetland aboveground biomass in the Poyang Lake National Nature Reserve using machine learning algorithms and Landsat-8 imagery. Journal of Applied Remote Sensing, 12(4), pp.046029-046029.

Wan, R., Wang, P., Wang, X., Yao, X. and Dai, X., 2018. Modeling wetland aboveground biomass in the Poyang Lake National Nature Reserve using machine learning algorithms and Landsat-8 imagery. Journal of Applied Remote Sensing, 12(4), p.046029.

Wang, J., Xiao, X., Bajgain, R., Starks, P., Steiner, J., Doughty, R.B. and Chang, Q., 2019. Estimating leaf area index and aboveground biomass of grazing pastures using Sentinel-1, Sentinel-2 and Landsat images. ISPRS Journal of Photogrammetry and Remote Sensing, 154, pp.189-201.

Were, D., Kansiime, F., Fetahi, T., Cooper, A. and Jjuuko, C., 2019. Carbon sequestration by wetlands: a critical review of enhancement measures for climate change mitigation. Earth Systems and Environment, 3(2), pp.327-340.

White, L., Brisco, B., Dabboor, M., Schmitt, A. and Pratt, A., 2015. A collection of SAR methodologies for monitoring wetlands. Remote sensing, 7(6), pp.7615-7645.

Wu, Q., 2017. GIS and remote sensing applications in wetland mapping and monitoring.

Xie, Y., Sha, Z., Yu, M., Bai, Y. and Zhang, L., 2009. A comparison of two models with Landsat data for estimating above ground grassland biomass in Inner Mongolia, China. Ecological Modelling, 220(15), pp.1810-1818.

Xu, D., Guo, X., Li, Z., Yang, X. and Yin, H., 2014. Measuring the dead component of mixed grassland with Landsat imagery. Remote Sensing of Environment, 142, pp.33-43.

Xu, L. and Baldocchi, D.D., 2004. Seasonal variation in carbon dioxide exchange over a Mediterranean annual grassland in California. Agricultural and Forest Meteorology, 123(1-2), pp.79-96.

Xue, J. and Su, B., 2017. Significant remote sensing vegetation indices: A review of developments and applications. Journal of sensors, 2017.

Yang, S., Feng, Q., Liang, T., Liu, B., Zhang, W. and Xie, H., 2018. Modeling grassland above-ground biomass based on artificial neural network and remote sensing in the Three-River Headwaters Region. Remote Sensing of Environment, 204, pp.448-455.

Yang, Y.H., Fang, J.Y., Pan, Y.D. and Ji, C.J., 2009. Aboveground biomass in Tibetan grasslands. Journal of Arid Environments, 73(1), pp.91-95.

Ye, Y., Zhou, C., Sun, Y. and Zhou, D., 2010, June. Estimation of wetland aboveground biomass based on SAR image: a case study of Honghe National Natural Reserve in Heilongjiang, China. In 2010 18th International Conference on Geoinformatics (pp. 1-6). IEEE.

Zeng, N., Ren, X., He, H., Zhang, L., Zhao, D., Ge, R., Li, P. and Niu, Z., 2019. Estimating grassland aboveground biomass on the Tibetan Plateau using a random forest algorithm. Ecological Indicators, 102, pp.479-487.

Zhao, H. and Gui, L., 2019. Nonparametric and parametric methods of spectral analysis. In Matec web of conferences (Vol. 283, p. 07002). EDP Sciences.

Zhao, P., Lu, D., Wang, G., Liu, L., Li, D., Zhu, J. and Yu, S., 2016. Forest aboveground biomass estimation in Zhejiang Province using the integration of Landsat TM and ALOS PALSAR data. International Journal of Applied Earth Observation and Geoinformation, 53, pp.1-15.

Zhao, Y., Mao, D., Zhang, D., Wang, Z., Du, B., Yan, H., Qiu, Z., Feng, K., Wang, J. and Jia, M., 2022. Mapping *Phragmites australis* Aboveground Biomass in the Momoge Wetland Ramsar Site Based on Sentinel-1/2 Images. Remote Sensing, 14(3), p.694.

Zhu, X. and Liu, D., 2015. Improving forest aboveground biomass estimation using seasonal Landsat NDVI time-series. ISPRS Journal of Photogrammetry and Remote Sensing, 102, pp.222-231.

Zinke, L., 2020. The colours of carbon. Nature Reviews Earth & Environment, 1(3), pp.141-141.

Zuhlke, M., Fomferra, N., Brockmann, C., Peters, M., Veci, L., Malik, J. and Regner, P., 2015, December. SNAP (sentinel application platform) and the ESA sentinel 3 toolbox. In Sentinel-3 for Science Workshop (Vol. 734, p. 21).

APPENDIX A

Table A1: Modelling accuracies for estimation of the LAI as an additional parameter in modelling AGB of palustrine wetland vegetation.

Modelling scenarios (down) and Season (across)	Summer			Winter		
	R^2	RMSE ($m^2.m^{-2}$)	relRMSE %	R^2	RMSE ($m^2.m^{-2}$)	relRMSE (%)
Scenario 1: Spectral bands only	0.611	1.509	23.024	0.740	1.237	26.892
Scenario 2: VIs only	0.422	1.674	28.454	0.764	1.253	23.904
Scenario 3: Bands + VIs	0.611	1.687	21.339	0.770	1.272	19.581